THE UNIVERSITY *of* EDINBURGH

The Effect of Volcanic Eruptions on the Hydrological Cycle

Carley Elizabeth Iles

Thesis submitted for the degree of
Doctor of Philosophy

The University of Edinburgh

2014

Declaration

I confirm that the work submitted is my own, except where work which is part of jointly-authored papers has been included. Two results chapters are based on papers published in or submitted to peer reviewed journals on which I am the lead author. Details of these publications are given below, including an outline of the contribution of each author. I confirm that appropriate credit has been given within the thesis where reference has been made to the work of others. No part of this work has been submitted for any other degree or professional qualification.

Chapter 2 is based on a paper published in the *Journal of Geophysical Research*:
Iles, C. E., G. C. Hegerl, A. P. Schurer and X. Zhang (2013), The effect of volcanic eruptions on global precipitation, *J. Geophys. Res.*,*118*(16) , 8770–8786, doi:10.1002/jgrd.50678.

I performed the data analysis and wrote the manuscript. My primary supervisor Gabi Hegerl provided scientific advice and edited the manuscript. Andrew Schurer provided the model data and Xuebin Zhang provided the precipitation dataset. All proofread the manuscript and gave feedback. My second supervisor Simon Tett also contributed through scientific discussion.

Chapter 3 is based on a paper submitted to *Environmental Research Letters*:
Iles, C. E. and G. C. Hegerl (2014), The global precipitation response to volcanic eruptions in the CMIP5 models, *Geophs. Res. Lett.* Submitted.

I conducted the analysis and wrote the paper, Gabi Hegerl provided scientific advice and edited the manuscript.

The other parts of the thesis were proofread by Gabi Hegerl and feedback given.

Carley Iles
Date: 09/07/14

Acknowledgements

Thanks go particularly to Gabi Hegerl for being an excellent supervisor, always making time for me in her busy schedule and for all the advice she has given me over the past few years. Thanks also go to my second supervisor, Simon Tett for useful discussions and input. I thank my co-authors Andrew Schurer, Xuebin Zhang and three anonymous reviewers for their input on the paper on which Chapter 2 is based. I would also like to thank the members of my research group: Andrew Schurer, Debbie Polson, Oliver Krueger, Mike Mineter, Andrew Harding, Oliver Brown, Massimo Bollasina, Tom Russon, Simone Morak, Alessio Bozzo and Helen Hanlon, and of course my fellow PhD students Emma Turner and Darren Slevin for their support and scientific discussions. I am grateful to my examiners, David Stevenson, Tim Osborn and Claudia Timmreck, for the time they spent reading my thesis and for their insightful comments. Thanks also go to the members of the 'pod' Gus Fraser-Harris, Rami-Eid, Becky Jackson, Alice Macente and Nicola Rigonat for being entertaining office mates and good friends, along with the rest of my friends both at Edinburgh University and Kings Church. Finally thanks go to my family, flatmates and particularly to Ben Ritchie for their moral support.

Abstract

Large explosive volcanic eruptions inject SO_2 into the stratosphere where it is oxidised to sulphate aerosols which reflect sunlight. This causes a reduction in global temperature and precipitation lasting a few years. Here the robust features of this precipitation response are investigated, using superposed epoch analysis that combines results from multiple eruptions. The precipitation response is first analysed using the climate model HadCM3 compared to two gauge based land precipitation datasets. The analysis is then extended to a large suite of state-of-the art climate models participating in the Coupled Model Intercomparison Project Phase 5 (CMIP5). This is the first multi-model study focusing on the precipitation response to volcanoes. The large ensemble allows analysis of a short satellite based dataset which includes ocean coverage. Finally the response of major world rivers to eruptions is examined using historical records. Whilst previous studies focus on the response of just a few rivers or global discharge to single eruptions, here the response of 50 major world rivers is averaged across multiple eruptions. Results are applicable in predicting the precipitation response to future eruptions and to geoengineering schemes that seek to counteract global warming through reducing incoming solar radiation.

The main model-simulated features of the precipitation response include a significant global drying over both land and ocean, which is dominated by the wet tropical regions, whilst the dry tropical ocean regions get significantly wetter following eruptions. Monsoon rainfall decreases, whilst in response to individual eruptions the Intertropical Convergence Zone shifts away from the hemisphere with the greater concentration of volcanic aerosols. The ocean precipitation response is longer lived than that over land and correlates with near surface air temperature, whilst the land response correlates with aerosol optical depth and a reduction in land-ocean temperature gradient

Many of these modelled features are also seen in observational data, including the decrease in global mean and wet tropical regions precipitation over land and the increase of precipitation over dry tropical ocean regions, all of which are significant in the boreal cold season. The land precipitation response features were robust to choice of dataset. Removing

the influence of the El Nino Southern Oscillation (ENSO) reduces the magnitude of the volcanic response, as several recent eruptions coincided with El Nino events. However, results generally remain significant after subtraction of ENSO, at least in the cold season. Over ocean, observed results only match model expectations in the cold season, whilst data are noisy in the warm season. Results are too noisy in both seasons to confirm whether a long ocean precipitation response occurs. Spatial patterns of precipitation response agree well between observational datasets, including a decrease in precipitation over most monsoon regions. A positive North Atlantic Oscillation-like precipitation response can be seen in all datasets in boreal winter, but this is not captured by the models. A detection analysis is performed that builds on previous detection studies by focusing specifically on the influence of volcanoes. The influence of volcanism on precipitation is detectable using all three observational datasets in boreal winter, including for the first time in a dataset with ocean coverage, and marginally detectable in summer. However, the models underestimate the size of the winter response, with the discrepancy originating in the wet tropics.

Finally, the number of major rivers that undergo a significant change in discharge following eruptions is slightly higher than expected by chance, including decreased flow in the Amazon, Congo, Nile, Orange, Ob and Yenisey. This proportion increases when only large or less humanly influenced basins are considered. Results are clearer when neighbouring basins are combined that undergo the same sign of CMIP5 simulated precipitation response. In this way a significant reduction in flow is detected for northern South American, central African and less robustly for high-latitude Asian rivers, along with a significant increase for southern South American and SW North American rivers, as expected from the model simulated precipitation response.

Lay Summary

Large explosive volcanic eruptions inject reflective particles (sulphate aerosols) high up into the atmosphere which then spread out globally, reflecting sunlight. This causes a decrease in global temperature lasting a few years, along with a reduction in global rainfall. Here the details of this rainfall response are investigated using a combination of rainfall measurements and climate model simulations. Historical data from major world rivers are then examined to investigate whether the influence of volcanic eruptions can also be seen therein. Since volcanic eruptions cause global cooling, geoengineering measures based on the same principles have been proposed. Understanding the response of the water cycle to eruptions thus sheds light on potential geoengineering side effects. Results are also relevant in predicting the response of the water cycle to future eruptions.

The main features of this volcanic rainfall response agree between models and observed data and include a global drying response, which is dominated by a decrease in rainfall in the wet tropical regions. In contrast the dry tropical ocean regions get wetter. However, the models tend to underestimate the size of the response in the boreal cold season (i.e. November through to April). In climate models the response of rainfall over oceans consistently lasts longer than that over land. However, this cannot be confirmed by observations, as ocean precipitation records are short, capturing the response to only two major eruptions and hence show too much variability to identify a clear volcanic response. Monsoon rainfall reduces following eruptions in both models and observations, whilst in the models the Intertropical Convergence Zone (an equatorial band of converging winds and rising air associated with rain) shifts away from the hemisphere with the largest concentration of sulphate aerosols. Volcanic eruptions have previously been found to be followed by a positive phase of the North Atlantic Oscillation (a fluctuation in the pressure difference between Iceland and the Azores which affects the strength of westerly winds and thereby winter temperature and precipitation in Europe). A corresponding rainfall pattern can be seen in observational data in winter, but this is not captured by climate models, in agreement with previous studies.

Finally, it was found that some rivers undergo a change in discharge following eruptions, for instance a decrease in flow for the Amazon, Congo, Nile, Orange, Ob and Yenisey. Results are clearer when neighbouring river basins undergoing the same sign of model-simulated rainfall response are combined. In this way a notable reduction in flow is experienced for northern South American, central African and northern Asian rivers, along with an increase in flow for southern South American and SW North American rivers, as might be expected from the model simulated precipitation response over these regions.

Contents

List of Figures

List of Tables

Chapter 1: Introduction and Background

1.1 Introduction

The Earth's climate has warmed by 0.85°C since 1880, with a high probability that at least half of the warming since 1950 is attributable to anthropogenic greenhouse gas emissions [*Bindoff et al*., 2013]. A further 0.3 to 4.8°C of warming is predicted by the end of the century depending on the emissions scenario and climate model employed [*IPCC*, 2013]. This climatic change is expected to have adverse effects on both people and ecosystems, e.g. through sea level rise, changes in climate extremes, changes in growing conditions for crops and geographical ecosystem shifts [*IPCC*, 2014]. Some of these impacts could be ameliorated if a temperature increase could be avoided. In contrast, large explosive volcanic eruptions cause a decrease in global temperature lasting a few years, through injecting sulphate aerosols into the stratosphere where they reflect incoming solar radiation [e.g. *Robock*, 2000 and references therein]. This has led to consideration of geoengineering schemes based on artificially injecting sulphate aerosols into the stratosphere to replicate the volcanic cooling response. However, as well as reducing temperatures, volcanic eruptions also affect other components of the climate system, including atmospheric circulation and the hydrological cycle, causing a temporary decrease in precipitation on a global scale [e.g. *Robock*, 2000 and references therein, *Trenberth and Dai*, 2007; *Stenchikov et al*., 2006, *Gillett et al*., 2004]. This suggests that such geoengineering schemes are likely to have similar side effects which require further investigation, for which volcanic eruptions provide a useful analogue.

However, compared to the effect of volcanic eruptions on temperature, understanding of the response of precipitation and other hydrological cycle components to eruptions, particularly streamflow, is more limited. Furthermore, previous studies suggest that climate models underestimate the magnitude of the precipitation response to eruptions [*Lambert et al.,* 2004; 2005, *Gillett et al*., 2004], which has direct consequences for model-based geoengineering studies. Particularly given its importance to both people and ecosystems, more research is needed into the response of the hydrological cycle to eruptions. This would also aid

understanding of past precipitation and drought records, and the prediction of the precipitation response to future eruptions. Hence the question to what extent volcanic eruptions influence global precipitation, and the mechanisms and timescales at which the response occurs are also scientifically important.

In this thesis the robust features of the precipitation response to volcanic eruptions are investigated using both observational data and climate model simulations. In order to separate the volcanic response from climate variability we apply several techniques, including superposed epoch analysis, which involves averaging across the response to several eruptions. Robustness of results to using alternative observational datasets or climate models is investigated and quantitative comparisons between observations and model simulations drawn, including a detection analysis which is tailored specifically to the volcanic response. Finally, the response of major world rivers to eruptions is investigated using historical streamflow records.

1.2 Background

This section commences by outlining how the impact of volcanic eruptions is studied, including the type of eruption that affects climate, an outline of the superposed epoch analysis technique and a brief discussion of how climate models are used to investigate the climate impact of volcanoes. The impact of volcanic eruptions on various aspects of climate is then discussed, focusing particularly on research into their effect on the hydrological cycle. Research into the response of the hydrological cycle to solar-radiation management based geoengineering schemes is also briefly outlined. Finally, research gaps are identified, aims and objectives set out, and an outline of the thesis described, highlighting how this research builds on previous studies.

1.2.1 Investigating the effects of volcanic eruptions in climate studies

Type of eruption

It is large, explosive volcanic eruptions that inject sulphur dioxide (SO_2) and hydrogen sulphide (H_2S) into the stratosphere that impact climate. SO_2 and H_2S are oxidised to

sulphate aerosols over a time scale of weeks, and these spread out zonally to encircle the globe within 2-3 weeks, and meridionally over the timescale of months, transported polewards by the Brewer-Dobson circulation [e.g. *Robock*, 2000 and references therein]. Aerosol clouds from tropical eruptions tend to spread out over both hemispheres, whilst those of high latitude eruptions are confined to the hemisphere of eruption [e.g., *Robock*, 2000; *Timmreck*, 2012 and references in both]. These aerosols reflect sunlight, causing global surface and tropospheric cooling. For example, the 1991 Pinatubo eruption caused a $4Wm^{-2}$ reduction in short-wave radiation reaching the Earth's surface [*Stenchikov et al*., 1998]. Sulphate aerosols tend to linger in the stratosphere for a couple of years and are removed through large scale subsidence at the poles, sedimentation into the troposphere, and tropopause folding [e.g. *Haywood et al*., 2010]. Lower injection heights and higher latitudes of eruption lead to quicker removal [e.g. *Haywood et al*., 2010]. High latitude eruptions will tend to have a smaller impact on climate compared to tropical eruptions for a given sulphur emission due to the combination of quicker aerosol removal, limited geographical extent of the aerosol cloud and lower incoming solar radiation levels at high latitudes. Effusive eruptions which only emit aerosols to the troposphere have much less impact on climate because aerosols there only have a lifetime of a few days [*Highwood and Stevenson*, 2003]. Although the eruption of Laki in 1783-4 was mostly effusive, it did affect northern hemisphere temperature and monsoon precipitation because of sulphur emitted to the stratosphere during its explosive phases [*Oman et al*., 2006a; 2006b]. However, studies disagree about the amount of sulphur reaching the stratosphere and therefore the magnitude of its climate effects [*Highwood and Stevenson*, 2003; *Oman et al*., 2006a; 2006b]. Effusive and Laki-style eruptions are not considered in this thesis.

It is the amount of sulphur rather than magmatic material (ash and tephra) injected into the stratosphere that is important for climatic impacts. Carbon dioxide and water vapour emitted from volcanoes are negligible compared to background levels and so are not important for climate [*Robock*, 2000]. Since there is little water in the stratosphere, volcanic particles acting as cloud condensation nuclei is a phenomenon confined to the troposphere, and therefore short-lived. [*Robock*, 2000]. Nevertheless, climate effects are not linearly related to

sulphur burden of the stratosphere, as higher sulphate loads lead to more coagulation of aerosols which have a smaller effect on short-wave radiation per unit mass [*Timmreck et al*., 2009]. Figure 1.1 shows a time series of aerosol optical depth (AOD) over the last 150 years, thereby indicating when the recent climatically important volcanic eruptions occurred and towards which hemisphere their aerosol clouds were biased (see also Table 2.1 and Figure 2.1, Chapter 2).

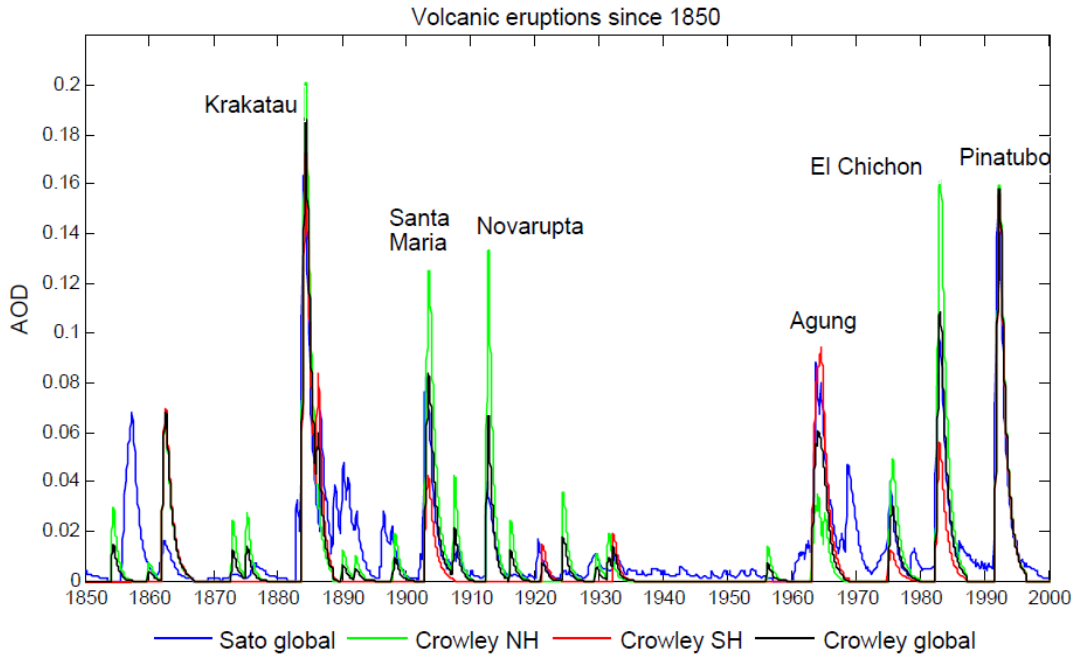

Figure 1.1: Time series of global mean Aerosol Optical Depth (AOD) since 1850 from the *Sato et al*. [1993] (blue) and *Crowley et al*., [2008] (black) datasets, thereby indicating the main climatically important volcanic eruptions over the recent period. *Crowley et al*. [2008] AOD data is also shown for the northern hemisphere (green) and southern hemisphere (red) separately to give an indication of the eruption latitude and position of the aerosol cloud.

Epoch analysis

Many studies on the effect of volcanic eruptions on climate are based on a technique called superposed epoch analysis [e.g. *Fischer et al*., 2007; *Hegerl et al*., 2003; 2011]. This involves averaging the climate response across multiple eruptions in order to reduce internal variability and thereby see the influence of volcanic eruptions more clearly. This technique can be applied to both observations and climate model simulations and is the main analysis technique employed in this thesis.

Investigating the impact of volcanic eruptions using climate models

In order to be used to examine the effect of volcanic eruptions on climate, General Circulation Models of the atmosphere and ocean (GCMs) must be forced with volcanic aerosols. In older models this involved a simple reduction of the solar constant. More recently models such as the ones used for the Couple Model Intercomparison Project Phase 5 (CMIP5) generally specify volcanic forcing as aerosols with a specified size distribution based on historical observations. Examples of such forcing datasets are *Crowley et al*. [2008], *Sato et al*. [1993] and its update *Hansen et al*. [2002] (see Figure 1.1) or Ammann et al. [2003] and its update *Ammann et al*. [2007]. These forcing datasets are compiled using a number of techniques. For example, the *Crowley et al*. [2008] dataset is based on sulphate measurements from ice cores from Greenland and Antarctica calibrated to satellite estimates of AOD and effective radius for the 1991 Pinatubo and much smaller Hudson eruption. The *Hansen et al*. [2002] dataset is based on satellite, aircraft, balloon, and ground-based observations of AOD and effective radius of sulphate aerosols. Both of these datasets estimate AOD in four latitudinal bands. The *Ammann et al*. [2003] and its update *Ammann et al*. [2007] datasets are also commonly used to force GCMs and use a simple model to recreate the probable distribution of aerosols following eruptions including seasonal differences in transport. They assume a constant effective radius of 0.42μm. This dataset provides higher latitudinal resolution (64 bands), which is particularly useful in the pre-satellite era. Alternatively in some models, such as MRI-CGCM-3, aerosol emissions are specified and the climate model is left to simulate reactions and transport. This is more computationally expensive and it is generally only the mass of aerosols that is calculated, whilst the size distribution is specified [*Timmreck*, 2012]. In all cases climate models are then left to simulate the climate system response to the volcanic forcing.

Whereas in the real climate system there is only one rendition of each volcanic eruption and its response is partially obscured by noise, in climate models it is possible to perform an ensemble of runs for each eruption, each with different initial conditions. Due to the chaotic nature of the atmosphere, each run will have different internal variability associated with it and by taking the ensemble mean this variability will tend to cancel out, making the volcanic

influence clearer. Ensemble means can also be taken across multiple models. Note that responses to volcanism that involve circulation (see 1.2.2) will remain visible if correctly simulated.

GCMs also have the advantage compared to observations of having spatially and temporarily complete data, including for variables that are difficult to measure, such as evaporation or precipitation over the ocean. In this way they can be used to compliment observations, providing they appear to simulate the climate response correctly. Finally, GCMs are also useful in exploring the mechanisms through which volcanic eruptions affect climate. In a climate model it is possible to hold some variables constant, such as sea surface temperatures (SSTs), allowing their contribution to the volcanic response to be discerned.

The observed and model simulated climate response of a variable to eruptions can be compared through fingerprinting techniques (also referred to as detection analyses) [e.g. *Lambert et al*., 2004; 2005; *Gillett et al*. 2004]. These are regression based techniques used to establish whether the modelled fingerprint (i.e. a space-time pattern) of climate response to a forcing agent can be detected in observational data, whether or not this is inconsistent with internal variability and whether the modelled magnitude is correct. Optimal fingerprinting is essentially the same but includes a step to reduce the effect of climate variability on the fingerprints in order to reduce uncertainty on the estimated climate response [see *Hegerl and Zwiers*, 2011]. Here we apply fingerprint detection methods to identify the volcanic signal in observations, using results of epoch analysis to determine fingerprints.

1.2.2 Volcanic eruptions and climate

As well as reflecting incoming solar radiation and thereby causing surface and tropospheric cooling, sulphate aerosols also absorb near infrared radiation and outgoing long wave radiation, thereby warming the lower stratosphere [*Wielicki et al*., 2002]. For low latitude eruptions, this enhances the equator to pole stratospheric temperature gradient, which is thought to cause a stronger polar vortex and a stationary wave pattern of tropospheric circulation that resembles the positive phase of the North Atlantic Oscillation (NAO- a

fluctuation in the pressure difference between Iceland and the Azores which affects the strength of westerly winds and thereby winter temperature and precipitation in Europe). This is associated with warming over northern hemisphere continents in winter, in contrast to the general global post-eruption cooling [e.g. *Robock and Mao*, 1992; 1995] and brings wetter conditions to Northern Europe and drier conditions to Southern Europe. This response is found in observational studies, and earlier model studies, but is not well captured by more recent (CMIP3 and CMIP5) climate models [*Driscoll et al.*, 2012; *Stenchikov et al*., 2006; *Charlton-Perez et al*., 2013]. Nevertheless, this NAO response is reasonably robust in observational studies, increasing confidence that it is a real phenomenon. For instance *Fischer et al*. [2007] found a significant winter warming in northern Europe in the mean response across 15 large low latitude eruptions since 1500, with 14/15 eruptions followed by this pattern. A significant NAO-like 500 hPa geopotential height pattern was found in the mean response to the more recent 10 of these eruptions for which data exists. Furthermore, *Driscoll et al*. [2012] found a significant (95% level) NAO response in sea level pressure data averaged across 9 tropical eruptions that occurred since 1850. 7 out of 9 eruptions were followed by a positive NAO index, whilst the aerosol clouds of the remaining 2 were biased towards the southern hemisphere, which may have affected the dynamical response. However, *Hegerl et al.* [2011] found that the winter warming response over Europe was only marginally detectable against randomly selected winters, despite being present for many eruptions. The existence of physical explanations, such as the one detailed above, add confidence that this NAO response is a real phenomenon, although these mechanisms are still uncertain, e.g. *Stenchikov et al*. [2002] found that stratospheric aerosol heating did not need to be included to simulate the NAO response, but that the reduced equator-pole tropospheric temperature gradient was enough. For very big eruptions, such as that in 1258, climate model simulations have suggested that the direct radiative cooling response can override this dynamical winter warming response [*Schneider et al*., 2009].

Another circulation response to eruptions is the weakening of monsoon winds, with associated reductions in precipitation, which are found in both observations and model simulations. This arises because the land masses cool more than the oceans following

eruptions due to their lower heat capacity, reducing the summer temperature gradient between them [*Schneider et al*., 2009; *Joseph and Zeng*, 2011; *Peng et al*., 2010; *Cao et al*., 2012]. Results from CMIP3 models suggest that volcanic eruptions are also followed on average by a positive phase of the Southern Annular Mode in spring and autumn, which is associated with a strengthened polar vortex and reduced sea-level pressure over the Antarctic [*Karpecho et al*., 2010], although observations suggest a negative SAM following the last three eruptions. [e.g. *Karpecho et al*., 2010; *Roscoe and Haigh*, 2007]. A positive phase of the SAM is associated with a poleward shift of the southern hemisphere midlatitude storm track, causing increased precipitation at high latitudes and decreased precipitation at midlatitudes in all seasons, whilst rainfall increases in the subtropics in autumn and spring [e.g. *Hendon et al*., 2014 using a satellite-gauge dataset (GPCP)].

Other effects of volcanic eruptions include a decrease in ocean heat content and uptake and a concomitant decrease in sea level [e.g. *Stenchikov et al*., 2009 using the GFDL CM2.1 GCM]. The Atlantic Meridional Overturning Circulation (AMOC) has been found to strengthen following eruptions in modelling studies, peaking around a decade after large eruptions [*Stenchikov et al*., 2009; *Zanchettin* et al., 2012]. This is caused by post-eruption cooling of the upper ocean along with increased salinity at mid and high northern latitudes in areas of deep water formation arising from decreased northern hemisphere precipitation and runoff [*Stenchikov et al*., 2009]. Meanwhile, salinity decreases at lower latitudes due to decreased evaporation [*Zanchettin* et al., 2012, using the MPI-ESM]. All the above have been found to recover on timescale of several decades to a century in climate models [*Stenchikov et al*., 2009; *Zanchettin* et al., 2012]. Sea ice has been found to respond on a decadal timescale in model studies, increasing in extent and mass following eruptions [e.g. *Stenchikov et al*., 2009; *Zanchettin et al*., 2012], whilst a few decadally spaced eruptions have been found to cause multi-decadal to centennial increases in sea ice that could have contributed to the onset of the little ice age [*Schneider et al*. 2009 and *Zhong et al*., 2011 using model simulations; *Miller et al*., 2012 using a model and proxy data]. A delayed winter warming associated with a prolonged positive phase of the NAO was found to occur a decade following eruptions on average by both *Zanchettin et al*. [2013] in observational

reconstructions and *Zanchettin et al*. [2012] using a GCM. Finally, ozone depletion has been observed following volcanic eruptions; sulphate aerosols act as a surface upon which ozone depleting reactions occur when chlorine is present [*Robock*, 2000].

There is considerable debate in the literature about whether volcanic eruptions can trigger El Nino events. The most recent three eruptions were followed by El Nino events, albeit a weak one for the 1963 Agung eruption. Based on observational records, *Adams et al*. [2003] and *Emile-Geay et al.* [2008] found an increased probability of El Nino events following large eruptions, whilst *Self et al.* [1997] found no link and *Chen et al*. [2004] showed that all major El Ninos since 1956 could be predicted up to 2 years ahead just using initial sea surface temperatures. Of the 3 twentieth century eruptions occurring at the beginning of El Nino events, El Chichon (1982) and Pinatubo (1991) occurred after the corresponding El Nino event had started [*Self et al.*, 1997]. If volcanic eruptions did affect ENSO, then this would be a mechanism through which they would also affect precipitation.

1.2.3 Volcanic eruptions and the hydrological cycle

Volcanic eruptions have been found to influence various components of the hydrological cycle, which is the focus of this thesis. Tropospheric water vapour tends decrease quasi-exponentially with decreasing temperature at the Clausius Clapeyron rate of around 6.5% per Kelvin [e.g. *Allen and Ingram* 2002]. Accordingly, *Li and Sharma* [2013] find that water vapour decreases across the whole globe following the Pinatubo eruption in the CMIP3 multi model mean, with the largest decrease in the tropics. Global mean water vapour also decreases in observational datasets following Pinatubo, but with increases in some regions such as the eastern equatorial Pacific [*Li and Sharma*, 2013]. However this increase could arise from incomplete removal of the ENSO signal and a poor signal to noise ratio since observational data exists for only one eruption. Using a combination of observations and model simulations, *Soden et al*. [2002] and *Forster and Collins*, [2004] find that the post-eruption decrease in global mean tropospheric water vapour amplifies the post-volcanic cooling response, since water vapour acts as a greenhouse gas. In contrast, *Joshi and Jones*, [2009] suggest that some eruptions increase lower stratospheric water vapour which reduces

the cooling response in the climate model HadGEM1. They suggest that this mechanism might explain the smaller observed temperature response to the 1883 Krakatau eruption compared to climate model simulations.

Both observational and modelling studies have consistently found a decrease in global mean precipitation following large explosive eruptions, lasting a few years (e.g. *Robock and Liu* [1994] using the GISS model, *Schneider et al*. [2009] using NCAR CCSM3; *Gu et al.* [2007] and *Gu and Adler* [2011] using observational precipitation data for eruptions in the latter part of the 20th century, *Trenberth and Dai* [2007] using observed land precipitation data, and *Broccoli et al*. [2003] for Pinatubo in both the GFDL R30 model and observational data). This decrease in global precipitation is due to a reduction in short-wave radiation reaching the surface, reducing evaporation, stabilizing the atmosphere and reducing the saturation mixing ratio of the air [*Bala et al*., 2008; *Cao et al*., 2012]. In addition, radiative cooling of the atmosphere to space is balanced by latent heat release associated with condensation and precipitation, and these all reduce for a cooler post-eruption atmosphere [*Allen and Ingram,* 2002; *O'Gorman et al*., 2012]. Precipitation decreases over both global land and ocean following eruptions, in contrast to ENSO related variations in which it shifts between the two [*Gu et al*., 2007; *Gu and Adler*, 2011; *Liu et al.*, 2012]. The influence of volcanic forcing on the smoothed time series of globally averaged land precipitation has been formally detected through optimal fingerprinting studies on its own [*Gillett et al*., 2004], and in combination with other forcings (*Lambert et al*. [2004], but only for 5 of 9 GCMs in *Lambert et al*. [2005]). The models that did exhibit this volcanic precipitation response tended to underestimate its magnitude.

The main regions experiencing decreased precipitation following low latitude eruptions tend to be the tropics [*Robock and Liu*, 1994; *Trenberth and Dai*, 2007; *Schneider et al*., 2009], and monsoon regions [*Schneider et al*., 2009; *Joseph and Zeng*, 2011; *Wegmann et al*., 2014]. The former has been associated with a weakened Hadley Circulation (*Robock and Liu* [1994] in the GISS model), or a contracted one (*Schneider et al*. [2009] in NCAR CCSM3), whilst the monsoon response is associated with a weakened land-ocean temperature gradient as described above. These features are seen in both modelling and observational studies,

although the monsoon response is less robust in the observations over Asia [e.g. *Joseph and Zeng*, 2011; *Anchukaitis et al*., 2010]. Other features of the precipitation response to low latitude eruptions identified in previous modelling studies include an increase over large parts of the subtropics [*Schneider et al.*, 2009], a decrease over the Sahel in summer [*Robock and Liu*, 1994; *Schneider et al*., 2009] and a shift of the intertropical convergence zone (ITCZ) away from the hemisphere with the greatest concentration of aerosols [*Haywood et al*., 2013]. Using a precipitation reconstruction based on instrumental and proxy data, *Fischer et al*. [2007] found an NAO-like precipitation response over Europe in winter. *Oman et al*. [2006b] and *Robock et al*. [2008] find that the Asian and African monsoons weaken in climate model simulations in response to high northern latitude eruptions and high northern latitude sulphate aerosol geoengineering respectively. This has also been associated with reductions in Sahelian precipitation [*Oman et al*., 2006b; *Haywood et al*., 2013], which is confirmed by observed precipitation records [*Haywood et al*., 2013] and historical streamflow records from the Nile and Niger [*Oman et al*., 2006b]. This Sahelian drying is also tied to shifts in the position of the ITCZ which in turn shifts the African monsoon [*Haywood et al*., 2013].

Concerning streamflow, in addition to *Oman et al*., [2006b] mentioned above, *Trenberth and Dai* [2007] found a significant decrease in global streamflow using historical records following the 1991 Pinatubo eruption, even once the influence of ENSO had been removed, and a moderate decrease following El Chichon in 1982 and Agung in 1963. Spatial patterns of streamflow response following Pinatubo from a land surface model forced with observed precipitation were very similar to the precipitation response itself. The only other study mentioning the streamflow response to eruptions is *Timmreck et al*. [2012] who used MPI-ESM simulations to investigate the climate response to the Toba super eruption in 73ka (100x Pinatubo stratospheric injection of sulphur) in 5 river catchments that were important regions for human evolution. They found a decrease in streamflow lasting around 2 years in all catchments: the Nile, Ganges-Brahmaputra, Mekong, Krishna and Orange rivers. For some rivers (Nile, Ganges- Brahmaputra and Orange, and several others in Africa, tropical Asia and Australia) the initial decrease was followed by anomalously high streamflow (and

precipitation) in years 3-5, linked to a la Nina-like SST anomaly in the Pacific that was thought to strengthen the Indian monsoon.

1.2.4 Geoengineering and the hydrological cycle

As mentioned in Section 1.1, geoengineering schemes that replicate the volcanic cooling effect through reducing incoming solar radiation have been considered in order to counteract global warming and its temperature related impacts, e.g. through placing mirrors in space, artificially injecting sulphate aerosols into the stratosphere, marine cloud brightening or even painting roofs white [e.g. *Caldeira et al*., 2013; *Boucher et al*., 2013]. The sulphate aerosol technique most closely resembles volcanic forcing, the key difference to a simple reduction in the solar constant being that sulphate aerosols absorb near infrared solar radiation and outgoing longwave radiation, thereby warming the lower stratosphere. This has implications for dynamics and also increases downwelling longwave radiation as the aerosols re-emit in the infrared, increasing the forcing needed for a given surface temperature reduction [e.g. *Ammann et al*., 2010; *Ferraro et al*., 2014; *Fyfe et al*., 2013; *Niemeier et al*., 2013]. Nevertheless, the climate response to sulphate aerosol based geoengineering may differ from that to past volcanic eruptions in that the forcing is prolonged, with constant renewal of aerosols, and occurs on a backdrop of elevated CO_2 concentrations. It should be pointed out that whilst these geoengineering schemes can restore global mean temperatures, they do not address other effects of elevated CO_2 levels such as ocean acidification or changes in the terrestrial carbon cycle, whilst sulphate aerosol based schemes can cause ozone depletion [*Caldeira et al.*, 2013].

The effects of solar-radiation management geoengineering has been increasingly studied in recent years through model experiments, including as part of GeoMIP (Geoengineering Comparison Project) [Kravitz et al 2013a], although many of these studies involve very idealised experiments e.g. the GeoMIP ‘G1’ experiment which involves reducing the solar constant to maintain top of the atmosphere radiative balance during an abrupt quadrupling of CO_2. Whilst less comparable to volcanic eruptions, these studies do shed light on how the

climate system, including the hydrological cycle responds to short-wave radiative forcing. The following discussion is based solely on the results of model experiments.

Both solar reduction and sulphate aerosol techniques have been found to be effective in reducing global mean temperatures to desired levels, albeit with overcompensation in the tropics and residual warming at high latitudes for latitudinally uniform shortwave forcing [e.g. *Ban-Weiss and Caldeira*, 2010, *Kravitz et al*., 2013b, *Schmidt et al*., 2012; *Ammann et al*., 2010]. However, all short-wave geoengineering studies find that when temperature is reduced to desired levels, global precipitation decreases too much [e.g. *Tilmes et al*., 2013; *Kravitz et al*., 2013b, *Ricke et al*., 2010; *Bala et al*., 2008; *Fyfe et al*., 2013; *Ban-Weiss and Caldeira*, 2010; *Robock et al*., 2008]. On the one hand the increase in temperature associated with elevated CO_2 concentrations (with no-geoengineering) tends to increase precipitation through increasing the water vapour holding capacity of the atmosphere, whilst a warmer atmosphere tends to undergo more radiative cooling to space which is balanced by latent heat release associated with precipitation. On the other hand CO_2 also acts to decrease precipitation through stabilising the atmosphere and inhibiting radiative cooling to space through absorbing longwave radiation (referred to here as 'the direct CO_2 effect'). The net effect under elevated CO_2 concentrations is an increase in precipitation that is weaker than the thermal response alone [e.g. *Bala et al*., 2008; *O'Gorman et al*., 2012; *Allen and Ingram*, 2002; *Lambert and Allen*, 2009]. A decrease in short-wave forcing acts directly at the surface, decreasing evaporation and increasing atmospheric stability with no compensating effect, making it more effective at influencing precipitation [e.g. *Bala et al*., 2008; *Cao et al*., 2012; *Lambert and Allen*., 2009]. In a geoengineered world, temperature effects are minimal, and so the direct CO_2 effect becomes important [e.g. *Tilmes et al*., 2013]. Whilst a decrease in global precipitation is undesirable, changes for solar reduction techniques are smaller than for climate change with no geoengineering, although can be bigger for some regions [*Schmidt et al*., 2012; *Tilmes et al*., 2013; *Kravitz et al*., 2013b]. Due to their greenhouse effect, sulphate aerosols cause a greater reduction in precipitation than a simple solar reduction [e.g. Fyfe et al., 2013; Ferraro et al., 2014; Niemeier et al., 2013]. The effect of elevated CO_2 concentrations on plants further reduces precipitation, particularly over land

through stomata closure leading to reduced transpiration [*Fyfe et al*. 2013; *Tilmes et al*., 2013, *Kravitz et al*., 2013c, *Cao et al*., 2012]. This effect is of comparable magnitude to the radiative effects mentioned above [*Fyfe et al*., 2013].

Spatial patterns of precipitation change to geoengineering are not directly comparable to those for volcanism, since in a geoengineered world higher CO_2 levels are also affecting precipitation. However, model studies suggest that most areas dry in a geoengineered world, including monsoon regions, although models are less consistent over India. Precipitation increases over the Middle East and in the location of the ITCZ in the Pacific, although agreement between models in these regions is poor [*Kravitz et al*., 2013b, *Tilmes et al*., 2013, *Schmidt et al*., 2012]. Evaporation and latent heat fluxes decrease in most places, except in deserts and the high latitudes, particularly over the ocean, although with poor agreement in these areas [*Kravitz et al*., 2013b, *Tilmes et al*., 2013, *Schmidt et al*., 2012]. Some studies find ITCZ shifts in response to broadly hemispherically symmetric geoengineering, but the direction of shift is inconsistent between studies and does not occur in all models [e.g. *Schmidt et al*., 2012; *Ban-Weiss and Caldeira*, 2008; *Jones et al*., 2010; *Kravitz et al*., 2013b]. When geoengineering is strongly biased to one hemisphere, the ITCZ shifts away from the hemisphere with the greater forcing [*Haywood et al*., 2013; *Ban-Weiss and Caldeira*, 2010; *Yoshimori and Broccoli*, 2008]. Finally, *Tilmes et al*. [2013] found a reduction in precipitation intensity in a geoengineered world, including in monsoon regions.

1.3 Research gaps

Compared to the temperature response to volcanic eruptions, the precipitation response is less well understood. There are a number of avenues that have yet to be explored, some of which are addressed in this thesis. For example, there are few studies that investigate the observed precipitation response across multiple eruptions (see section1.2.1), and those that do tend to be regional in nature and based mostly on proxy data (e.g. *Fischer et al*. [2007] for Europe, *Anchukaitis et al*. [2010] for Asia and *Wegmann et al*. [2014] for Europe and Asia). *Joseph and Zeng* [2011] are an exception but focus only on the tropical land masses. There is scope to investigate this observed precipitation response in more detail, identifying its robust features, including regional and seasonal characteristics. In addition, epoch analysis has not been performed on observed ocean precipitation data, although *Gu et al*. [2007] and *Gu and Adler* [2011] examine its response to volcanism through lagged correlation and regression analysis with aerosol optical depth, but do not examine the spatial features of the response.

There is also a need for more quantitative comparisons of the volcanic precipitation response between models and observations. Climate models tend to simulate precipitation less well than temperature, with some persistent systematic biases e.g. insufficient precipitation in the equatorial West Pacific, too much in the convergence zones south of the equator in the Atlantic and Eastern Pacific, an overly zonal South Pacific Convergence zone, and overly frequent light rainfall events [*Flato et al*., 2013]. Some studies on the volcanic precipitation response are based on model simulations only [e.g. *Robock and Liu*, 1994; *Schneider et al*., 2009; *Peng et al*., 2010; *Haywood et al*., 2013]. Others compare the precipitation response between models and observations qualitatively only. For example, *Joseph and Zeng* [2011] compare the observed precipitation response over tropical land regions to the most recent 3 eruptions with simulations from a model of intermediate complexity with a slab ocean and find the observed and modelled response to be similar. However, *Anchukaitis et al*., [2010] find that paleo-drought indices and GCM simulations disagree over SE Asia. Previous studies that formally detect the influence of external forcing on precipitation through optimal fingerprinting techniques tend not to focus specifically on volcanoes, but note that time series of volcanic forcing appears correlated with global mean land precipitation [e.g.

Lambert et al., 2004; *Lambert et al*., 2005]. However, *Gillett et al*. [2004] detected the influence of volcanic eruptions on a 5 year smoothed time series of global mean land precipitation using the Parallel Climate model. Nevertheless there is scope to perform a detection analysis that is more targeted at volcanic eruptions through combining it with epoch analysis, focusing on interannual variability and incorporating information on the spatial patterns of response. This would be valuable given that these previous detection studies suggest the magnitude of the precipitation response to eruptions is underestimated by models, whilst internal variability and the precipitation response to greenhouse gases also appear underestimated [*Zhang et al*., 2007; *Polson et al*., 2013a; 2013b]. Finally, with the exception of *Lambert et al*. [2005], which does not specifically focus on volcanic forcing, most modelling studies are based on a single model, and a multi-model study would be valuable in assessing whether the response of precipitation to eruptions is consistent between models.

The response of rivers to volcanic eruptions is an area that has not been studied much and has real implications for the people who depend on them. Rivers also integrate surplus precipitation over a drainage basin, reducing noise associated with localised precipitation events. Existing studies either focus on the global response of streamflow to individual eruptions [*Trenberth and Dai*, 2007] or focus on a small number of river basins [*Oman et al*., 2006b; *Timmreck et al*., 2012]. There have not yet been any studies that look at streamflow changes across multiple eruptions or that analyse results for a large number of basins either individually or grouped into regions.

1.4 Aims and objectives of this thesis

Aim

The aim of this thesis is to further understanding of the effect of large explosive volcanic eruptions on the hydrological cycle.

Objectives

- To identify robust features of the precipitation response to large explosive volcanic eruptions on regional and seasonal scales by averaging the response across multiple eruptions, using a combination of observational datasets and climate model simulations. In order to clearly identify the response, significance testing, removing the influence of ENSO and testing sensitivity to choice of dataset and model is important.

- To draw quantitative comparisons between the observed precipitation response and that simulated by climate models, including a detection analysis tailored specifically to the volcanic response. This includes establishing whether climate models underestimate the magnitude of the precipitation response as suggested by previous studies.

- To investigate the response of streamflow to volcanic eruptions using observational records from major rivers worldwide, both individually and grouped into regions informed by the modelled precipitation response. This again includes significance testing and removing the ENSO influence.

1.5 Thesis outline

Chapter 2 is an adaptation of a published paper (Iles, C. E., G. C. Hegerl, A. P. Schurer and X. Zhang (2013), The effect of volcanic eruptions on global precipitation, *J. Geophys. Res*.,118(16) , 8770–8786, doi:10.1002/jgrd.50678). In this chapter the robust features of the precipitation response to volcanic eruptions are investigated using an ensemble of last millennium runs of the climate model HadCM3, comparing to a gauge-based land

precipitation dataset for twentieth century eruptions. This involves using epoch analysis to investigate the regional and seasonal aspects of the volcanic precipitation response in greater detail than has been done previously, including breaking the response into land and ocean, extratropics, and wet and dry tropical regions. The effects of removing the influence of ENSO are investigated, and significance of results tested through a Monte Carlo technique. A detection analysis is performed that builds on previous detection studies by specifically targeting the volcanic response and incorporating spatial information. The hydrological sensitivity (change of precipitation per unit temperature) is calculated for volcanic forcing for the first time and is compared to values for greenhouse gases and internal variability. Key findings include: the tropical wet regions get drier, including monsoon regions, and dry ocean regions wetter following eruptions, which is the opposite pattern to that predicted under global warming; the magnitude of the modelled precipitation response is underestimated in the boreal cold season, originating from the wet tropics; and HadCM3 simulates a long ocean precipitation response (5 years) that follows the near-surface air temperature response, while the precipitation response over land is faster and shorter lived (3 years), following AOD and a reduction in land-ocean temperature contrast.

Chapter 3 is an adaptation of a paper submitted to Environmental Research Letters (Iles and Hegerl 2014, The global precipitation response to volcanic eruptions in the CMIP5 models). In this chapter the analysis in Chapter 2 is extended to models forming part of the CMIP5 (Coupled Model Intercomparision Project Phase 5) archive to see whether the features identified using HadCM3, including the underestimate of the magnitude of the precipitation response, are robust across CMIP5 models. Many of these models are more recent than HadCM3, with higher resolutions and extend further into the stratosphere. This is the first multi-model study focusing on the post-volcanic precipitation response. Model results are compared to a satellite dataset containing ocean coverage, making it the first epoch-style study on observed ocean precipitation data and the first time the influence of volcanic eruptions has been formally detected in a dataset that includes ocean coverage Results proved robust to using alternative observational datasets. The main precipitation response features identified in HadCM3 are also found in CMIP5, including the long ocean response

and the underestimate of the magnitude of response in the boreal cold season. In addition, the ITCZ is found to shift away from the hemisphere with the greater concentration of aerosols in response to individual eruptions in the multi-model mean.

In Chapter 4 the influence of volcanic eruptions on streamflow is investigated by performing epoch analysis on historical records from 50 major world rivers spread across the globe. Rivers are examined both individually and combined into regions, informed by the modelled precipitation response, in order to improve signal to noise ratios. The influence of ENSO is removed and significance of results is tested through a Monte Carlo technique. This is the first study to analyse the streamflow response across multiple eruptions and to examine the response of many rivers worldwide. Individual rivers undergoing a significant response included the Amazon, Congo, Nile, Orange, Ob, Yenisey and Yangtze. For the regional analysis a significant decrease in streamflow was found in northern South America, Central Africa, high latitude Asia, and the wet tropical regions as a whole, and a significant increase in southern South America, and SW North America as expected from the modelled precipitation patterns. A publication based on this chapter is in preparation.

Finally in Chapter 5 the main findings of this thesis are summarised, the main challenges and limitations outlined, wider implications of the findings discussed and ideas for further research suggested.

Chapter 2: The effect of volcanic eruptions on global precipitation

Declaration

This chapter is adapted from a published paper on which I am the first author and Gabi Hegerl, Andrew Schurer (both School of Geosciences, University of Edinburgh) and Xuebin Zhang (Climate Research Division, Environment Canada) are co-authors: Iles, C. E., G. C. Hegerl, A. P. Schurer and X. Zhang (2013), The effect of volcanic eruptions on global precipitation, *J. Geophys. Res.,118*(16) , 8770–8786, doi:10.1002/jgrd.50678. I performed the data analysis and wrote the manuscript, my supervisor Gabi Hegerl provided scientific advice and edited the manuscript, Andrew Schurer provided the model data and Xuebin Zhang provided the precipitation dataset. All three proofread the manuscript and gave feedback. My second supervisor Simon Tett also contributed through scientific discussion. The paper's introduction has been significantly shortened to avoid repetition, and the deleted material moved to the main introduction in Chapter 1.

2.1 Introduction

In this chapter robust features of the precipitation response to 18 large low-latitude volcanic eruptions that occurred between 1400 and 2000 are identified using an ensemble of 11 HadCM3 simulations, analyzing the response separately for climatologically wet and dry regions. The difference in timing between the land and ocean precipitation response is examined and the sensitivity of global precipitation to forcing is calculated. The extent to which the main land precipitation features identified in response to 18 eruptions in HadCM3 can also be identified in observational gauge data for 5 twentieth century eruptions is then examined. The extent to which model and observations agree is then assessed through performing a detection analysis that regresses the observed patterns onto the model patterns and determines whether precipitation variability not associated with volcanism can generate comparable regression coefficients. This builds on previous detection studies [*Lambert et al*., 2004; 2005; *Gillett et al*., 2004], by specifically targeting the volcanic response through focusing on interannual timescales and including information about the spatial patterns of response. Results are shown to be robust to using an alternative observational dataset.

Section 2.2 describes the observational data and model runs used, Section 2.3 outlines the methods employed, whilst results are presented and discussed in Section 2.4, and conclusions drawn in Section 2.5.

2.2 Data

2.2.1 Observational data

The observational precipitation dataset used is an updated version of that detailed in *Zhang et al*. [2007] (hereafter Z07). This is a 5x5 degree gridded gauge based dataset that runs from January 1900 to December 2009. It uses a subset of stations from version 2 of the Global Historical Climatology Network's (GHCN) precipitation dataset [*Vose et al*., 1992] that have at least 25 years of data during the 1961-1990 base period and at least 5 years of data in every decade from 1950-1999 [Z07]. Data are stored as monthly anomalies with respect to this base period. Half year values for the boreal cold (November-April; NDJFMA) and warm seasons (May-October, MJJASO) were calculated by taking the mean of the monthly anomalies where there were at least four months of data present in a given season. We present results for these half year seasons rather than traditional seasons since they capture the main differences in the precipitation response between the cold and warm seasons, whilst signal to noise ratios are improved relative to seasonal or monthly values. Results were very similar when using 3-month seasons (not shown).

In order to test whether results were robust to using a different dataset, the analysis was repeated using the Global Precipitation Climatology Centre's (GPCC) Full Data Reanalysis Version 6 [*Becker et al*., 2013]. This is a 2.5 x 2.5 degree resolution gauge dataset that runs from January 1901 to December 2010. Whilst Z07's dataset focuses on homogeneity through time, GPCC makes use of as many station records as possible (67200 stations with at least 10 years of data) and is spatially interpolated, giving complete land coverage over the time period. These differences lend themselves well to testing how sensitive results are to the method of dataset construction and spatial coverage differences.

2.2.2 Model runs

We used simulations from the coupled climate model HadCM3. This comprises a 3.75x2.5 degree lon-lat resolution atmospheric model, with 19 levels in the vertical and an upper boundary at 10 hPa. This is coupled to an ocean model of 1.25 degree horizontal resolution with 20 vertical levels [*Pope et al*., 2000; *Gordon et al*., 2000]. HadCM3 has been used extensively in the literature and can be used to simulate climate change over millennia since it is not too computationally expensive [*Schurer et al*., 2014]. Having a relatively low upper boundary in the atmosphere it may not capture the observed Northern Annular Mode circulation responses in the cold season [*Stenchikov et al*., 2006; *Tett et al*., 2007], although recent studies found no improvement when using models with much higher vertical extents and stratospheric resolution [*Charlton-Perez et al.*, 2013; *Driscoll et al.*, 2012]. Many aspects of the hydrological cycle are well represented by HadCM3, although the Hadley and Walker circulations are too strong, resulting in an overestimation of precipitation in wet regions, whilst evaporation is overestimated in tropical and subtropical regions [*Pardaens et al*., 2003; *Inness and Slingo* 2003; *Turner et al*., 2005]. The Asian monsoon is reasonably well simulated [*Annamalai et al*., 2007], as is ENSO variability [*Collins et al*., 2001; *Joseph and Nigam*, 2006], (see also Section 2.3.3). We found that both the main features of the precipitation response in HadCM3 and the detection analysis results were consistent with results of models from the CMIP5 archive (see Chapter 3 and C .E. Iles, G.C Hegerl, The global precipitation response to volcanic eruptions in the CMIP5 models, submitted to *Environmental Research Letters*, 2014). Hence we consider this model appropriate to study the large scale precipitation response to volcanism.

We used all 11 runs available to us that were forced by volcanic aerosols. Some of these also included other external forcings (for more detail see *Schurer et al*. [2014]). They all span the years 1400-2000. The ‘ALL’ ensemble consists of 4 runs that were forced with historical changes in greenhouse gas forcing, variations in solar activity, volcanic aerosols, land use

change, anthropogenic aerosols, tropospheric and stratospheric ozone and orbital variations. The 'NoLUSE' ensemble consists of 4 runs with the same forcings as the 'ALL' ensemble but with land use fixed at 1400 conditions. Finally, the 'VOLC' ensemble consists of 3 runs forced with historical volcanic aerosols (Figure 2.1) whilst other forcings were kept constant at 1400 conditions or excluded in the case of anthropogenic aerosols. All 11 ensemble members were used throughout this analysis. Since the analysis focuses on changes within a decade following eruptions relative to the preceding 5 years, the difference in the slower varying forcings should not matter. We tested this for the global mean precipitation response (Figure 2.2) and the spatial patterns (not shown) and found the response to be indistinguishable between ensemble types.

The volcanic forcing dataset used is that detailed in *Crowley et al*. [2008] (Figure 2.1a). This is a reconstruction of aerosol optical depth (AOD) in 4 latitudinal bands based on ice core records from Antarctica and Greenland, calibrated to satellite estimates of AOD for the 1991 Pinatubo and much smaller Hudson eruption. The *Hansen et al*. [2002] AOD dataset is shown from 1850 onwards for comparison and is based on satellite, aircraft, balloon and ground-based observations [*Hansen et al*., 2002]. The volcanic forcing is implemented in HadCM3 as stratospheric aerosols with a constant size distribution, specified in 4 latitudinal bands. They are distributed evenly across all layers above the tropopause in the vertical, with a uniform mass mixing ratio [*Jones et al*., 2005]. The aerosols interact with radiation, such that the lower stratospheric warming effect is reproduced as well as the surface cooling [*Tett et al*., 2007].

2.3 Methods

There are three main components to the analysis. The first is to identify robust features of the precipitation response to strong eruptions in HadCM3 with full data coverage, using a large ensemble of eruptions over the period 1400-2000. Secondly, we examine whether these features identified in HadCM3 can also be seen in response to 20th century eruptions in the observations, and how closely HadCM3 matches the observations for these same eruptions

when it is masked to replicate the observational data spatial coverage. Lastly, we determine whether the observed land precipitation response following volcanic eruptions is detectable against internal variability, sub-dividing the global response into the northern hemisphere extratropics, tropical wet and dry regions.

2.3.1 Selection of volcanic events

Since precipitation is very variable, a technique called epoch analysis was used. This involves averaging the response across multiple eruptions in order to reduce internal variability and make the volcanic influence clearer. For the model response, eruptions with peak global mean AOD >0.05 whose aerosol clouds affected both hemispheres were chosen, based on *Crowley et al*. [2008]'s data (Figure 2.1a). This ensures that eruptions should be

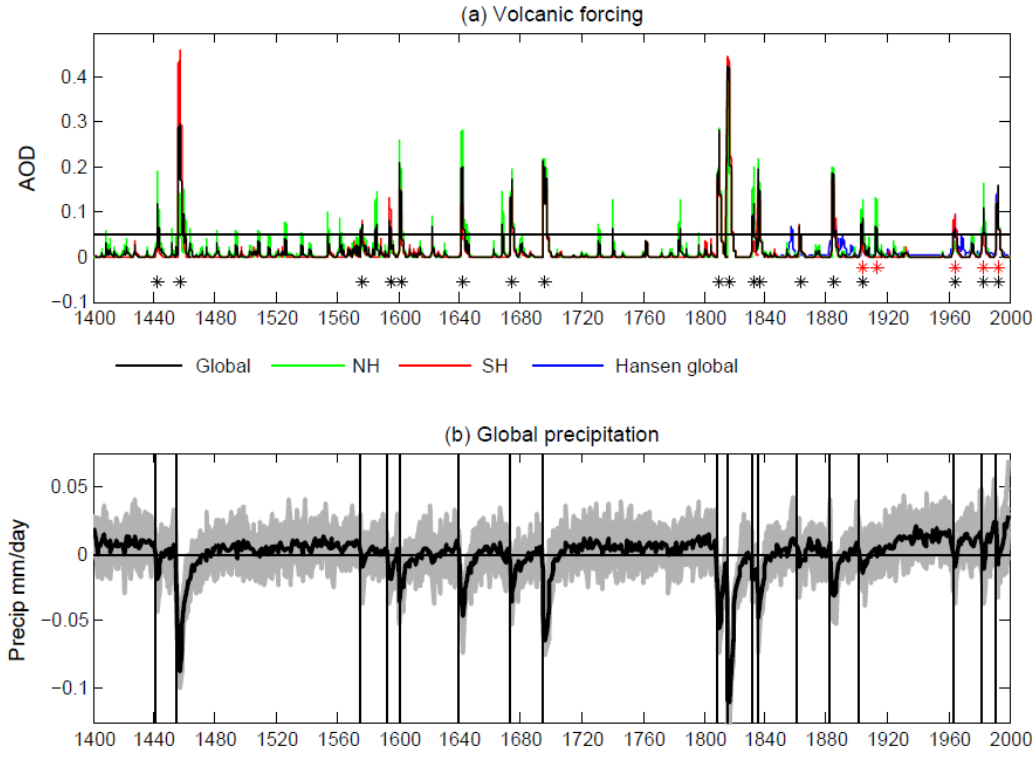

Figure 2.1. (a) Aerosol optical depth (AOD) from *Crowley et al*. [2008]: global mean AOD (black), Northern Hemisphere (green), Southern Hemisphere (red). *Hansen et al*. [2002] AOD is shown in blue for comparison. Black asterisks indicate eruptions used for the 1400-2000 HadCM3 results, red asterisks denote eruptions used for the 20th century analysis. Black horizontal line denotes the 0.05 AOD cut-off used for selecting the 18 eruptions for the climate model results and applies to the global mean AOD. (b) Time series of simulated global mean precipitation for 1400-2000 from all 11 ensemble members of HadCM3, expressed as anomalies with respect to the 1400-2000 climatology. Thick black line is the ensemble mean, ensemble members are shown in grey and eruptions dates are indicated by vertical black lines.

Table 2.1 Eruption Dates and Year 1 Definitions

Estimated Eruption date[a]	Volcano and location[b]	NDJFMA Year 1[c]	MJJASO Year 1	Start month of year 1 for annual data
1441 1st July		1442	1442	Oct 1441
1455 1st July		1456	1456	Oct 1455
1575 1st July		1576	1576	Oct 1575
1593 1st July		1594	1594	Oct 1593
1600 1st Jan	Huaynaputina, Peru 16.61°S, 70.85°W	1601	1600	April 1600
1640 1st July	Philipines	1641	1641	Oct 1640
1673 1st Jan	Indonesia	1674	1673	April 1673
1694 10th March		1695	1694	July 1694
1809 1st Jan		1810	1809	April 1809
1815 mid April	Tambora, Indonesia 8.25°S, 118.00°E	1816	1815	Aug 1815
1831 10th Sept		1832	1832	Jan 1832
1835 20th Jan	Cosiguina, Nicaragua 12.98°N, 87.57°W	1836	1835	May 1835
1861 1st Dec		1863	1862	March 1862
1883 mid August	Krakatau, Indonesia 6.10°S, 105.42°E	1884	1884	Dec 1883
1902 24th Oct*	Santa Maria, Guatemala 14.76°N, 91.56°W	1903	1903	Feb 1903
1912 6th June**	Novarupta, Alaska 58.27°N, 155.16°W	1913	1913	Oct 1912
1963 mid March*	Agung, Indonesia 8.34°S, 115.51°E	1964	1963	July 1963
1982 28 March*	El Chichon, Mexico 17.36°N, 93.23°W	1983	1982	July 1982
1991 15th June*	Pinatubo, Philippines 15.13°N, 120.35°E	1992	1992	Oct 1991

[a]Eruption dates were defined as the date at which aerosol could first be seen in the *Crowley et al*. [2008] dataset for a given eruption. This was set to 1st Jan or 1st July where more precise eruption dates were unknown. Dates for the 1902, 1912, 1963, 1982 and 1991eruptions were obtained from the Global Volcanism Project http://www.volcano.si.edu/world/largeeruptions.cfm.
[b]Locations are taken from *Hegerl et al*. [2011], except for the 20th century eruptions which are from the Global Volcanism Project. All eruptions are low-latitude except the 1912 Novarupta eruption.
[c]The year for NDJFMA refers to the year of the months January-April rather than November-December.
* Denotes eruptions also used for the 20th century analysis
** The 1912 eruption was used for the 20th century analysis, but was omitted for the 1400-2000 model one as it is a high latitude eruption.

large enough to have an effect on climate, whilst excluding high latitude eruptions. For reference the 1991 Pinatubo eruption had a peak global mean AOD of 0.16 and the 1963 Agung eruption 0.06 using this same data. 18 eruptions were selected through this method (Table 2.1). For the 20th century, the 5 largest eruptions as measured by global mean AOD were chosen (Figure 2.1a, Table 2.1). These are low latitude apart from Novarupta in 1912.

We do not take into account differences in seasonal timing of eruptions as [*Toohey et al*., 2011] find this makes little difference to all-sky short wave radiative flux for a Pinatubo-sized eruption (17Tg SO_2 injection), although it does make a difference for super-eruptions (700Tg SO_2). Figure 5.1 shows the observed spatial patterns of precipitation response to these 5 twentieth century eruptions to give an indication of whether averaging across them is justified. There are features that are fairly consistent across eruptions, e.g. drying in southern Africa and southern Europe in boreal winter, and in equatorial Africa in summer, although in other locations the response is either less consistent, or obscured by noise.

2.3.2 Epoch analysis

For each eruption and grid cell, precipitation anomalies for each of the 10 years following the eruption, or up until the next eruption if that occurred first, were calculated with respect to a 5 year pre-eruption mean [see also *Hegerl et al*., 2003, 2011; *Fischer et al*., 2007]. This minimizes the effect of trends or low frequency climate variability on our results, for example due to increasing greenhouse gases in the 'ALL' and 'NoLUSE' runs. We then averaged across all the eruptions for each grid cell before making spatial averages. We define "year 1" as the first season in question that starts after the eruption date. For example, if the eruption went off in June 1991, year 1 for NDJFMA would be 1992 (defined as the calendar year that January to April falls in rather than November and December), and year 1 for MJJASO would be 1992. Volcanic aerosols take a few months to spread out globally and reach their peak forcing [*Ammann et al*., 2003]. This is why we do not use MJJASO 1991 as year 1. "Year 0" would then be 1991 for both seasons, and year 2 1993. This means that in some cases year 0 contains some degree of volcanic forcing. Table 2.1 defines year 1 for both seasons for each eruption used. Where annual data are used for epoch analysis, the start month of year 1 is defined as occurring 3 complete months after the eruption date.

For Z07's data, which has variable spatial coverage through time, we set a requirement of at least 2 out of 5 years of data being present for calculating the pre-eruption mean for a given eruption before a grid cell was used. Requiring more years made little difference to results, whereas requiring only one made a much more noticeable difference (not shown). There

were only 2 years of data available for making the pre-eruption mean for the 1902 eruption since the dataset starts in 1900, so both of these years were required to be present (for GPCC, which starts in 1901, and for Z07 data in Figure 2.10 for comparability with GPCC, the pre-eruption mean for 1902 was augmented with data starting from 5 years *after* the eruption, when the land precipitation response will have decayed. When presenting spatial patterns data are sometimes expressed as percent of climatological precipitation, since otherwise some impact-relevant changes are overwhelmed by large changes in very wet regions in the tropics. In that case, percentages are calculated for a given grid cell as the anomaly divided by the grid point climatology for the full analysis period (i.e. 1400-2000) times 100. For spatial averages absolute values were used to avoid overemphasis of changes in very dry grid boxes. Where HadCM3 is compared to Z07's data for the 20th century eruptions, it was first regridded and masked to match the observational data coverage.

Significance of the average precipitation response to volcanic eruptions was assessed using a Monte Carlo technique. For seasonal data the analysis described above was repeated 1000 times using randomly selected years as year 0, and only results beyond 5-95% of these Monte Carlo results were considered significant. This meant choosing 5 random eruption years per cycle for the 20th century results, and 18 for the 1400-2000 model results and using these to conduct an epoch analysis (see for example *Fischer et al.* [2007], *Hegerl et al.* [2003, 2011]). This led to 1000 epoch analysis results based on random years, which were used to calculate confidence intervals for sampling variability by taking the 5^{th} and 95^{th} percentiles of the range of results. The same random year was not allowed to be chosen twice per cycle to replicate the observed distribution. When using annual data, a random eruption month had to be chosen as well as a year and so 10,000 cycles were run due to the increased number of possible random eruption dates.

When performing Monte Carlo analysis on the observed or masked model spatial patterns the situation is complicated by changing spatial data coverage through time. For a given grid cell and Monte Carlo cycle not every randomly selected eruption has data. The number with data can also change between Monte Carlo cycles. For each grid cell and post-eruption year (e.g. year1, year2 etc.) we use only random eruption combinations in which the number of

eruptions with data is the same as for the real eruptions, and discard combinations with less. If more random eruptions have data than was the case for the real eruptions we choose a random sub-selection of them. To make sure that enough useable eruption combinations are available for all grid cells, we performed 5000 cycles rather than 1000. We allowed overlap with the next eruption for the spatial patterns analysis. This is because the real eruptions are fairly well spaced, meaning that up until and including year 8 there is no overlap with subsequent eruptions. However, the random eruptions tend to be less well spaced, and truncating data at the time of the next eruption means that if all 5 real eruptions had data in year 8, it is less likely that all 5 random eruptions will, reducing the number of usable random eruption combinations for later years overall.

2.3.3. Removing the ENSO influence

The El Nino Southern Oscillation (ENSO) has a large influence on global precipitation patterns, tending to decrease precipitation over land and increase it over the ocean during El Nino years, and vice versa for La Nina years [*Gu et al*., 2007; *Gu and Adler*, 2011; *Liu et al.*, 2012]. Regressing out its influence enables the volcanic precipitation response to be seen more clearly and avoids confusing it with ENSO variability. This is particularly the case for observational data where there are few eruptions to average over, and where the most recent three eruptions were followed by El Nino events, albeit a weak one for the 1963 Agung eruption. For results based on the model ensemble mean, the large number of ensemble members, each with different natural variability, overcomes this problem as does the large number of eruptions used for the 1400-2000 results. Nevertheless we removed the ENSO influence from the model when performing a detection analysis for consistency (Section 2.4.2). There has been debate in the literature about whether or not volcanic eruptions can trigger El Nino events (see discussion in Section 1.2.2). We find no evidence of an El Nino response to eruptions in our HadCM3 runs. Because of this and the findings of *Self et al*. [1997] and *Chen et al*. [2004] detailed in Section 1.2.2, we ignore the possibility of a link between volcanic eruptions and El Nino events in this study.

We used the cold tongue index (CTI) as a measure of ENSO. This is defined as the average sea surface temperature (SST) anomaly over the 6°N-6°S, 180-90°W region in the central-eastern pacific, minus the global mean SST anomaly. Due to this subtraction, the CTI index should be less affected by a general cooling of global SSTs following eruptions compared to Nino 3.4 for example; nor will it be affected by global warming. CTI data for the 20th century were obtained from the Joint Institute for the Study of the Atmosphere and Ocean (JISAO) at the University of Washington (available at http://www.jisao.washington.edu/data/cti/). This index has been used in other studies of interannual and decadal climate variability, e.g. *Zhang et al*. [1997]; *Kenyon and Hegerl* [2008, 2010]; and yields similar results to using Nino 3.4 [*Kenyon and Hegerl*, 2008].

For each grid cell and season, a regression coefficient for precipitation on CTI was calculated, using detrended time series of half year values for non-volcanically influenced years (i.e. not year 0 to 5 following an eruption). These coefficients were then used to calculate the ENSO-related precipitation anomalies for their respective grid cells, which were then subtracted from the actual precipitation to arrive at non-ENSO related precipitation**.** Removing the ENSO influence decreases the standard deviation of the observed global mean annual time series of land precipitation from 0.062 mm day^{-1} to 0.045 mm day^{-1} (Figure 2.8). We also removed the ENSO influence from the twentieth century model results and found that it made very little difference to the ensemble mean (not shown). We therefore present only the raw model results without removing the ENSO influence, with the exception of the detection analysis in Figure 2.12. For the latter, ENSO-precipitation regression coefficients were defined for each ensemble member separately and the ENSO influence was removed from each member before averaging across the ensemble. The ENSO-related precipitation patterns in the model and observations were very similar, except that the area of increased precipitation associated with El Nino events in NDJFMA extends too far into the Western Pacific in the model, in agreement with the findings of *Joseph and Nigam*, [2006]. HadCM3 simulates the amplitude, frequency and seasonal phase locking of ENSO variability well, whilst its SST footprint is reasonable but extends too far westwards into the West Pacific warm pool [*Collins et al*. 2001; *Joseph and Nigam*, 2006].

2.4 Results

2.4.1 Climate model results

A clear decrease in global mean precipitation can be seen following eruptions in the HadCM3 runs, both in the ensemble mean and ensemble members, the size of which appears to be related to the magnitude of the volcanic forcing (Figure 2.1b). A clear, highly significant reduction can also be seen when averaging across these 18 eruptions, both for the global mean (Figure 2.2a) and when land and ocean are examined separately (Figure 2.2b and 2c respectively), in agreement with previous studies [e.g. *Robock and Liu*, 1994; *Trenberth and Dai*, 2007; *Schneider et al*., 2009; *Gu et al.*, 2007; *Gu and Adler*, 2011]. This reduction is more rapid and of greater magnitude over land than ocean, the ensemble mean reaching a minimum of -0.05 mm day^{-1} over land in year 1 (which is -2.3% of the global land pre-eruption mean) and remaining significant until year 3, compared to a minimum of around -0.035 mm day^{-1} (-1.1%) in year 3 for the ocean, remaining significant until year 7.

We compared the timing of the global precipitation and near surface air temperature response to eruptions over land and ocean to gain insight into the difference in timing of the precipitation response (Figure 2.3). Findings were consistent when the tropics were examined separately (not shown). Over ocean, precipitation and temperature decrease on a similar timescale to each other. This is consistent with the model results of *Joseph and Zeng* [2011] who find that evaporation lags SSTs by 1 month and that precipitation responds one month after that, suggesting that precipitation changes are being driven by changes in SSTs. In contrast, over land we find that precipitation responds before temperature, also in agreement with *Joseph and Zeng* [2011]. We plot the anomaly in land minus ocean temperature (Figure 2.3) and find that it correlates reasonably well with land precipitation, suggesting that weakening of monsoon circulations may be involved [e.g. *Cao et al*., 2012, *Peng et al*., 2010]. We also plot aerosol optical depth (Figure 2.3), which matches the timescale of the land precipitation response very well, implying also a directly forced component. In contrast, *Gu and Adler* [2011] found that precipitation led temperature over both land and ocean, based on an analysis of a merged satellite and gauge dataset (GPCP

[*Adler et al*., 2003]) for the Pinatubo and El Chichon eruptions. This, however, might be affected by sampling variability.

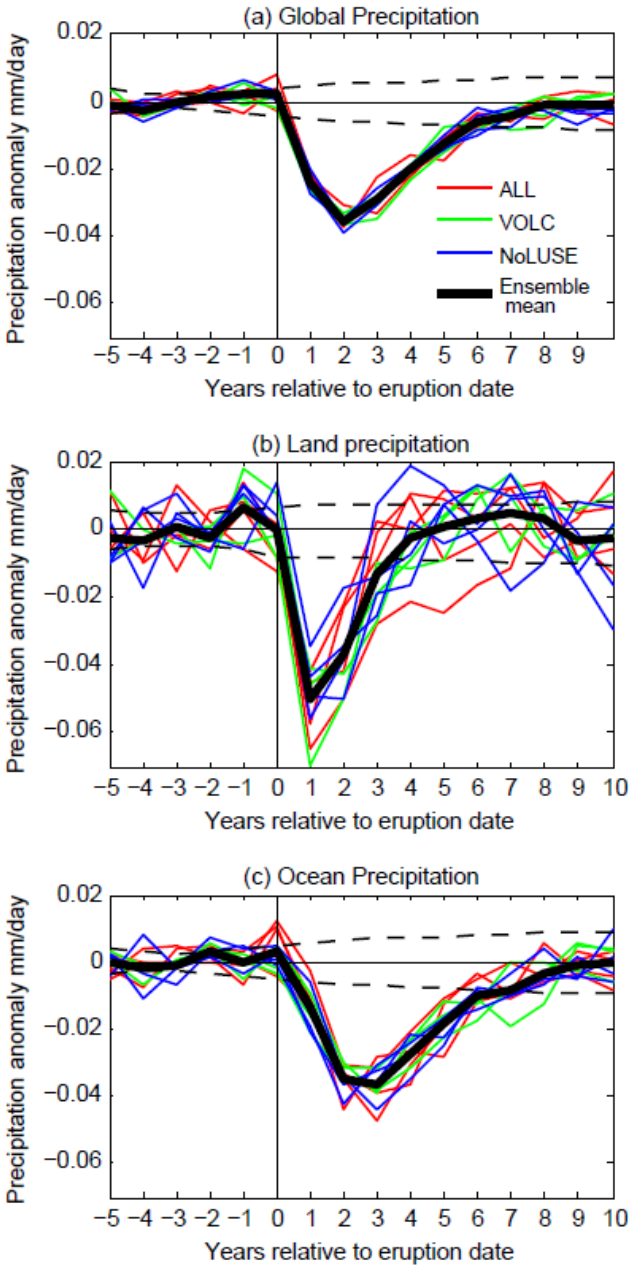

Figure 2.2. Average precipitation response to 18 large low latitude volcanic eruptions in HadCM3, global mean (a), global land areas (b) and global ocean (c). Thick black line is the ensemble mean response, colored lines are ensemble members (red- "ALL" ensemble, green- "VOLC" and blue- "NoLUSE". Black dashed lines denote the 5-95% confidence limits for the ensemble mean based on a Monte Carlo Technique. Vertical black line denotes timing of eruptions.

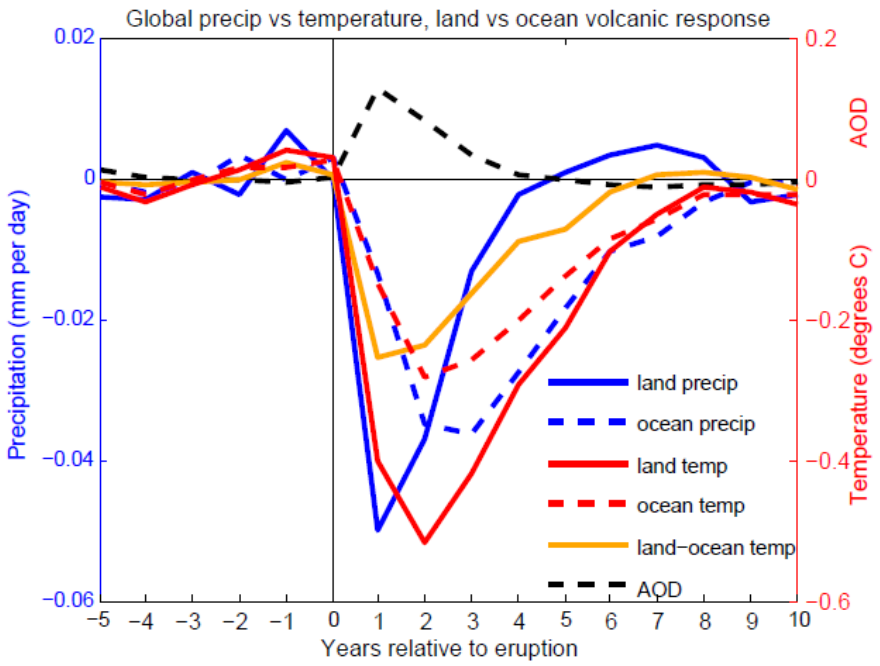

Figure 2.3. Ensemble mean average global precipitation (blue) and 1.5m air temperature (red) response to 18 eruptions in HadCM3 over land (solid) and ocean (dashed). Orange line is the anomaly in land minus ocean temperature. Black dashed line is global mean AOD from *Crowley et al.*, [2008].

Figure 2.4 shows the ensemble mean spatial patterns of precipitation response to 18 eruptions in the 4 cold and warm seasons following the eruptions. The patterns are broadly the opposite of, but physically consistent with projections under climate change in which the wet regions get wetter and the dry regions get drier with warming [*Held and Soden*, 2006; *Trenberth*, 2011; see also *Meehl et al.*, 2007 Figure 10.9 and 10.12]. They generally agree with the volcanic response found in other recent modeling studies [e.g., *Schneider et al*., 2009; *Joseph and Zeng*, 2011]. The main areas exhibiting drying are the extratropics and the monsoon regions in their respective warm season, with the exception of the monsoon regions of India and Papua New Guinea, which get wetter. An increase in rainfall is seen over northern Africa, the Middle East, the Southern Indian Ocean and the Atlantic subtropics. These patterns shift northwards in MJJASO relative to NDJFMA, following the passage of the overhead sun. This monsoon response and seasonal shift agree with the model results of *Joseph and Zeng* [2011]. The main features of the response persist until year 3 or 4 although details of the response vary from year to year. The ocean response generally takes until year

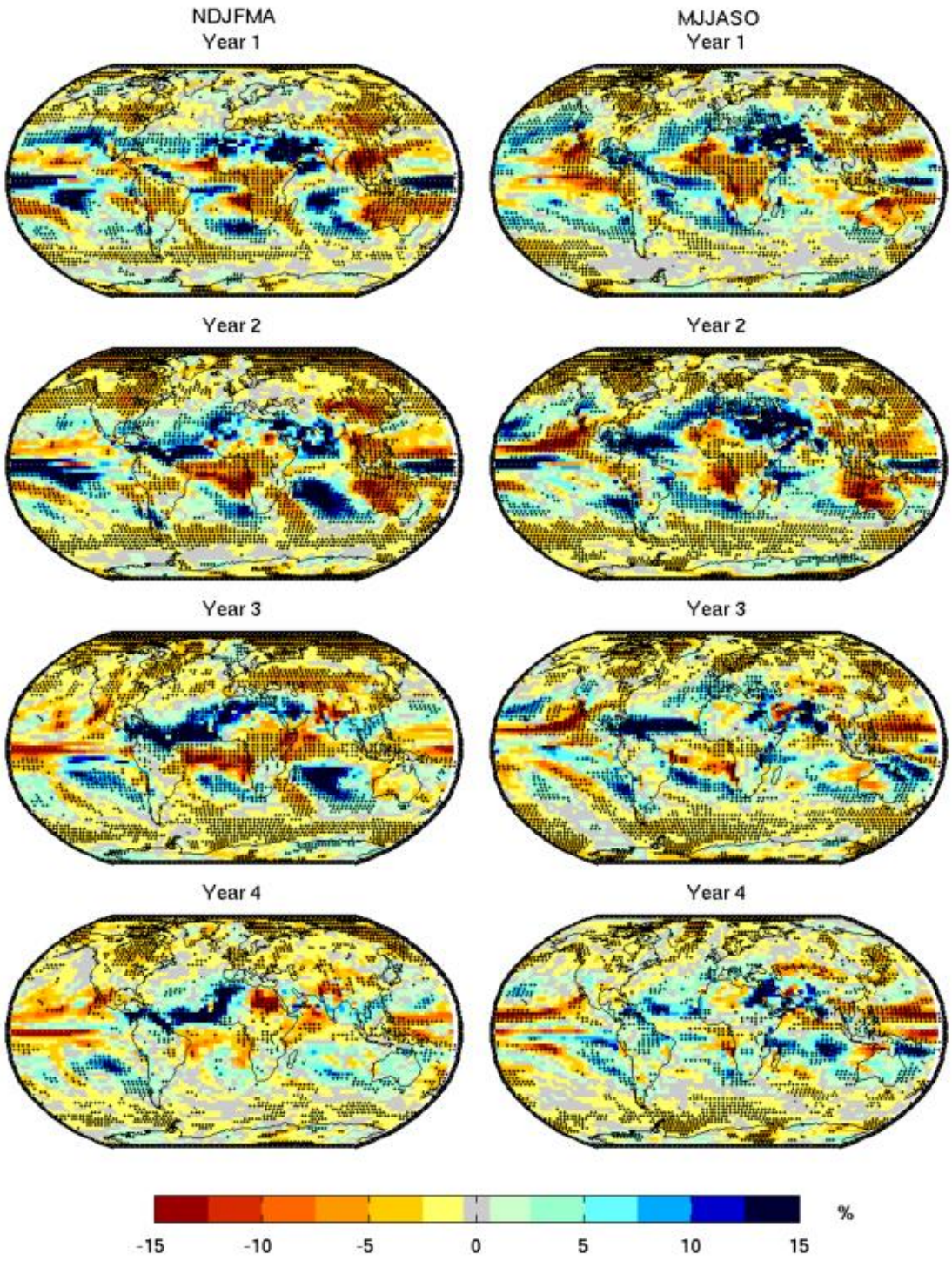

Figure 2.4. HadCM3 ensemble mean precipitation response to 18 eruptions for four years following the eruptions, expressed as percentage changes relative to grid cell climatology. Dots indicate significance at the 90 % level. Small changes are shown in grey.

2 to fully establish (see also Figure 2.2) and then remains more stable over time, with the exception of the Pacific. There is little evidence of a positive NAO pattern of precipitation in the boreal winter following the eruptions, consistent with the findings of *Tett et al*. [2007]. This lack of dynamic response also occurs in CMIP5 models, and its cause is presently not well understood [*Driscoll et al*., 2012]. Table 2.2 shows the number of grid cells exhibiting a significant response for each year and season in Figure 2.4 compared to that expected by chance. The percentage of grid cells experiencing a significant drying is well above what we would expect by chance until around year 6. There are also more grid cells than expected that get significantly wetter, but to a lesser extent and only until year 3 or 4.

Table 2.2 Percentage of grid cells showing a significant precipitation change at each year following eruptions in the HadCM3 1400-2000 runs[a]

		yr0	yr1	yr2	yr3	yr4	yr5	yr6	yr7	yr8	yr9	yr10
cold season	drier	3.0	**23.7**	**38.2**	**32.8**	**20.9**	**13.4**	6.6	**11.3**	4.3	6.7	6.0
	wetter	5.7	**10.8**	9.8	9.5	5.3	3.7	3.2	4.3	4.0	2.6	3.9
warm season	drier	4.4	**25.4**	**36.1**	**29.7**	**19.4**	**13.3**	**11.4**	7.2	4.2	4.1	8.3
	wetter	5.4	**13.2**	**13.8**	**10.4**	7.8	3.5	5.6	4.6	3.0	3.5	5.3

[a] Grid cells that get significantly "drier" are those with anomalies less than the 5th percentile derived from a Monte Carlo technique, grid cells that get significantly "wetter" are greater than the 95th percentile. 5% of grid cells should be significantly dry or wet by chance. Values greater than 10 are in bold.

Previous studies find shifts in the position of the Intertropical Convergence Zone (ITCZ) in response to volcanic forcing. Since hemispherically symmetric volcanic forcing causes a greater reduction in temperature in the summer hemisphere relative to the winter one, the ITCZ should not migrate as far polewards as it normally would [*Schneider et al*., 2009; *Yoshimori and Broccoli*, 2008; *Stenchikov*, pers. com., 2012]. However, the ITCZ also shifts away from the hemisphere with the greater concentration of aerosols in response to asymmetric forcing [e.g. *Haywood et al*., 2013]. There is some evidence of a shift in the position of the ITCZ in Figure 2.4. For example in NDJFMA there is a northward shift in the Atlantic in years 2-4 and a northward shift of the South Pacific Convergence zone in years 1-2. Over the Indian Ocean there appears to be a southward shift. In MJJASO there is a southward shift over the Pacific in year 2 and over the Atlantic in year 1. These shifts for year 2 are clearer in Figure 2.5e-f. Since these results are the average of multiple eruptions whose aerosol clouds are biased towards different hemispheres, the ITCZ shifts will be

confused. ITCZ shifts in response to individual eruptions are explored in Chapter 3. Overall, however, the precipitation response patterns appear to be better explained by changes in the Hadley circulation and a weakening of the monsoon circulations.

To explore this further we split the tropical and subtropical region into climatologically wet and dry regions which has been shown to help capture precipitation changes due to radiative forcing, e.g. *Allan et al.* [2010], *Liu et al.* [2012] and *Chou et al.* [2013]. A cut-off of 40° latitude was chosen between the tropics/subtropics and extratropics (41.25° for the 1400-2000 model results) .This choice was based on the edge of the subtropical regions that get wetter following eruptions in Figure 2.4, but many of the model results are robust to using narrower or wider tropical/subtropical band. (We hereafter refer to this 40°N-40°S band as the "tropics", although technically the tropics are limited to 23.3°N/S). The wet regions were defined as the climatologically wettest third of grid cells within this tropical band, whilst the dry regions were defined as the remaining two thirds. The driest and middle third were combined since they behaved similarly. The thirds were defined according to the ensemble mean climatology for the model results, and were defined separately for each season and after any land or ocean masking, or masking according to observational data coverage. This method was chosen as opposed to a set precipitation criterion since it can be applied to different datasets and the model whose climatological precipitation may differ in magnitude, or whose circulation patterns may differ from the observations. Our results are robust to using different criteria. Furthermore, when grid cells were classified as wet or dry regions based on individual ensemble members rather than the ensemble mean climatology, only 1-1.5% of grid cells changed between wet and dry for the 1400-2000 results, and 5% for the masked twentieth century results. We chose not to move regions that are considered wet and dry between analysis years as *Allan et al*. [2010] do as our analysis focuses on year-to-year responses, which are quite noisy, particularly when based on observations.

The wet regions show a clear and highly significant precipitation decrease for both seasons, and both over land and ocean, of around 0.16-0.18 mm day^{-1} (Figure 2.5). The land response is more rapid than the ocean response, peaking in year 1 rather than year 2, in agreement with the results for the global mean. In contrast, the dry regions exhibit a smaller but

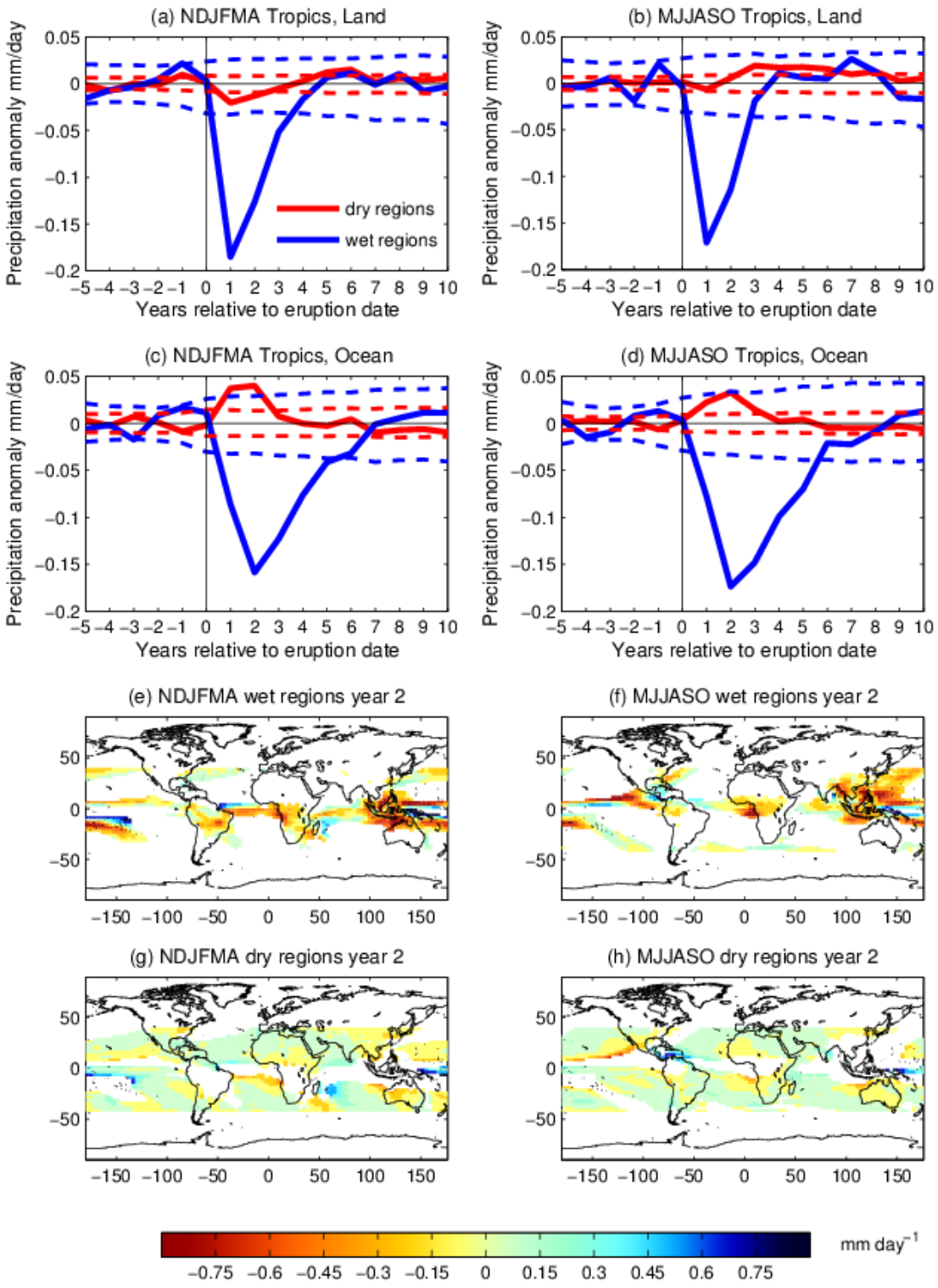

Figure 2.5 (a-d) HadCM3 ensemble mean tropical (40°N-40°S) precipitation response averaged across 18 eruptions. Blue line is for the climatologically wet regions, red line the climatologically dry regions. Left column NDJFMA, right column MJJASO, top row is land precipitation, bottom row is ocean precipitation. Dashed lines indicate the 5-95% confidence limits, blue for the wet regions, red for the dry regions. (e-h) Ensemble mean spatial precipitation patterns for year 2 following the same 18 eruptions, masked to show only the climatologically wet regions (e,f), and dry regions (g,h), NDJFMA is on the left and MJJASO on the right. Units are mm per day.

significant increase in precipitation of 0.04 mm day^{-1} over the ocean, which is more short-lived than the wet regions response. Over land the dry regions experience a small, but significant, decrease for NDJFMA and a small but insignificant decrease followed by a prolonged and significant increase for MJJASO. The similarity between the two seasons despite different spatial response patterns (Fig 5e-h) suggests that this wet-dry split captures the response well. Figure 2.5e-h shows the spatial patterns for year 2. The areas experiencing drying generally fit very well with the climatologically wet regions (Figure 2.5e-f). The ocean precipitation drying response over these wet regions persists until year 4 and seems to come from the ITCZ and South Pacific Convergence Zone. The climatologically dry regions are more spatially heterogeneous in their response (Figure 2.5g-h). Potential shifts in the position of the ITCZ and South Pacific Convergence zone can be seen as described above, leading to a visible divergence from the wet get drier paradigm, although this only affects a small fraction of the area. Results mostly seem to suggest changes in monsoon and Hadley circulations, although the more noisy response over dry land areas could be due to limited moisture availability.

A significant decrease in precipitation can be seen for the extratropics, for both seasons, and for both land and ocean (Figure 2.6). However, the Southern Hemisphere extratropical land response is less clear, perhaps due to noise in this small spatial area. Apart from the southern hemisphere land, the precipitation response generally peaks in year 2 and remains significant until year 5 or 6. It is larger over ocean than over land with no obvious difference in timing between the two, in contrast to the results for the global mean and the tropics.

Finally we examine how much annual global mean precipitation changes for a given change in temperature in response to volcanic forcing, greenhouse gases and due to internal variability (Figure 2.7). For this we used single forcing runs, i.e. the VOLC ensemble (3 runs, forced only with volcanic aerosols, other forcings are kept constant at pre-industrial levels), and greenhouse gas only runs (GHG, 4 simulations), together with the 1200 year control run in which all forcings are held constant at 9th century levels (see *Schurer et al*. [2014] for more detail). For the VOLC runs we plot the ensemble mean global precipitation anomaly for each eruption against the corresponding temperature anomaly relative to the

global-scale 5-year pre-eruption mean, separately for each of the 4 years following the eruptions. The temperature-precipitation relationship associated with interannual internal variability is shown using data from the control run (grey crosses). For the effect of greenhouse gases we plot the precipitation difference for the 1980-1999 mean minus 1840-1859 mean for each run, against the equivalent for temperature, and plot a line from the ensemble mean result to zero.

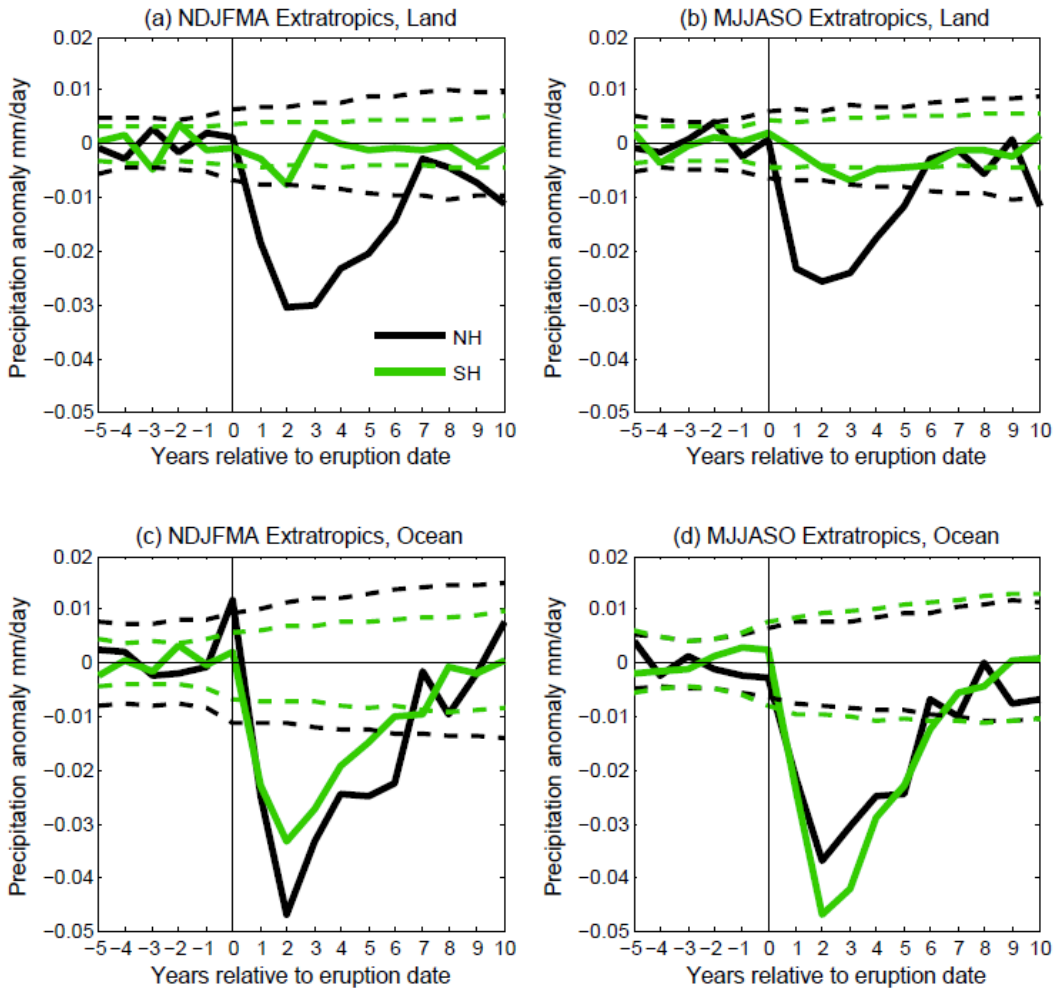

Figure 2.6. HadCM3 ensemble mean extratropical (40-90°) precipitation response averaged across 18 eruptions. Left column NDJFMA, right column MJJASO, top row is land precipitation, bottom row is ocean precipitation. Black line is the Northern Hemisphere, green line is the Southern Hemisphere. Dashed lines indicate the 5-95% confidence limits, black for the Northern Hemisphere, green for the Southern Hemisphere.

The resulting slopes are 3.3 % K^{-1} for volcanic years in the VOLC runs compared to 2.7 % K^{-1} for non-volcanic years, 2.0 % K^{-1} for internal variability in the control run and 1.5 % K^{-1} for greenhouse gases. This greater sensitivity to shortwave forcing compared to greenhouse gases is consistent with other studies [e.g. *Liu et al*., 2013; *O'Gorman et al*., 2012; *Cao et al*., 2012; *Bala et al*., 2008; *Allen and Ingram*, 2002; *Yoshimori and Broccoli*, 2008], although this is the first study to focus specifically on volcanic forcing. Global precipitation is linked to the amount of radiative cooling of the atmosphere to space, and both increase with warming. However, CO_2 also reduces the ability of the atmosphere to radiate long-wave radiation to space, reducing the increase in precipitation with temperature [*O'Gorman et al*., 2012; *Allen and Ingram*, 2002; *Lambert and Allen*, 2009]. Volcanic aerosols have a much smaller long-wave effect, whilst their influence is felt most strongly at the surface through reduced shortwave related heating and evaporation. Therefore precipitation is more sensitive to changes in volcanic aerosols than CO_2 [*Bala et al*., 2008; *Lambert and Allen*, 2009; *Allen and Ingram*, 2002]. The slope for internal variability in the control run is predominantly due to ENSO variability [see also *Allan and Soden*, 2008].

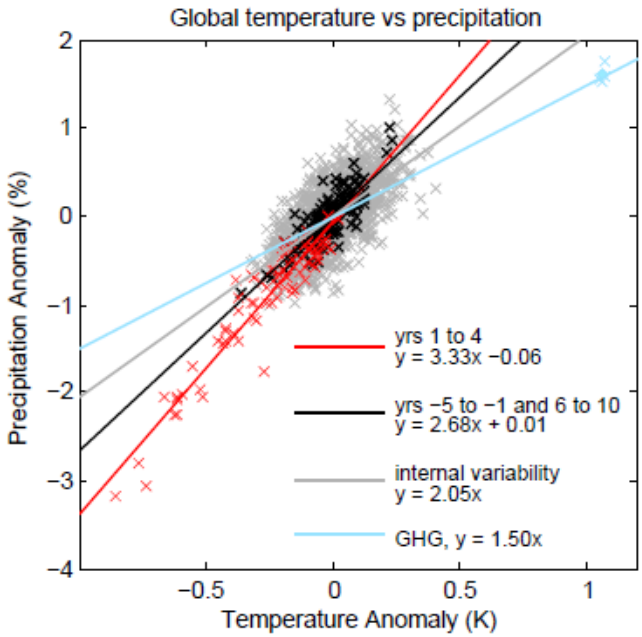

Figure 2.7: Global mean annual mean temperature versus precipitation anomalies for volcanically influenced (red) and non-volcanically influenced (black) years for the ensemble mean of volcanic only driven simulations of the last millennium. Grey crosses show interannual variability for the control run, and blue crosses the 1980-1999 mean minus 1840-1859 from the greenhouse gas only runs, the blue line connects the ensemble mean change (blue diamond) to zero.

2.4.2 Twentieth Century Results

Having identified the main features of the precipitation response in HadCM3 with full data coverage and many strong eruptions, we now turn our attention to the observations. We will examine whether the precipitation response is identifiable given the larger amount of noise associated with fewer eruptions, a single representation of observed change rather than an ensemble as in the model results, and limited spatial coverage over land regions only. We also examine whether model and data are consistent. All 11 HadCM3 runs are regridded and masked according to observational data coverage, in order to assess to what extent they agree with the observational findings.

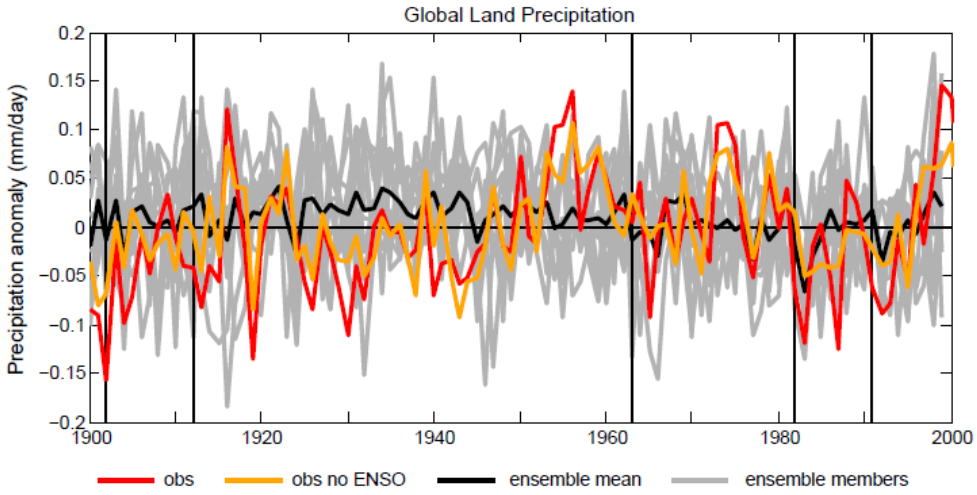

Figure 2.8. Time series of observed and modeled global mean precipitation from 1900-2000 (anomalies with respect to the 1961-1990 climatology). Red line indicates the observations, orange line the observations with ENSO influenced linearly regressed out, thick black line is the ensemble mean. Ensemble members (all 11) are shown in grey and eruptions dates are indicated by vertical black lines.

Figure 2.8 compares the observed and modeled time series of twentieth century global mean land precipitation, with eruption dates denoted by vertical black lines. The volcanic response is less clear than it was in Figure 2.1b, although a reduction in precipitation can be seen in the ensemble mean following the 1963, 1982 and 1991 eruptions, and is also reflected in a downward shift of the ensemble envelope. A reduction can also be seen in the observations following the 1982 and 1991 eruptions. The magnitude of the observed response better matches the ensemble mean once the ENSO influence is removed (Figure 2.8). The delayed decrease after the 1963 eruption in the observations largely disappears once ENSO is

removed, whilst the reduction around 1912 coincides better with the eruption date after ENSO removal.

When the precipitation response is averaged across all 5 twentieth century eruptions, a significant decrease in global mean land precipitation can be seen for both seasons in both the observations and the model ensemble mean when masked to replicate the observational coverage (Figure 2.9 a, b). Whilst the timescale of this response is similar between model and observations, the observed response is larger than the ensemble mean reaching 0.12 mm day^{-1} for NDJFMA compared to 0.03 mm day^{-1} for the model and 0.07 and 0.04 mm day^{-1} respectively for MJJASO. In NDJFMA the model underestimate is significant, with the observed response lying outside the ensemble envelope at 2.94 ensemble member standard deviations away from the ensemble mean in year 1. Removing the ENSO influence brings the observed response closer to the ensemble mean, particularly for MJJASO, although the latter is no longer significant. In NDJFMA, whilst the observed response in year 1 is much closer to the ensemble mean after removing ENSO, in year 2 it is still significantly greater than the model response at 2.17 standard deviations away from the ensemble mean, with ENSO also removed from the model (not shown). El Nino events are associated with decreased precipitation over land [e.g. *Gu et al*., 2007; *Liu et al*., 2012]. Therefore given the coincidence of 3 of these 5 eruptions with El Nino events, we would expect removing its influence to decrease the apparent size of the volcanic response as seen in our results. We also removed the ENSO influence for all the model results in Figure 2.9 (not shown), but this made very little difference to the ensemble mean, due to the large number of ensemble members with different ENSO variability.

Agreement between the model and observations is poor for the northern hemisphere extratropical land masses (Figure 2.9c, d) (the Southern Hemisphere extratropics are not shown due to poor data coverage). The observations exhibit a significant peak in precipitation in year 0 for MJJASO (further analysis could not pin this to an individual event or cause, suggesting it to be due to spurious sampling variability), and a lesser insignificant one in year 1 for NDJFMA, both of which remain once the ENSO influence has been removed. Some of the observed peak in year 1 NDJFMA seems to originate from a positive

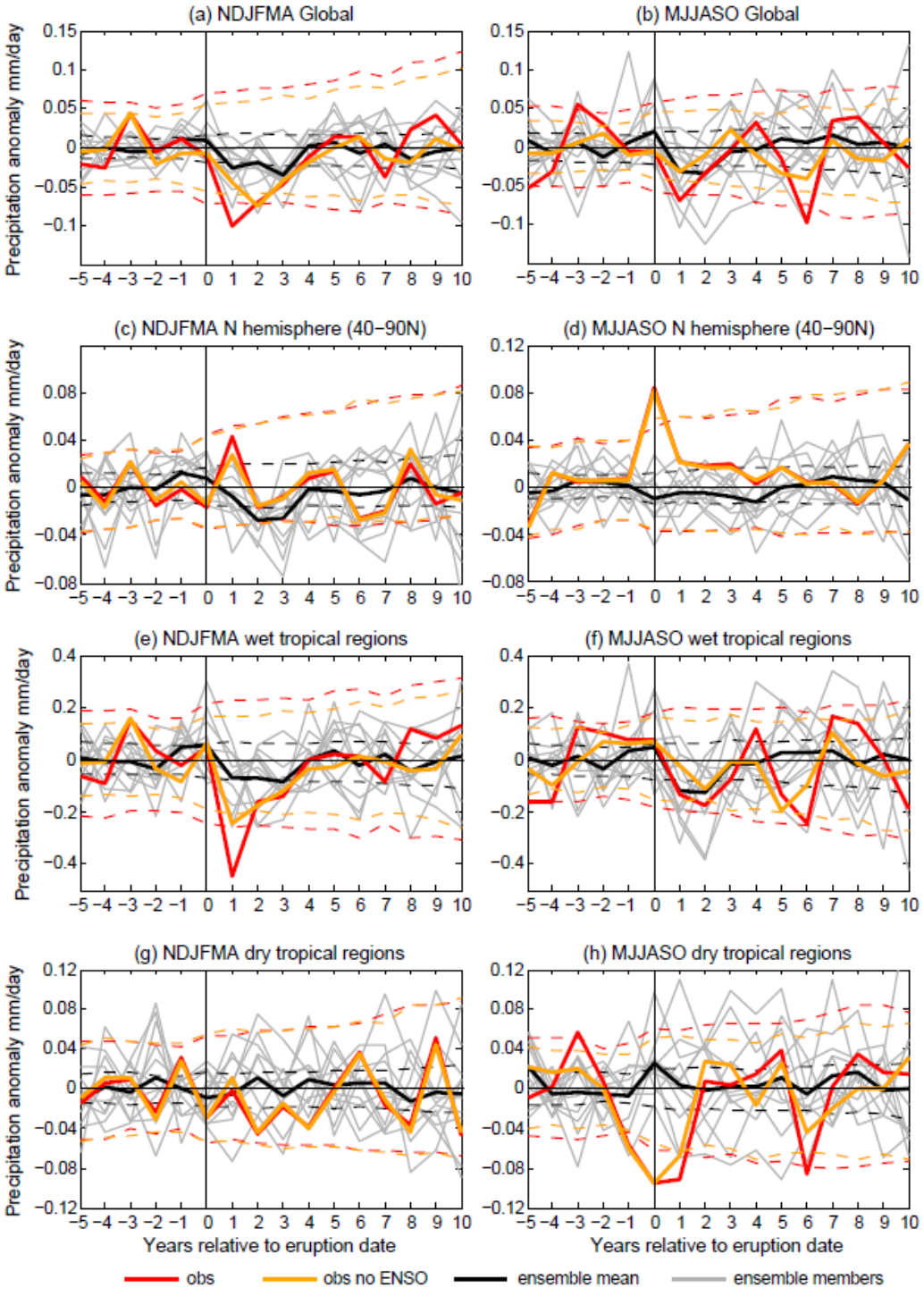

Figure 2.9 Average land precipitation response to 5 eruptions for (a,b) the globe, (c,d) the Northern Hemisphere extratropics (40-90°N), (e,f) climatologically wet tropical regions, and (g,h) climatologically dry tropical regions. Observations are shown in red, observations with ENSO influence linearly regressed out in orange, HadCM3 ensemble mean in black and ensemble members in grey. Vertical black line indicates timing of eruptions. Dashed lines are 5-95% confidence intervals: red applies to the observations, orange for the observations with ENSO influence removed, and black to the ensemble mean.

NAO pattern over Europe, characterized by wetter than average conditions in Northern Europe and drier conditions in southern Europe, which is present for 3 of 5 eruptions (see also Figure 2.11). In contrast, the model ensemble mean shows a significant drying for years 2-3 in NDJFMA and an insignificant drying for years 0-4 in MJJASO and no visible NAO response consistent with findings for CMIP5 models [e.g. *Driscoll et al*., 2012].

The results for the entire tropical land masses (not shown) are very similar to but larger than those for the global land mean, suggesting that the global land mean largely reflects the precipitation changes over the tropics. The tropical land masses, in turn, seem to be mostly reflecting the wet tropical land regions, where changes are of larger magnitude still (Figure 2.9 e, f). The observed tropical wet land regions decrease in NDJFMA is highly significant and lies outside the ensemble envelope, at 3.56 ensemble member standard deviations from the ensemble mean. When repeated as percentage changes to account for potential differences in climatological precipitation, the observations are still 2.3 standard deviations away from the ensemble mean (not shown). This drying signal largely comes from the 1991, 1982 and to a lesser extent 1902 eruptions. The 1982 and 1991 eruptions have more weight due to better data coverage and are again coincident with El Nino, exaggerating the drying signal over land [e.g. *Gu et al*., 2007; *Liu et al*., 2012], but even with the ENSO influence removed the observed response remains significant and 2.04 standard deviations away from the ensemble mean. Investigating the cause of this discrepancy is beyond the scope of this paper, but possibilities include model errors in ocean heat uptake, climatology, SST response, monsoon responses or other circulation responses to eruptions. Other possibilities include larger observed variability due to station data being sparse and recording point values rather than area ones, observational errors or incomplete removal of the ENSO signal. In MJJASO the observed decrease in the wet tropical land regions is not significant, but matches the size of the ensemble mean response better. However, there is a second larger dip in years 5-6, occurring after we expect the volcanic response to have decayed. This seems to be partly accounted for by ENSO variability in year 6. The modeled wet land regions response is significant for both seasons. The dry land region response in NDJFMA is not

significant for either the observations or ensemble mean (Figure 2.9g, h), whilst in MJJASO the observations appear very noisy.

Observational results are broadly similar if GPCC data are used with their complete land coverage (Figure 2.10), and are very similar for the two observational datasets if only points where both have data are used (not shown). The main difference is that the agreement in magnitude between the masked model and observations for the global, tropical and tropical wet regions in MJJASO response is worse when GPCC is compared to HadCM3 using the full land coverage of GPCC (see Figure 2.10b for the global mean results); the observed response is larger than in Z07's data, particularly for the wet tropics (not shown), and the model response is smaller using the larger area coverage. The degraded agreement with GPCC is possibly, at least in part, due to interpolation of sparsely data covered regions in GPCC. Results for NDJFMA are more similar between both datasets (Figure 2.10a).

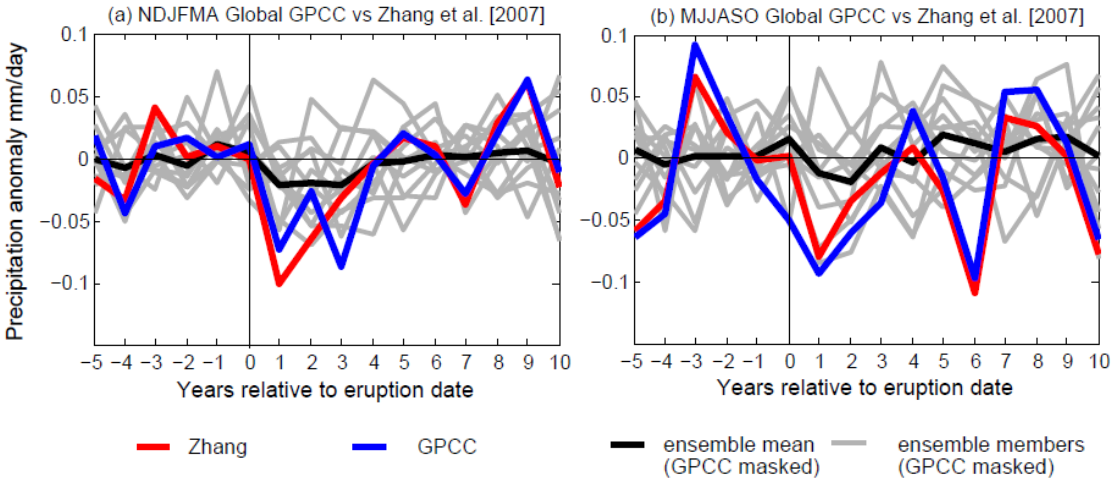

Figure 2.10. Average global land precipitation response to 5 eruptions in 2 observational datasets with their original coverage, *Zhang et al.* [2007] (red), GPCC (blue), compared to HadCM3 masked according to the GPCC coverage, ensemble mean (black) and ensemble members (grey), for NDJFMA (a) and MJJASO (b).

We also repeated the 20th century analysis excluding the 1912 high latitude Novarupta eruption, and excluding both early 20th century eruptions, 1902 and 1912, when data coverage was poor. This did not make much difference to the observational results. Adding the two next biggest eruptions to the existing five (1907 and 1974), made the results noisier,

as these were quite small eruptions in comparison. The masked model results were broadly the same whichever eruptions were used.

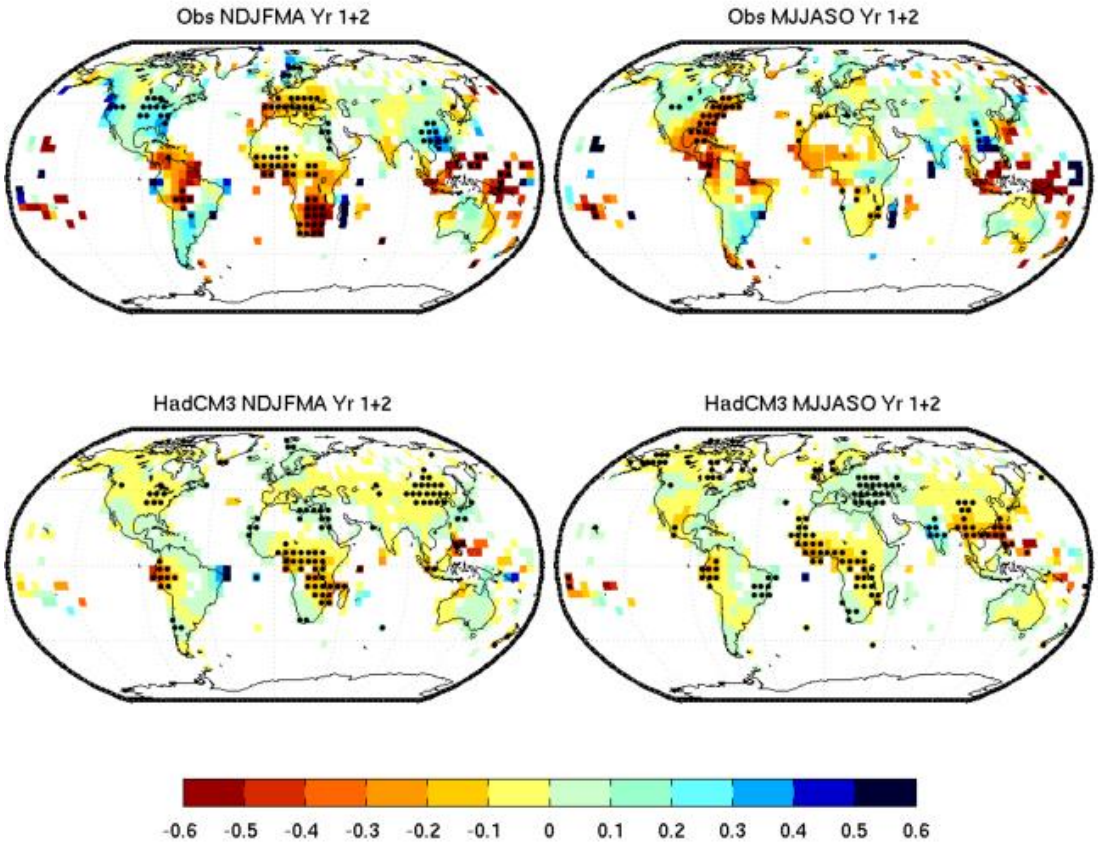

Figure 2.11. Average precipitation response to 5 eruptions for years 1 and 2 combined (mm per day). Observations (*Zhang et al.* [2007]) are shown on top, and the HadCM3 ensemble mean, masked according to the observational data coverage on the bottom. Stipples indicate significance at the 90% level (see also Table 2.3). Both the observations and model results are spatially smoothed (see text).

Figure 2.11 shows the average spatial patterns for these twentieth century eruptions for Z07's data and the masked model ensemble mean. Both are smoothed by a 5 point filter in which the central grid cell is given twice the weight of each of the adjacent four. Our observed patterns match the observational results of *Trenberth and Dai* [2007] and *Joseph and Zeng* [2011] fairly well, except that we do not see their drying signal over S.E Asia. The number of grid cells experiencing a significant change in precipitation for both the observations and the model for the 20th century eruptions is fairly close to that expected by chance (Table 2.3), although slightly higher in year 1 and years 1 and 2 combined,

suggesting that the spatial patterns are rather noisy. The patterns in Z07's data are of much greater amplitude than those in HadCM3, at least in part due to the cancellation of noise in the ensemble mean. The monsoon regions response is less clear in both the masked model and observations than it was for the 18 eruptions model case. There appears to be a southward shift of the ITCZ over Africa in MJJASO in year 1 (not shown), in agreement with the findings of *Stenchikov* [pers. com, 2012] over the same region in summer. This is not seen in the model data for the 20th century eruptions, nor for the 18 large eruptions. There is also a positive NAO-like pattern in year 1 in NDJFMA in the observations, and a similar but much weaker insignificant pattern in the model. The observed spatial patterns look very similar if GPCC is used instead of Z07's data.

Table 2.3 As for Table 2.2 but for *Zhang et al*. [2007]'s observational data and the HadCM3 ensemble mean masked according to the observational coverage for the twentieth century.

Obs		yrs1+2	yr0	yr1	yr2	yr3	yr4	yr5	yr6	yr7	yr8	yr9	yr10
cold season	dry	9.7	4.5	**13.2**	4.6	4.6	6.1	3.8	4.2	2.9	6.0	4.3	8.2
	wet	5.3	4.2	**10.8**	2.5	4.3	5.4	2.5	2.6	1.5	4.0	5.0	7.1
warm season	dry	5.0	3.8	5.3	5.3	3.8	2.8	3.5	5.3	3.5	2.5	4.8	4.9
	wet	1.7	7.2	2.4	3.5	3.5	3.5	3.3	3.9	4.8	2.8	5.2	4.4

HadCM3		yrs1+2	yr0	yr1	yr2	yr3	yr4	yr5	yr6	yr7	yr8	yr9	yr10
cold season	dry	**11.3**	7.5	**10.2**	9.1	4.0	4.3	5.3	5.3	3.1	1.8	2.9	7.1
	wet	4.2	8.1	4.6	5.2	1.8	3.3	3.6	4.0	4.2	2.2	4.6	8.8
warm season	dry	**14.3**	7.5	**12.3**	8.2	5.7	4.7	2.1	4.1	3.1	2.4	1.7	2.1
	wet	6.3	**11.8**	7.8	3.2	4.1	2.8	4.2	4.3	5.6	6.2	3.8	5.6

As the analysis up to this point uses multiple significance tests, some of which would be expected to detect a change by chance, we performed a fingerprint analysis to determine whether the overall response is significant and whether model and data are consistent. The volcanic response in precipitation has been so far only detected by *Gillett et al*. [2004] for global land precipitation. The model they used (NCAR PCM) significantly underestimated the observed response. We build on this study by incorporating information on the spatial response patterns, sub-dividing the global land response into the northern hemisphere

extratropics, tropical wet and dry regions. (We exclude the southern hemisphere extratropics due to poor spatial data coverage). We also better represent the time response of volcanic forcing. For each year following the eruptions we regress a 3 element vector of the observed response, averaged across all 5 eruptions, onto the equivalent for observationally masked model ensemble mean (the 3 elements correspond to the 3 regions above, whose response is that shown in Figure 2.9). This yields a scaling factor describing whether the modeled response is bigger or smaller than that in the observations. We test whether or not scaling factors are significantly different from that expected by chance by conducting Monte Carlo analysis, in which the analysis is repeated 1000 times choosing random eruption years for the observations and regressing the resulting fingerprint against the model fingerprint, as described in Section 2.3.2. We might expect significant results in years 1-2 and maybe 3 based on the model results for land precipitation (see Figures 2.2b, 2.5a,b). We also repeated the analysis regressing results for each ensemble member separately against the ensemble mean of the remaining ensemble members to assess whether the observations were consistent with the ensemble members. In order to maximize the power of the detection approach, we also combined years 1 and 2, since this is when we expect the clearest response based on the model results, by using a 6 (rather than 3) element vector for the regression.

The volcanic response is detectable in NDJFMA in year 1 and years 1 and 2 combined at the 99% level using a one-sided test (Figure 2.12). It is marginally detectable in MJJASO at the 90% level in year 2 and years 1 and 2 combined. This is a greater number of significant results than expected by chance, and shows that there is indeed a significant volcanic influence on precipitation at large scales, even though the response is hard to detect at a grid point scale. The large scaling factor indicates that the model underestimates the magnitude of the precipitation response in year 1 and years 1 and 2 combined in NDJFMA, and to a lesser extent in years 2 and 3. However, some individual ensemble member results are similar, suggesting that this is not a significant underestimate. Analysis of the fingerprint vector indicates that this underestimate in year 1 seems to be mostly originating in the wet tropics (consistent with results described above) and it is substantially reduced once the ENSO influence has been removed. The wet tropical regions dominate all of the coefficients

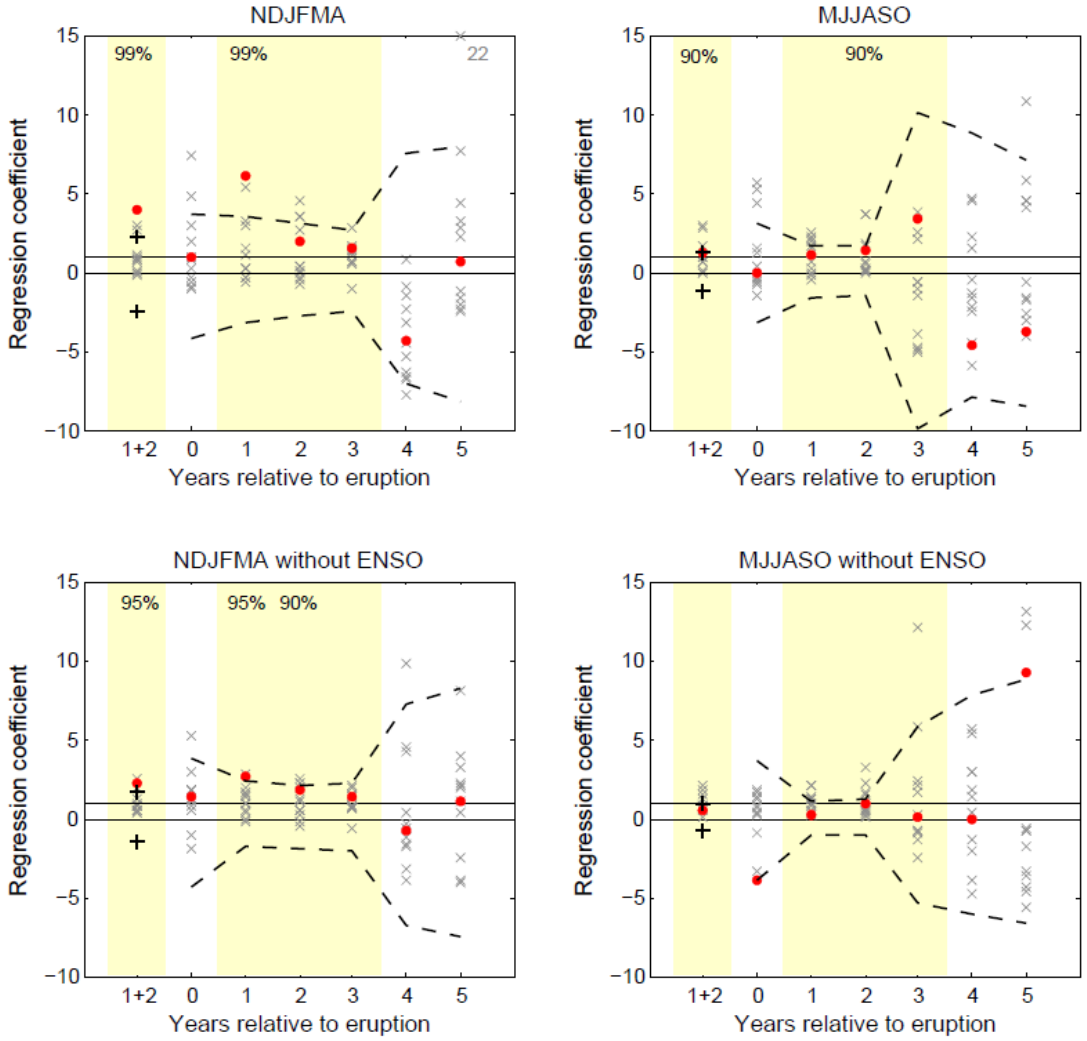

Figure 2.12 Regression coefficients obtained by regressing the observed average spatial patterns onto the model ensemble mean spatial patterns (red dots-see text for details). Black dashed lines are the 5-95% confidence limits for these regression coefficients (see text for details). Black crosses are confidence limits for years 1 and 2 combined. Grey crosses are the coefficients obtained by regressing single ensemble members onto the ensemble mean of the remaining members. Lower plots are based on the results after the ENSO influence has been regressed out from both the observations and model data. Yellow shading denotes years in which we expect to see a detectable response based on the model results. Where results are significant, the level at which they are significant is indicated above the relevant regression coefficient at the top of the plots.

due to the large magnitude of variations there. In MJJASO there appears to be good agreement between model and observations in years 1 and 2, but this breaks down in year 1 once the ENSO influence has been removed. In years 4 and 5 agreement between the model and observations deteriorates, presumably because the volcanic response is now decaying, similarly indicated by the widening of the uncertainty bars (note that the larger coefficients

and widening uncertainty bars are due to the fingerprint decaying leading to small values in the denominator of the regression equation). The ensemble members exhibit the best agreement with the ensemble mean in the two years following the eruption, suggesting that they have some level of agreement in their volcanic response. The scaling factors derived from the observations generally lie within the range of the ones calculated from the ensemble members, suggesting that while we found a significant underestimate in the wet tropics (see also Figure 2.9), there is no significant model underestimate in the overall response.

2.5 Conclusions

The aim of this study was to identify robust features of the precipitation response to large volcanic eruptions. We examined first the response to 18 large low latitude eruptions in an ensemble of 11 HadCM3 runs. We found a significant reduction in global mean precipitation, in agreement with previous studies [e.g. *Robock and Liu*, 1994; *Trenberth and Dai*, 2007; *Schneider et al.*, 2009*; Gu et al.*, 2007; *Gu and Adler*, 2011]. Over the ocean, the response remained significant for around 5 years and matched the timescale of the near-surface air temperature response, suggesting that the precipitation response could be driven by changes in sea surface temperature. In contrast, the land response remained significant for 3 years and reacted faster than land temperature. These findings agree with *Joseph and Zeng* [2011]. We further found the land precipitation response correlated well with aerosol optical depth and a reduction in land-ocean temperature contrast, suggesting a directly forced component and possible contributions from weakening monsoons. Spatial patterns did indeed show a drying signal in monsoon regions in agreement with previous studies [*Joseph and Zeng*, 2011; *Schneider et al*., 2009; *Trenberth and Dai*, 2007], with the notable exception of India, along with a wettening signal in the subtropics and drying in the extratropics. We built on previous studies by splitting the tropics into wet and dry regions. We found that the tropical areas experiencing drying after eruptions coincided very well with the climatologically wet regions, whilst the dry ocean areas, which are the primary moisture source regions [e.g. *Gimeno et al*., 2010], got wetter on average but were patchier. This is broadly the opposite pattern to, but physically consistent with, projections under global warming [*Held and Soden*, 2006; *Trenberth*, 2011; Meehl et al., 2007]. We found these

HadCM3 results to be consistent with the other CMIP5 models (Chapter 3 and Iles and Hegerl (2014), submitted). We also found a greater sensitivity of precipitation to temperature changes for volcanic forcing (3.3 % K^{-1}) compared to greenhouse gas forcing (1.5 % K^{-1}) or internal variability (2.0 % K^{-1}).

We then examined whether the volcanic response could be detected in observational land precipitation data for 5 twentieth century eruptions, replicating the observational data coverage in the model. Again we found a significant reduction in global mean precipitation in both the model and observations, lasting 2-3 years, although the signal to noise ratio was sharply reduced when data were limited to station-covered land regions (as found for 20th century forcing in *Balan-Sarojini et al.* [2012]). There was also a significant reduction in the wet tropical regions for model and observations in NDJFMA, but only for the model in MJJASO. The global land precipitation response in NDJFMA was significantly underestimated by the model, and this originated from the wet tropical regions. Once the ENSO influence had been removed from the observations, the global and wet tropical region results remained significant in NDJFMA and agreed better with the masked model, but became insignificant in MJJASO. Agreement between the model and observations was poor for the extratropics, whilst the tropical dry regions response was noisy. Spatial patterns were only marginally significant, and monsoon regions did not always dry in either the masked model or the observations. The observational findings were broadly consistent when an alternative dataset was used, although model-data agreement deteriorated for MJJASO in data sparse interpolated regions.

We performed a detection analysis to determine whether the volcanic response is detectible and consistent between models and observations. The fingerprint of the volcanic precipitation response from the model was detected in observations for the boreal cold season for year 1 following the eruption and years 1 and 2 combined, but it was only marginally significant for the boreal warm season. The detection analysis also suggested that the global-scale model response was smaller than that in the observed data, although the discrepancy appeared to be explained by internal variability and reduced once the influence of ENSO had been removed.

Chapter 3: The global precipitation response to volcanic eruptions in the CMIP5 models

Declaration

This chapter is adapted from a paper that has been submitted to Environmental Research Letters: Iles, C. E. and G. C. Hegerl (2014), The global precipitation response to volcanic eruptions in the CMIP5 models, *Geophs. Res. Lett.*, submitted. I conducted the analysis and wrote the paper, Gabi Hegerl (University of Edinburgh) provided scientific advice and edited the manuscript. Xuebin Xhang (Environment Canada) provided precipitation data and Debbie Polson (University of Edinburgh) provided help with acquiring CMIP5 data. The manuscript has been modified to avoid repetition of material in chapters 1 and 2.

3.1 Introduction

In this chapter we investigate whether the main findings of Chapter 2 (referred to here as I13 (*Iles et al*., 2013)) using HadCM3 are consistent with results using the CMIP5 models, many of which have higher horizontal and vertical resolutions and extend higher into the stratosphere than HadCM3. Furthermore, whilst I13 only used observational data over land, here we use an additional satellite-gauge dataset to investigate whether the long-lasting ocean response found in HadCM3, along with the wettening response in the dry tropical ocean regions are supported by observations. Finally we examine whether the CMIP5 models underestimate the precipitation response to volcanism, testing sensitivity to using alternative observational datasets.

3.2 Data

3.2.1 Model Data

We downloaded all twentieth century historical runs from the CMIP5 archive that were available in December 2012 (see Table S3.1). These are forced by observed records of both natural and anthropogenic forcings, such as solar variability, volcanic aerosols, greenhouse gases and land use change (see *Taylor et al.* [2012] for details). There is no recommended

volcanic forcing dataset, but many modelling groups use *Ammann et al*. [2003], its update [*Ammann et al*., 2007] or an updated version of *Sato et al.* [1993] (available at data.giss.nasa.gov/modelforce/strataer). We did not include HadCM3 in the analysis, for sake of comparison with I13. Multi-model means are constructed by averaging over all 88 available runs, even where there are differing numbers of runs per model. Using only a single simulation for each model yielded qualitatively similar results.

3.2.2 Observational data

The *Zhang et al*., 2007 (Z07) and GPCC twentieth century gauge-based land precipitation datasets detailed in Chapter 2, Section 2.2.1 were again used, as well as a shorter combined satellite-gauge record. There are substantial differences in the methods of construction between the datasets, allowing some assessment of the robustness of results to observational uncertainty. The GPCC dataset is spatially interpolated, resulting in full land coverage and is based on a very large number of station records (67,200 stations with at least 10 years of data). In contrast Z07 uses only stations that have at least 25 years of data in the 1961-1990 base period and at least 5 years of data in every decade from 1950-1999. It is not spatially interpolated, yielding a dataset with less spatial coverage, but that is more homogeneous and constrained by stations than GPCC (see Section 2.2.1 for more detail).

We also used the 2.5°x2.5° version of the Global Precipitation Climatology Project (GPCP) combined satellite-gauge dataset [*Adler et al.*, 2003]. This dataset is spatially complete and, unlike the other two datasets, includes ocean coverage. The dataset begins in 1979, since when there have been only 2 major eruptions, and only one since the introduction of a microwave based sensor in 1987 which has improved readings relative to the pre-microwave era.

3.3. Methods

3.3.1 Epoch analysis

As in I13 we used ‘epoch analysis’, which involves averaging across the precipitation response to several volcanic eruptions in order to reduce internal variability. We used the

five largest eruptions since 1900, as defined by global mean aerosol optical depth (AOD): the 1902 Santa Maria eruption; Novarupta in 1912; Agung, 1963; El Chichon, 1982 and Pinatubo, 1991 (Table S3.2, Figure S3.5b). For each grid cell and eruption, anomalies for each of the 10 years following an eruption, or up until the next eruption if that occurred first, were calculated with respect to a 5 year pre-eruption mean, to account for multidecadal changes in precipitation due to long-term trends or low frequency variability. We then averaged across all the eruptions available for each grid cell before spatial averaging. Where an eruption occurred too close to the beginning of a dataset (e.g., 1902), a shorter pre-eruption mean was used (see SI, this differs slightly from Chapter 2). Following I13, we use half year seasons: the boreal cold season (November to April, NDJFMA), and boreal warm season (May to October, MJJASO). "Year 1" denotes the season in question commencing after the eruption date, in order to give aerosols time to spread globally (Table S3.2).

As in I13, significance of results was tested using a Monte Carlo technique, in which the analysis is repeated 10,000 times using randomly selected years as eruption years (except for CMIP5 masked to Z07, and composite maps, where 1000 cycles were used due to computational constraints). 5-95% confidence intervals were then calculated from the distribution of these results (see I13 for more detail). Since GPCP has very limited temporal coverage (33 years), we obtained a second set of confidence intervals for it using the CMIP5 runs: for each region we combined the last 33 years of each run into one long time series after converting to anomalies and rescaling each run's standard deviation to the standard deviation of GPCP (which tends to be larger over oceans). We then performed Monte Carlo analysis on this new time series (see SI for detail).

Where wet or dry tropical regions are referred to, wet regions are defined as the wettest third of grid cells between 40°N and 40°S, after any masking according to land or ocean, or observational data coverage, and dry regions are the remaining two-thirds (following I13). These are defined separately for each model run or observational dataset.

3.3.2 Removing the influence of ENSO

As in Chapter 2 we repeat the analysis for the observational precipitation datasets after linearly removing the influence of ENSO. We again use the cold tongue index (CTI) as a measure of ENSO variability and calculate a regression coefficient for each grid cell and season between the detrended time series of CTI and precipitation, avoiding years 0-5 following an eruption. Note that this leaves only a limited number of ENSO events for the regression, particularly for GPCP, hence the removal of ENSO is somewhat noisy in that case (excluding fewer years following eruptions for GPCP did not improve results). We then subtract ENSO related precipitation from the precipitation time series at each gridpoint to arrive at a precipitation dataset with ENSO influence (at least partially) removed. We did not remove ENSO from the models since its signal should average out across the large number of simulations when constructing the multi-model mean.

3.4 Results

Figure 3.1 shows the time series of twentieth century precipitation for 50°N-50°S for land (b), ocean (c) and the two combined (a) for the CMIP5 models compared to observations. Latitudes poleward of 50^{o} are excluded to avoid biases in GPCP over the high latitudes in winter, particularly over oceans [*Adler et al*., 2012], although results using the whole globe are very similar (not shown). A clear decrease in precipitation following volcanic eruptions can be seen in the multi-model mean, particularly over oceans; and over land and ocean combined. This is also reflected in a lowering of the ensemble envelope. Over land the modelled response is noisier but still visible. The observed response is less clear, although a decrease in land precipitation can be seen following the 1991, 1982 and 1912 eruptions in all datasets. The observed datasets appear well correlated over land over the more recent period, but agree less well further back in time (see also *Polson et al*. [2013a]). Over ocean GPCP shows a noisy decrease around the time of Pinatubo in 1991, although this commenced before the eruption, and no response after El Chichon in 1982.

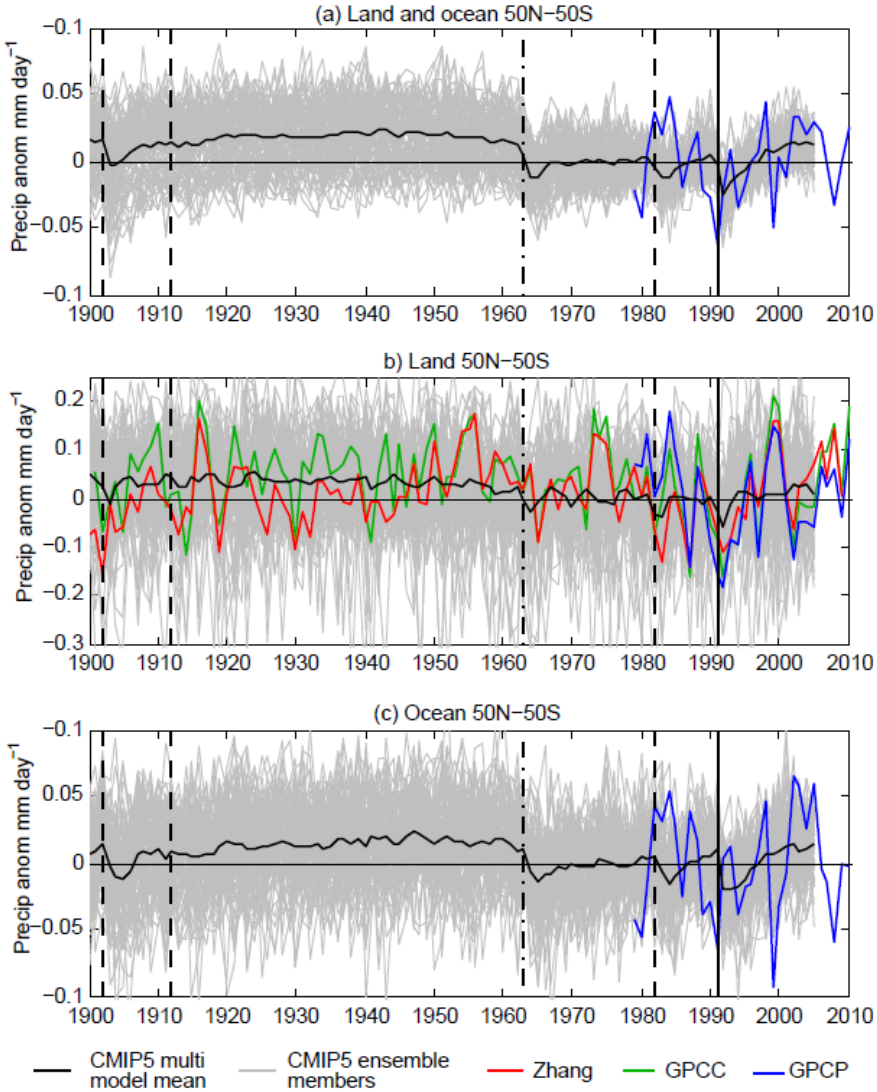

Figure 3.1: Time series of twentieth century precipitation for 50°N-50°S for observations (colored lines; blue line is GPCP, red Z07, green GPCC) compared to CMIP5 data (black line is the CMIP5 multi-model mean, grey lines are individual model runs. a) shows land and ocean areas combined, b) land regions and c) ocean regions. For b) CMIP5 and GPCP are masked to match the spatial coverage of GPCC, whilst Z07 has its own spatial coverage. Vertical black lines denote timing of eruptions (solid lines represent eruptions whose aerosol clouds are symmetrical between hemispheres, dashed lines represent a northern hemisphere bias, and dot-dashed lines a southern hemisphere bias). Anomalies are calculated with respect to the period covered by all datasets and model runs i.e. 1979-2005.

Figure 3.2 shows the CMIP5 multi-model mean spatial patterns of precipitation response averaged across all 5 eruptions for the 2 years following eruptions. Patterns are similar to those found in HadCM3 in I13. Monsoon regions dry in their respective warm seasons, whilst surrounding areas get wetter and the extratropics get drier on average. There appears to be a southward of the ITCZ over the Atlantic and Pacific oceans in MJJASO. Neither the multi-model mean (Figure 3.2a) nor individual models (Figure S3.1) show any evidence for

a precipitation pattern suggestive of a positive NAO in NDJFMA, consistent with *Driscoll et al*. [2012] and *Charlton-Perez et al*. [2013]. The modelled response lasts until year 2 over land and until year 3 (Figure S3.2) or 4 (not shown) over ocean, although the response over the Pacific is less stable over time, as was also the case in HadCM3 in I13.

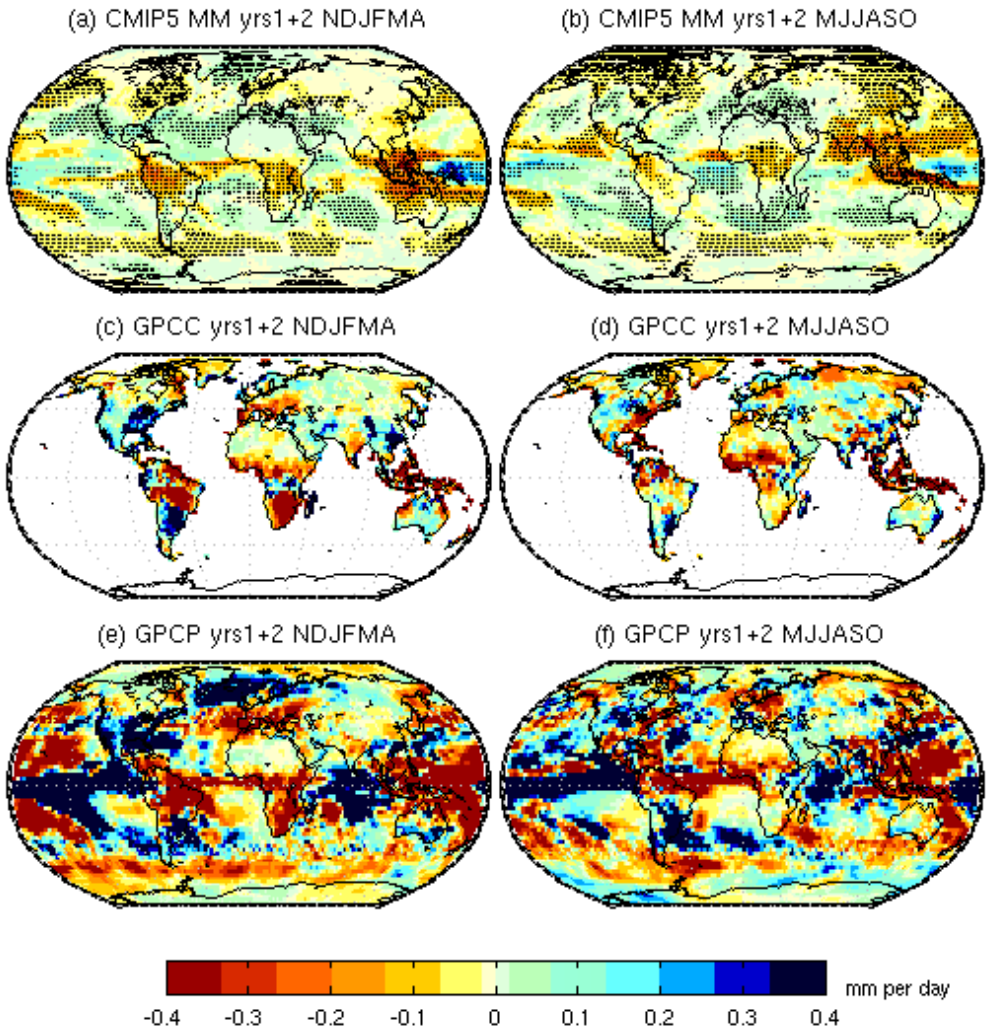

Figure 3.2: Average spatial patterns of precipitation response following 5 eruptions for years 1 and 2 combined (a, b) for the CMIP5 multi-model mean, (c, d) GPCC and (e, f) GPCP (using only two eruptions). (a ,c, e) are for NDJFMA, (b, d, f) for MJJASO. Stippling indicates significance at the 90% level for CMIP5. Units are millimeters per day.

The observed precipitation response patterns match well between observational datasets where they overlap, despite GPCP only covering 2 eruptions (Figure 3.2; Z07 is very similar to Figure S3.3 c-d (not shown)). Based on I13 observed patterns are expected to be only marginally significant. These patterns are of much greater magnitude than the multi-model

mean, probably due to the cancellation of noise in the latter. As in the models, the monsoon regions get drier following eruptions in the observations, although the exact location of these drying areas is slightly different and the Asian monsoon regions show a mixed response. Unlike in the models, there is a positive NAO precipitation pattern in NDJFMA in all the observed datasets [see *Fischer et al*., 2007]. Removing the ENSO influence generally makes little difference to results (Figure S3.3). Comparing observations and models over ocean is more difficult since GPCP results are noisy, but both show a wettening signal in the east equatorial pacific and south pacific convergence zone along with a drying signal in the location of the ITCZ over the Atlantic in both seasons.

Previous studies have identified shifts in the position of the ITCZ in response to volcanic forcing [e.g. *Schneider et al*., 2009; *Haywood et al*., 2013]. The ITCZ tends to move towards the warmer hemisphere. For an eruption with a hemispherically symmetric aerosol cloud this causes the ITCZ to move less far into the summer hemisphere, since the summer hemisphere undergoes a greater cooling relative to the winter one [*Yoshimori and Broccoli*, 2008; *Schneider et al*., 2009]. For asymmetric aerosol clouds *Haywood et al*. [2013] found the ITCZ to shift away from the hemisphere with the greatest increase in AOD using HadGEM2-ES. We also find this shift in response to asymmetric forcing in CMIP5, for example a northward shift in both seasons following the southern hemisphere biased Agung eruption (Figure S3.4 a,b), and a southward shift following the northern hemisphere biased 1982 El Chichon (Figure S3.4 c,d), 1902 Santa Maria and high latitude 1912 Novarupta eruptions (not shown). These shifts cause a smaller decrease, or even increase in hemispheric mean precipitation in the hemisphere with fewer aerosols (Figure S3.5). As most of the twentieth century eruptions had stronger aerosol loadings in the NH, the average response resembles such eruptions (Figure 3.2).

Figure 3.3 shows the post-volcanic precipitation response to the two most recent eruptions in GPCP compared to CMIP5 for various regions (the extratropics and dry tropical land regions are shown in Figure S3.6). Results for CMIP5 using all 5 eruptions are very similar, but more highly significant (not shown). CMIP5 results are very similar to those using HadCM3 in I13; there is a significant decrease in precipitation in the multi-model mean for the global

mean and wet tropical regions, over both land and ocean, and a significant increase over dry tropical ocean regions. As was the case for HadCM3, the response over ocean lasts longer than that over land and is smaller in magnitude. This longer ocean response occurs in all models with more than one ensemble member when averaging over all 5 twentieth century eruptions (Figure 3.4), but is not necessarily seen in individual runs using only 2 eruptions (Figure 3.3).

Over land, there is a significant decrease in observed precipitation in NDJFMA for the global mean and wet tropical land regions, and a decrease over these regions in MJJASO which is significant only if using CMIP5-based confidence intervals (see Section 3.3.1). Removing the influence of ENSO reduces the size of the response, although it remains significant in NDJFMA. The observed land response in NDJFMA is larger than the ensemble mean response, but is within the ensemble envelope (albeit on the upper edge for the wet tropics, year 1). Using the other two observational datasets (Figure S3.7) with their original spatial coverage and 5 eruptions yields qualitatively similar results (see I13 for Z07).

Over ocean, GPCP bears limited resemblance to the multi-model mean, at least in part due to the much larger variability in the average across two eruptions compared to the multi-model mean of 186 eruptions. Nevertheless, GPCP often reaches the edge of, or goes beyond the ensemble envelope, reflecting its higher variability over oceans compared to the CMIP5 models (not shown). For the global mean, GPCP only shows a decrease in NDJFMA once ENSO is removed, and only in year 1, compared to years 2-4 for the multi-model mean, whilst in MJJASO observed precipitation increases. In the wet tropical regions GPCP shows a significant decrease in year 1 in NDJFMA as expected, but this decrease is larger than in any ensemble member, noisy, and shorter-lived than the multi-model mean, whilst in MJJASO observed precipitation increases slightly, but is within the ensemble range. Finally over the dry tropical regions there is a significant increase in observed precipitation as expected in year 1 NDJFMA, which is larger than that of any individual ensemble member, and a noisy increase in MJJASO, which is significant using CMIP5 based confidence intervals. Some of the secondary peaks several years after the eruption in the observations

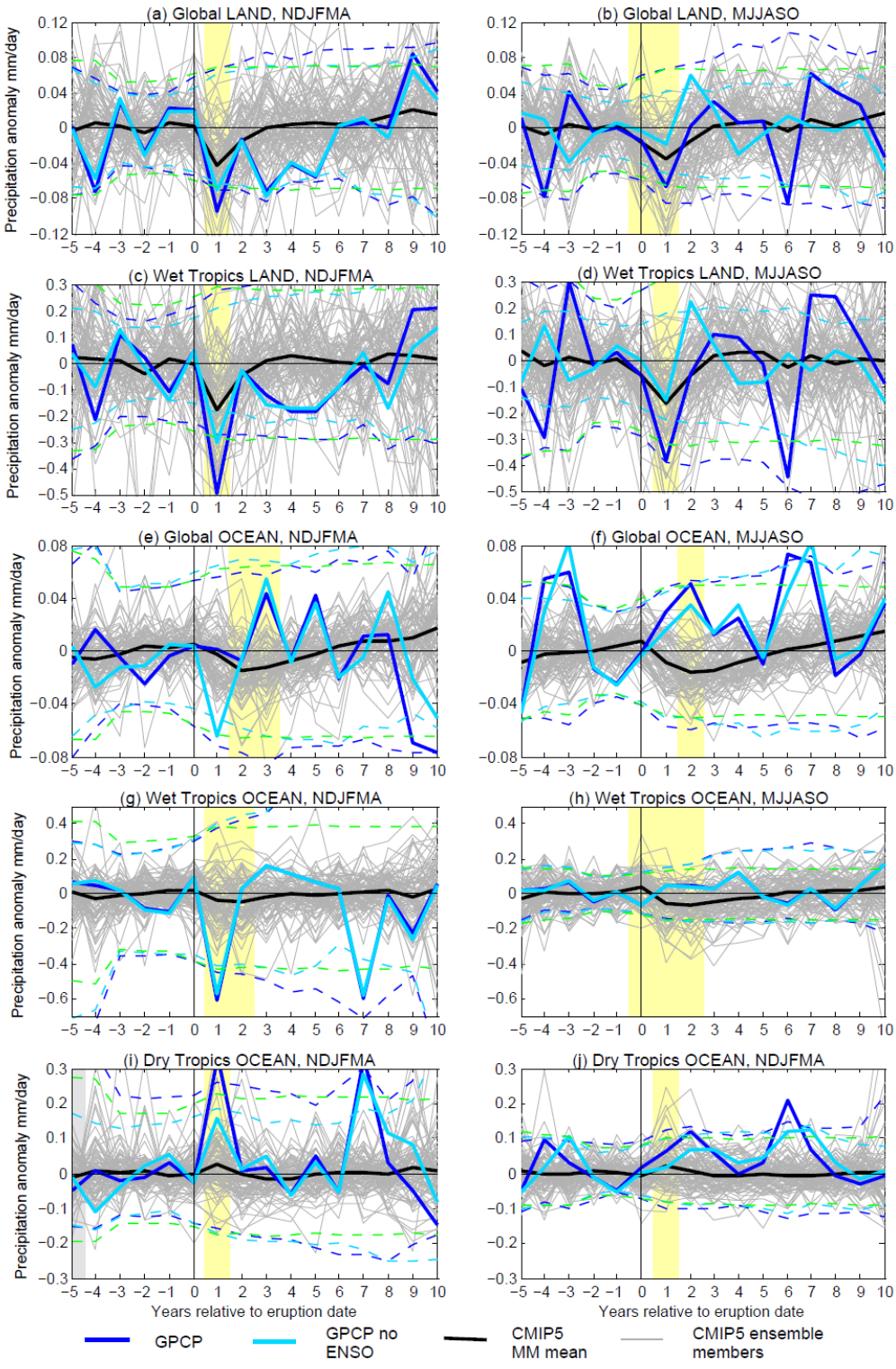

Figure 3.3 Precipitation response averaged over 2 volcanic eruptions in CMIP5 compared with GPCP observational data. (a-d) is for land precipitation, (e-j) is ocean precipitation, (a, b, e, f) global mean, (c, d, g, h) wet tropical regions, (i, j) dry tropical regions. GPCP is shown in dark blue, light blue once ENSO is removed; CMIP5 multi-model mean is shown in black and individual runs in grey. Vertical black line denotes timing of eruptions. Dashed lines are 5-95% confidence intervals, dark blue for GPCP, light blue for GPCP with ENSO influence removed and green for GPCP confidence intervals calculated from CMIP5. Yellow shading denotes years in which the multi-model mean response is significant (grey for pre-eruption years). From model results, significant responses are only expected in years 0-3.

may be due to incomplete removal of ENSO from GPCP (see Section 3.2). For example, the peaks in year 7 in NDJFMA coincide with the 1998 El Nino event, and the spatial patterns suggest some El Nino influence even after ENSO removal (not shown). In summary, while the multi-model mean response is significant in almost all diagnostics following an eruption, GPCP only shows significant responses that are robust to removing ENSO over the wet tropical ocean and land region, and over global land in the boreal cold season, suggesting a very marginally significant response overall. It is not possible to ascertain from these observational results over ocean whether the long ocean response seen in CMIP5 (Figure 3.4) is a real phenomenon.

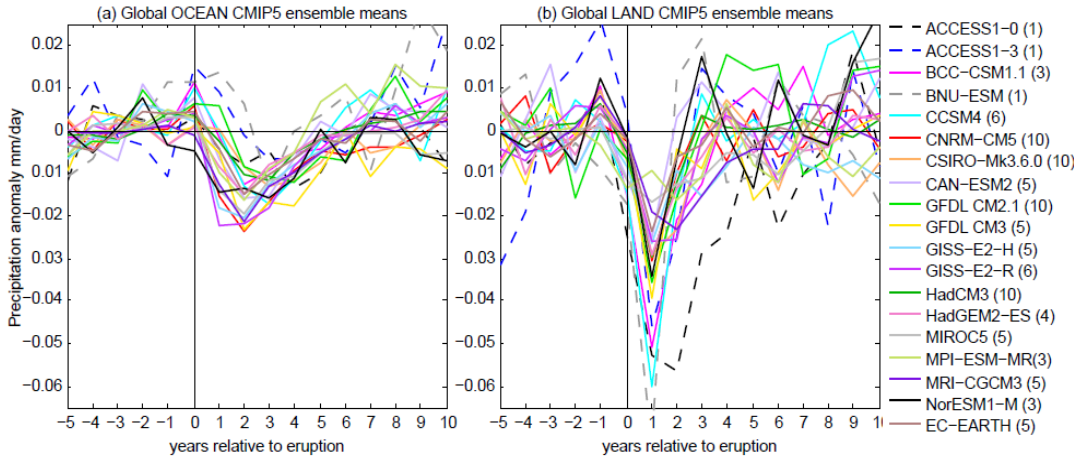

Figure 3.4: Ensemble mean global ocean (a) and land (b) precipitation response to 5 eruptions for each model. The number of ensemble members used for each model ensemble mean is shown in brackets in the legend. Dashed lines are used where there is only a single ensemble member.

Finally we perform a detection analysis as described in I13 to determine whether the overall response is significant and whether or not the models and data are consistent (Figure 3.5). We first split the global land response into the northern hemisphere extratropics, wet tropical and dry tropical regions to yield a 3 element vector for each year following the eruptions (the southern hemisphere extratropics are excluded due to their limited land area). For GPCP a four element vector is used consisting of dry tropical ocean regions, dry tropical land regions, wet tropical ocean regions, and wet tropical land regions. Extratropics are not used in the main analysis for GPCP to avoid less reliable high latitude data (however, results are robust to including the extratropics, see Figure S3.8). For each year following the eruptions

we regress this 3 (land data) or 4 (GPCP) element vector of the observed response averaged across all 5 eruptions (2 for GPCP) against the equivalent for the multi-model mean to yield a regression coefficient, or scaling factor which indicates whether the modelled response is bigger or smaller than that observed. For land data, the model data was first masked according to the data coverage of the observational dataset to which it is being compared. We test whether or not scaling factors are significantly different from those expected by chance through conducting a Monte Carlo analysis using random years for the observations as discussed above and regressing against the multi-model mean fingerprint. We then calculate 5-95% confidence intervals for the scaling factors. When a scaling factor exceeds the 95th percentile, it is large enough to be unlikely to occur due to climate variability, and the volcanic influence is said to be detected. We repeat the analysis using individual ensemble members instead of the observations, regressing against the mean of the remaining ensemble members to establish whether or not the observed response is consistent with the models. We also present results for years 1 and 2 combined, since this is when the clearest response is expected based on the multi-model mean response (Figure 3.3 and S3.6).

Figure 3.5 shows that the influence of volcanism is detectable (5% significance level) in NDJFMA in year 1 and years 1 and 2 combined in all three datasets. The large regression coefficients in these years suggest that CMIP5 underestimates the magnitude of the response, as HadCM3 also did to a greater extent in I13. In these years less than 5% of the ensemble members exhibit a response as big as that observed for almost all datasets, suggesting that the model underestimate is significant. In MJJASO the volcanic influence is only detectable at the 90% level in most datasets in these years. The magnitude of the observed coefficients agrees better with those of the models in MJJASO.

With the influence of ENSO regressed out from the observations, the volcanic influence is still detectable at the 95% level in NDJFMA in year 1 and years 1 and 2 combined in Z07 and GPCP, but not GPCC, which is based on more data but uses interpolation (see discussion in *Polson et al*. [2013a]). The magnitude of the coefficients decreases when removing ENSO, suggesting that ENSO was partly responsible for the large scaling factors in Figure 3.5a. In MJJASO removing ENSO decreases detectability making results marginal.

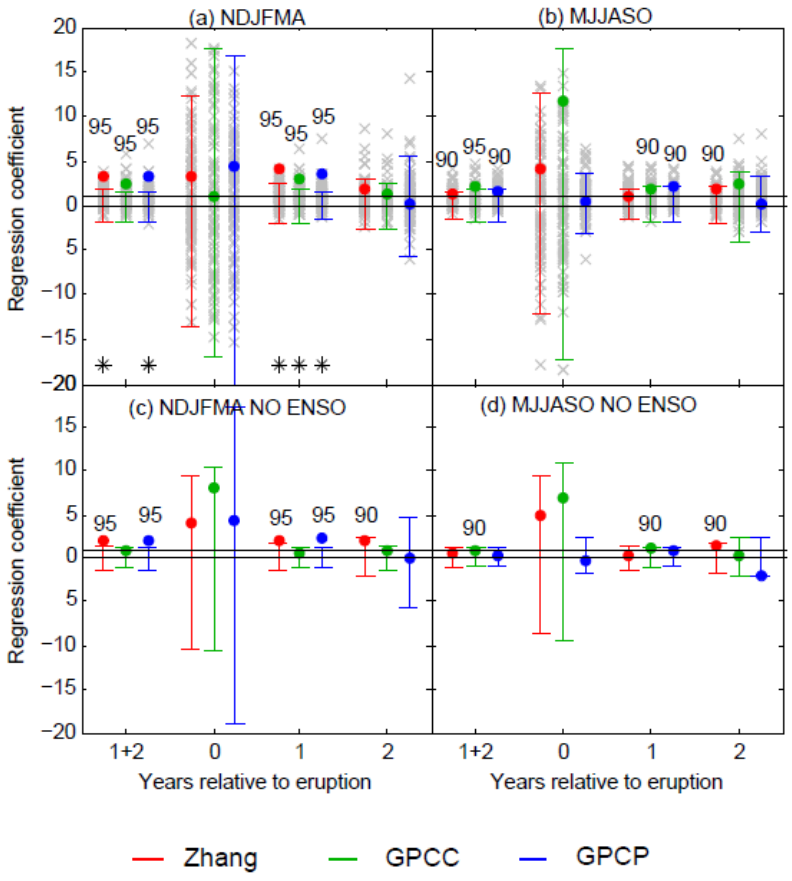

Figure 3.5: Detection of the volcanic signal: Regression coefficients obtained by regressing the observed average spatial patterns of precipitation response onto the CMIP5 multi-model mean patterns (circles -see text for details). Colored bars indicate 5-95% range of regression coefficients for internal climate variability. If a coefficient is greater than the 95th percentile the volcanic influence is detected. Grey crosses are coefficients obtained by regressing single ensemble members onto the mean of the remaining members. Numbers indicate the level at which the response is detectable. Red denotes results based on Z07, green GPCC, and blue GPCP. (c and d) are for results with the influence of ENSO removed. Asterisks indicate where less than 5% of the ensemble member-based coefficients are larger than the observed coefficients. (a and c) are for NDJFMA, (b and d) MJJASO.

We would expect the CMIP5 multi model mean fingerprint used in the detection analysis to be 'better' than the HadCM3 equivalent used in chapter 2 in the sense that the CMIP5 fingerprint is the average across more model runs (5 eruptions x 88 runs in CMIP5 (or 2 eruptions*88 runs when comparing with GPCP) vs 11x5 for HadCM3) and should therefore be less affected by noise, whilst the average across multiple models tends to be closer to reality than when using a single model. This is because model-specific errors in model formation or parameterisations tend to cancel out (unless they are shared across models). If the multi-model fingerprint is a more accurate representation of the precipitation fingerprint to volcanism, then we would expect scaling factors to be closer to unity. This occurs to a

certain extent, particularly in NDJFMA before ENSO removal, although coefficients still suggest that the model response is underestimated. Possible reasons for this could include model errors that are shared across multiple models, a noisy observational fingerprint that may not represent the response to volcanism very well, or incomplete ENSO removal from the observations (since most eruptions coincided with El Nino events, this will exaggerate the drying response over land if the ENSO response is not fully removed).

3.5 Conclusions

The main features of the precipitation response to large explosive volcanic eruptions in the CMIP5 models are consistent with those found in HadCM3 by I13. This includes a significant decrease in global, extratropical (see SI) and wet tropical regions precipitation over both land and ocean, and a significant wettening response over dry tropical ocean regions. The ocean response was longer-lived than that over land in all models with more than one ensemble member. Monsoon regions dried in agreement with other studies [e.g. *Joseph and Zeng*, 2011; *Schneider et al*., 2009], whilst the ITCZ moved away from the hemisphere with the greatest concentration of aerosols in the multi-model mean in agreement with *Haywood et al*. [2013]. Despite improvements in resolution and vertical extent, the CMIP5 models showed no evidence of a positive NAO response in the winter following eruptions, as was also the case in HadCM3.

We use observed gauge-based data over land; and additionally a combined satellite-gauge dataset (GPCP) to examine the observed precipitation response over oceans. Results using GPCP were noisy due to the short record length, covering only 2 eruptions. Nevertheless, over land a decrease in global and wet tropical regions precipitation following eruptions could be seen as expected, and this was significant in NDJFMA. Monsoon regions got drier in their respective warm season, with the exception of SE Asia, whilst there was a positive NAO response in winter. Regional mean findings were broadly consistent when alternative observational datasets were used, whilst spatial patterns were very similar. Over ocean, results were noisy, but the wet tropical ocean regions got significantly drier, and the dry regions significantly wetter as expected in NDJFMA, although with a larger magnitude than

any individual ensemble member. It was not possible to determine whether the long ocean response seen in the models was confirmed by observations due to the noisy nature of GPCP results. A detection analysis found the modelled influence of volcanism on precipitation was detectable in years 1+2 combined and year 1 following eruptions in NDJFMA in all observational datasets, and was marginally detectable in MJJASO in these same years. The response in NDJFMA was significantly underestimated by the models, particularly in the wet tropical regions. Removing the influence of ENSO brought the amplitude of the response in models and observations into better agreement, particularly in NDJFMA.

When the next large volcanic eruption occurs, which is likely to be in the next few decades based on the historical record [*Crowley et al*., 2008], the satellite record will be extremely valuable in further constraining the observed response, particularly over oceans.

Chapter S3: Supplementary Material

S3.1 Figures and tables

Table S1 details the CMIP5 runs used in the analysis. Table S2 details the dates and locations of the eruptions used and defines what counts as "year 1" for each season.

Table S3.1: CMIP5 Runs Used

Model Name	No. runs	Resolution	Model top height	Volcanic forcing dataset	Reference
ACCESS1.0	1	N96 L38 (1.25° lat, 1.875° lon)	40 km	*Sato et al*. [1993]	*Bi et al*. [2013] *Dix et al*. [2013]
ACCESS1.3	1	N96 L38 (1.25° lat, 1.875° lon)	40 km	*Sato et al*. [1993]	*Bi et al.* [2013] *Dix et al*. [2013]
BCC-CSM1.1	3	T42 L26 (~2.8° lat, 2.8° lon)	2.914 hPa	*Ammann et al*. [2003]	*Wu et al*. [2008] *Wu et al*. [2010] *Xin et al*. [2013]
BNU-ESM	1	T42 L26 (2.8° lat, 2.8° lon)	2.917 hPa	*Ammann et al*. [2003]	*Feng et al*. [2013]
CCSM4	6	0.9° lat, 1.25° lon L26	40 km	*Ammann et al*. [2003]	*Gent et.al*. [2011] *Meehl et al*. [2012]
CNRM-CM5	10	T127 L31	10 hPa	*Ammann et al*. [2007]	*Voldoire et al*. [2012]
CSIRO-Mk3.6.0	10	T63 L18 (~1.875° lat, 1.875° lon)	36 km	*Sato et al*. [1993]	*Jeffrey et al*. [2013] *Gordon et al*. [2002, 2010]
CanESM2	5	T63 L35 (~2.8° lat, 2.8° lon)	1 hPa	*Sato et al*. [1993]	*Chylek et al*. [2011] *Scinocca et al*. [2008]
EC-EARTH	5	T159/N80 L62 (Nominal 1.125° lat, 1.125° lon)	5 hpa	*Sato et al*. [1993]	*Koenigk et al*. [2012] *Hazeleger et al*. [2012]
GFDL-CM2.1	10	2° lat, 2.5° lon, L24	3 hPa (~35 km)	*Sato et al*. [1993], *Stenchikov et al*. [1998]	*Delworth et al*. [2006]
GFDL-CM3	5	C48 L48	0.01 hPa (~86 km)	*Sato et al*. [1993], *Stenchikov et al*. [1998]	*Donner et al*. [2011]
GISS-E2-H	5	2° lat, 2.5° lon, L40	0.1 hPa	*Sato et al*. [1993]	*Schmidt et al*. [2006] *Shindell et al*. [2013]
GISS-E2-R	6	2° lat, 2.5° lon, L40	0.1 hPa	*Sato et al*. [1993]	*Schmidt et al*. [2006] *Shindell et al*. [2013]
HadCM3[a]	10	2.5° lat, 3.75° lon	10 hPa	*Sato et al*. [1993]	*Collins et al*. [2001]
HadGEM2-ES	4	1.25° lat, 1.875° lon, L38	39+ km (~2.3 hPa)	*Sato et al*. [1993]	*Jones et al*. [2011] *Collins et al*. [2011]
MIROC5	5	T85 L40	3 hPa	*Sato et al*. [1993]	*Watanabe et al*. [2010]
MPI-ESM-MR	3	T63/L95	0.01 hPa	*Stenchikov et al*. [1998]	*Schmidt et al*. [2013] *Giorgetta et al*. [2013]
MRI-CGCM3	5	TL159L48	0.01 hPa	GEIA[b] [*Andres and Kasgnoc*, 1998]	*Yukimoto et al*. [2012]
NorESM1-M	3	1.9° lat, 2.5° lon, L26	2.917 hPa	*Ammann et al*. [2003]	*Bentsen et al*. [2013] *Iversen et al*. [2012].

[a] HadCM3 is not included in the results, apart from Figure S3.1 which shows spatial patterns of precipitation response to eruptions for each model separately.
[b] Global Emissions Inventory Activity database

Table S3.2. Eruption Dates and Year 1 Definitions

Eruption date	Volcano and location[a]	NDJFMA Year 1[b]	MJJASO Year 1	Start month of year 1 for annual data
24 Oct 1902	Santa Maria, Guatemala 14.76°N, 91.56°W	1903	1903	Feb 1903
6 June 1912	Novarupta, Alaska 58.27°N, 155.16°W	1913	1913	Oct 1912
Mid-March 1963	Agung, Indonesia 8.34°S, 115.51°E	1964	1963	July 1963
28 March 1982	El Chichon, Mexico 17.36°N, 93.23°W	1983	1982	July 1982
15 June 1991	Pinatubo, Philippines 15.13°N, 120.35°E	1992	1992	Oct 1991

[a] Locations are taken from Global Volcanism Project http://www.volcano.si.edu/world/largeeruptions.cfm. All eruptions are low-latitude except the 1912 Novarupta eruption.

[b] The year for NDJFMA refers to the year of the months January-April rather than November-December.

Figure S3.1 shows the ensemble mean spatial patterns of precipitation response for the individual models used in the analysis, averaged across 5 eruptions. For the most part, individual models also show a drying response over monsoon regions following volcanic eruptions in agreement with the multi model mean (Figure 3.2). Many models, but not all, show a southward shift of the ITCZ in boreal summer over the Atlantic. This is also visible, but less obvious, in the multi model mean. Some models also show a southward shift of this part of the ITCZ in winter, but fewer than show the summer shift. Shifts in the ITCZ are discussed in more detail in the main text. Precipitation patterns in the Pacific vary between models. None of the models show a convincing positive NAO response in winter.

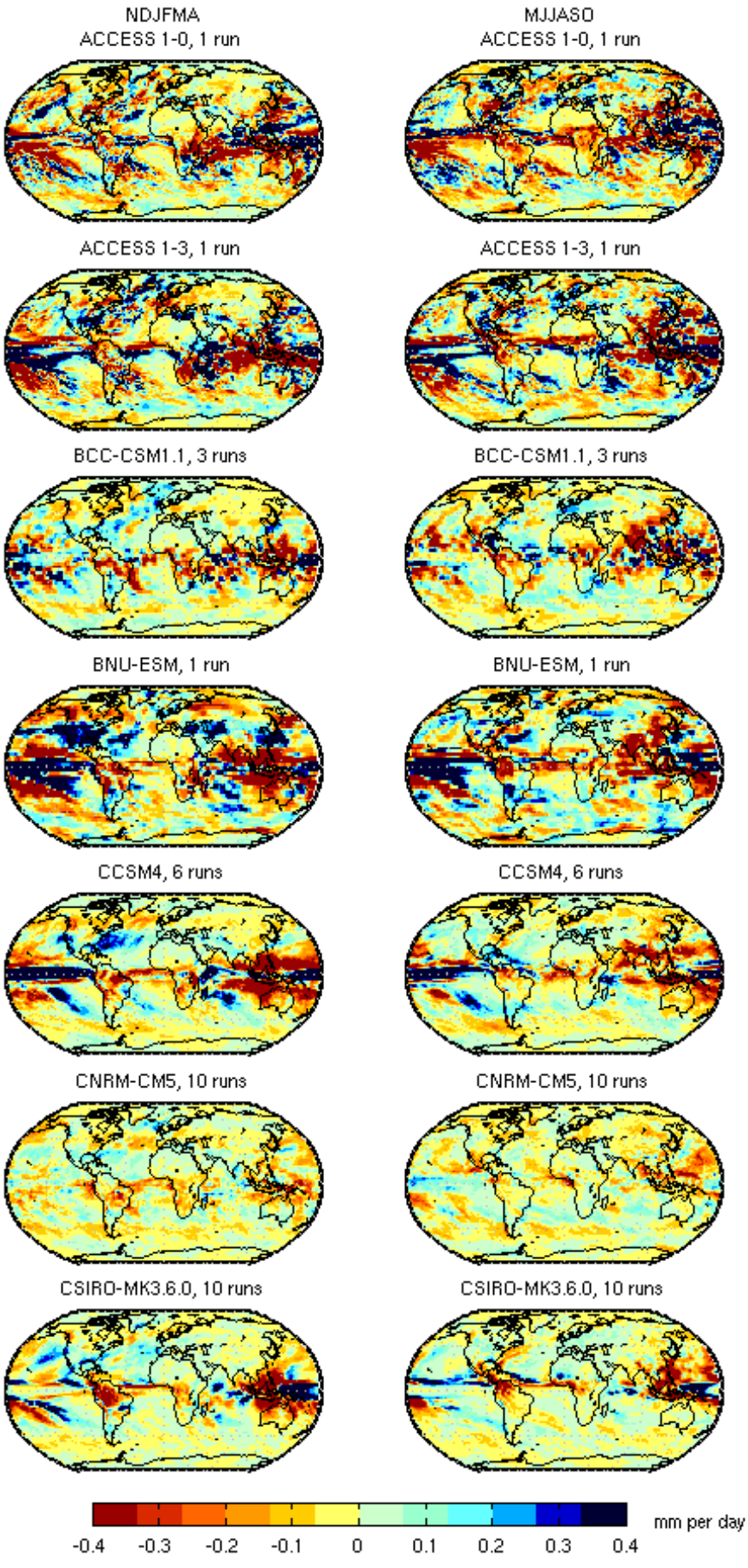
NDJFMA
ACCESS 1-0, 1 run
MJJASO
ACCESS 1-0, 1 run
ACCESS 1-3, 1 run
ACCESS 1-3, 1 run
BCC-CSM1.1, 3 runs
BCC-CSM1.1, 3 runs
BNU-ESM, 1 run
BNU-ESM, 1 run
CCSM4, 6 runs
CCSM4, 6 runs
CNRM-CM5, 10 runs
CNRM-CM5, 10 runs
CSIRO-MK3.6.0, 10 runs
CSIRO-MK3.6.0, 10 runs
-0.4
-0.3
-0.2
-0.1
0
0.1
0.2
0.3
0.4
mm per day

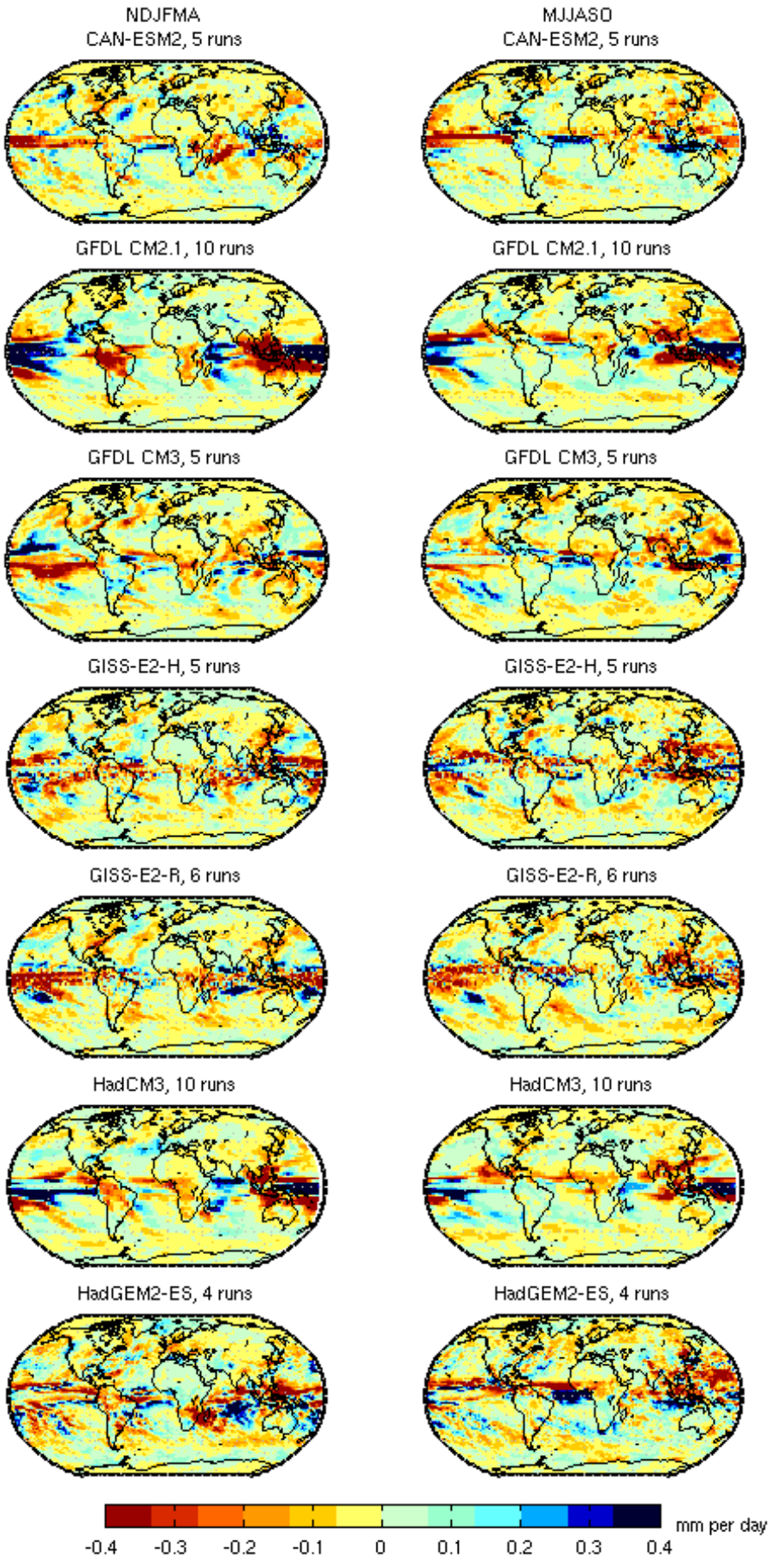
NDJFMA
CAN-ESM2, 5 runs
MJJASO
CAN-ESM2, 5 runs
GFDL CM2.1, 10 runs
GFDL CM2.1, 10 runs
GFDL CM3, 5 runs
GFDL CM3, 5 runs
GISS-E2-H, 5 runs
GISS-E2-H, 5 runs
GISS-E2-R, 6 runs
GISS-E2-R, 6 runs
HadCM3, 10 runs
HadCM3, 10 runs
HadGEM2-ES, 4 runs
HadGEM2-ES, 4 runs
mm per day
-0.4
-0.3
-0.2
-0.1
0
0.1
0.2
0.3
0.4

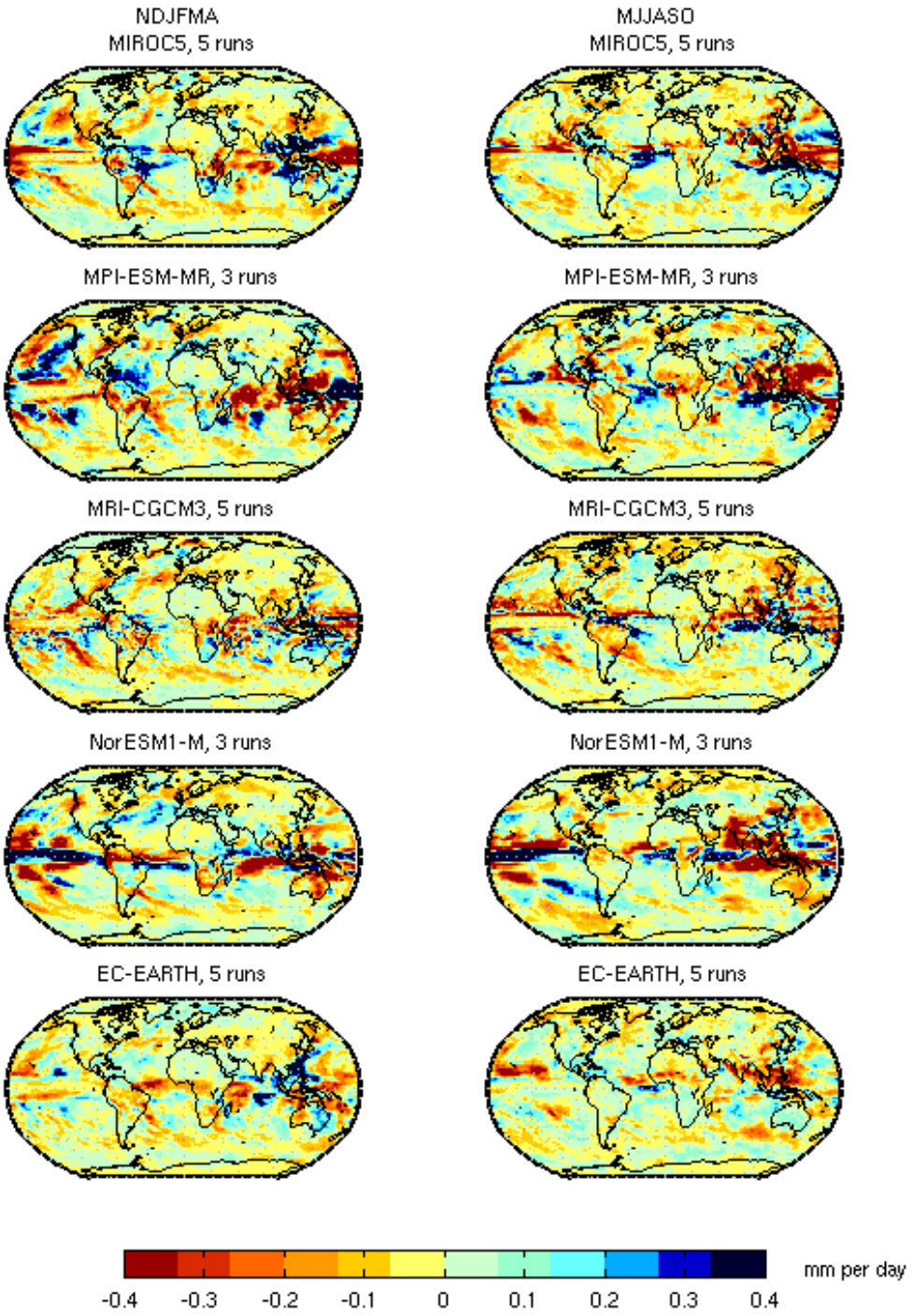

Figure S3.1: Ensemble mean precipitation response patterns to 5 eruptions for years 1 and 2 combined for each model used in this analysis. The patterns for HadCM3 are included for comparison. The number of runs contributing to the ensemble mean for each model is indicated above each plot. Left column is NDJFMA, right column MJJASO.

Figure S3.2 shows the evolution through time of the multi-model mean spatial patterns of precipitation response to eruptions. Stipples indicate where two thirds of the model runs

agree on the sign of the response. The precipitation response over land is strongest in year 1, is still visible but weaker in year 2, and has faded away by year three. The ocean response is longer lasting, but evolves through time, particularly in the eastern pacific. Agreement between model runs on the sign of precipitation response following eruptions is limited in many areas. However, one should bear in mind that each run has its own internal variability, such as that related to ENSO, which would reduce agreement. Nevertheless, more than two thirds of models agree on the drying signal in the monsoon regions in their respective warm season. If we use a criterion of 70% agreement, then very few grid cells agree on the sign of response, whereas using a criterion of 60%, the number of stippled grid cells increases noticeably (not shown).

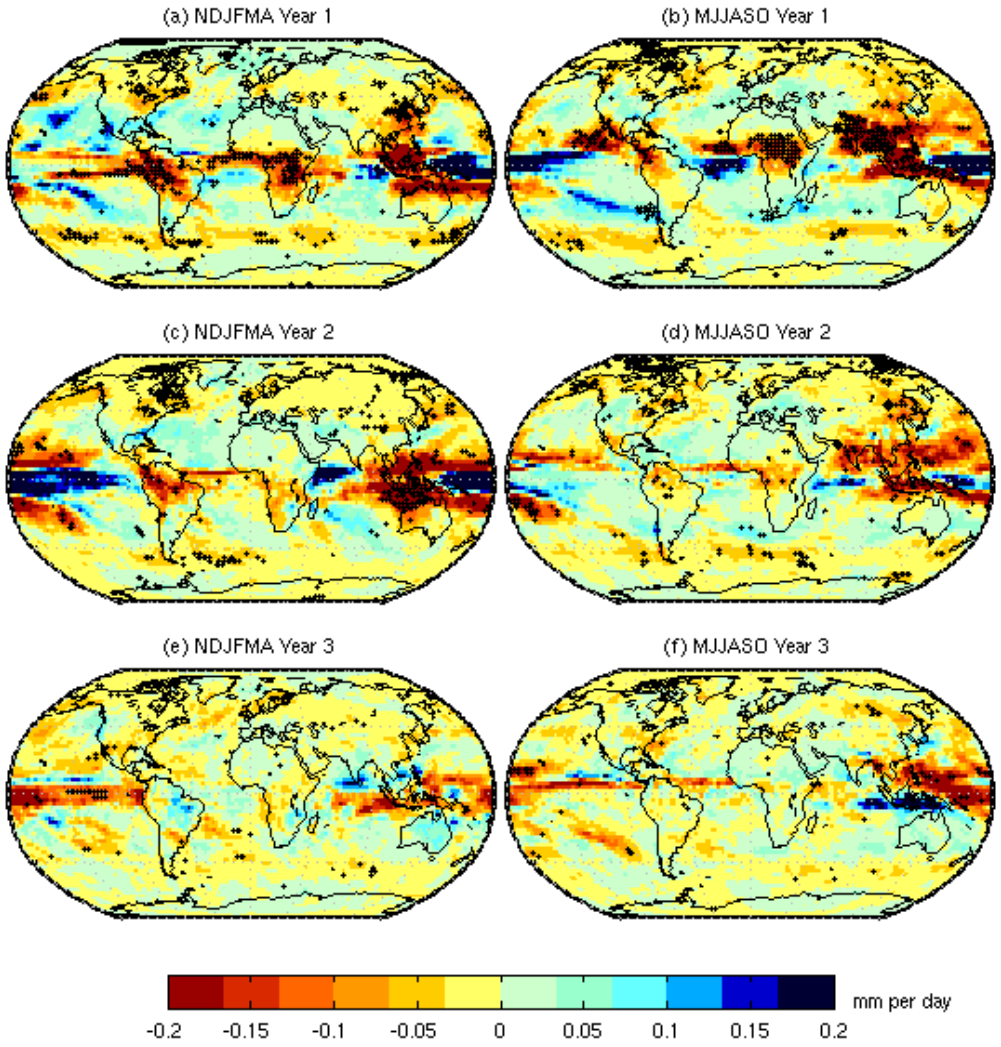

Figure S3.2 CMIP5 multi model mean spatial patterns of precipitation response for years 1 through to 3. Stipples indicate where two thirds of model runs agree on the sign of the change. (a, b) year 1, (c, d) year 2, (e, f) year 3. (a, c, e) NDJFMA, (b, d, f) MJJASO. Units are millimeters per day.

Figure S3.3 shows the average precipitation response to eruptions in the CMIP5 multi model mean and 3 observational datasets as in Figure 3.2 but with the influence of ENSO removed from the observations. Results using Z07's dataset are also added. Removing the influence of ENSO makes very little difference to results using Z07 or GPCC. In GPCP the main difference is that the westernmost Pacific switches from a drying to wetting signal in both seasons with ENSO removed. The eastern pacific pattern in GPCP in NDJFMA (g) suggests that ENSO was not completely removed through our procedure.

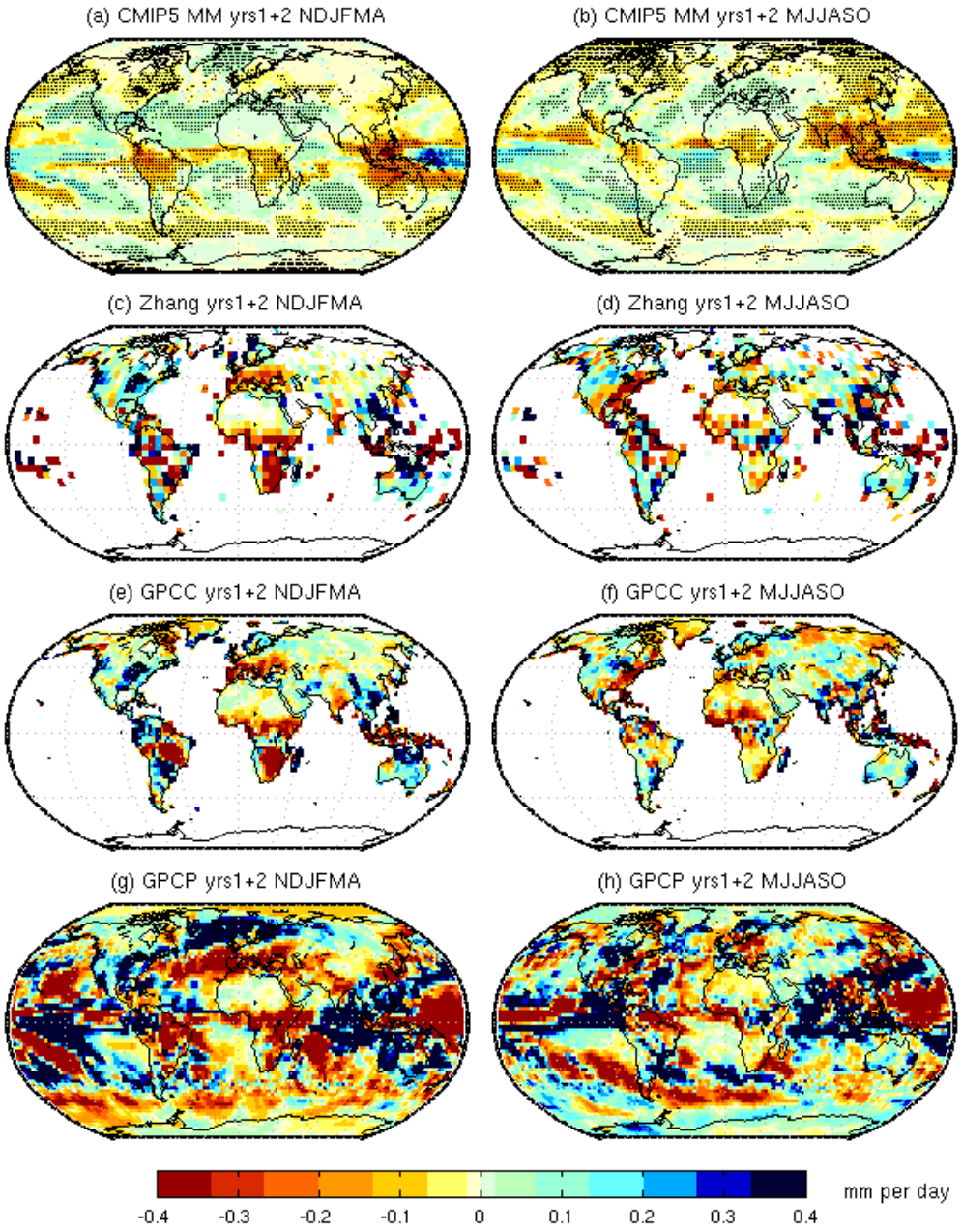

Figure S3.3 As in Figure 3.2 but with the influence of ENSO removed from the observations. Results for Z07 for 5 eruptions are added in (c) and (d). CMIP5 (a, b) is the same as in Figure 3.2. Units are millimeters per day.

Figure S3.4 shows how the precipitation response differs for eruptions whose aerosol clouds were biased towards either the southern or northern hemisphere, using the examples of the 1963 Agung and 1982 El Chichon eruptions respectively. Following Agung the ITCZ shifts northwards, away from the hemisphere most heavily influenced by aerosols, and following El Chichon it shifts southwards. (see also *Haywood et al*. [2013]). The same principle could also be seen at work in response to the other eruptions, including the 1912 high latitude eruption (not shown). The aerosol cloud following the 1991 Pinatubo eruption was symmetric between hemispheres. Although a southward shift of the ITCZ could still be seen in MJJASO over the Pacific and Atlantic, in NDJFMA any shifts were not clear, although there was some indication of a northward shift over the Atlantic (not shown). This is consistent with the summer hemisphere undergoing a greater reduction in temperature following eruptions than the winter one, limiting the poleward migration of the ITCZ into the summer hemisphere, as discussed in the main text [*Schneider et al*., 2009].

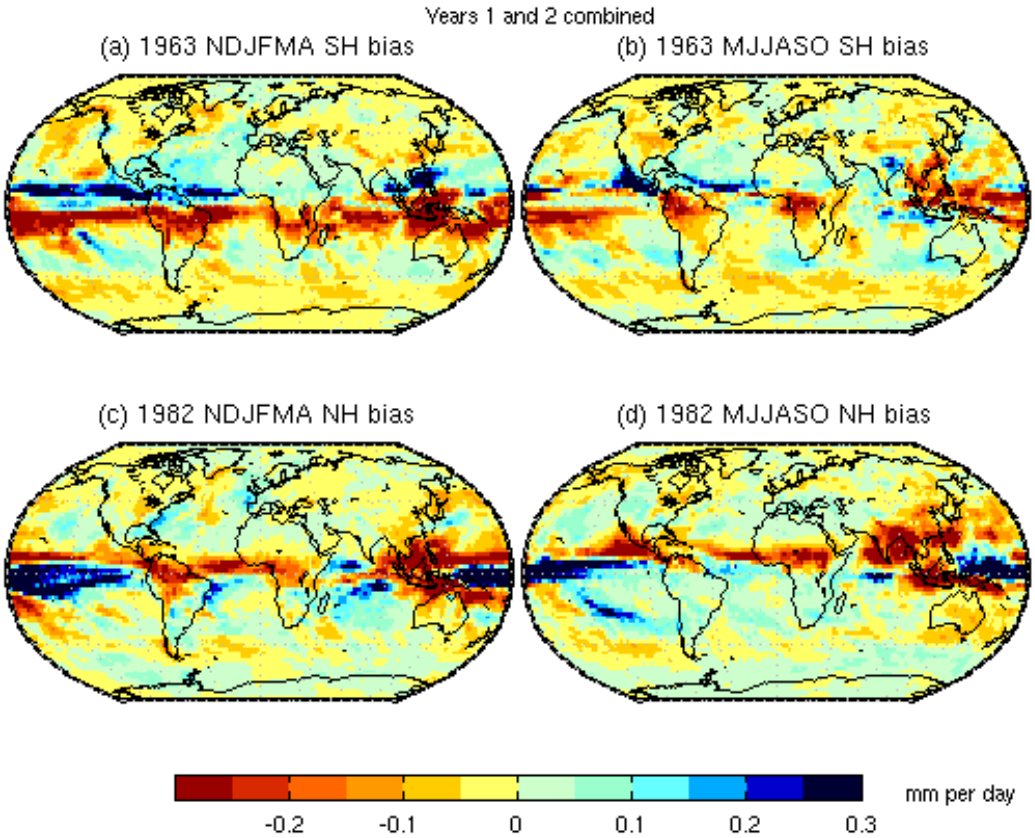

Figure S3.4 CMIP5 multi model mean spatial patterns of precipitation response for the two years following the southern hemisphere biased 1963 Agung (a, b) and northern hemisphere biased 1982 El Chichon (c, d) eruptions for the boreal cold season (a, c) and warm season (b, d). Units are millimeters per day.

Figure S3.5 shows the time series of hemispheric mean precipitation for the CMIP5 multi model mean compared to the distribution of volcanic aerosols between the hemispheres. The hemisphere with the greatest increase in aerosol optical depth experiences the greatest decrease in precipitation, whilst the opposite hemisphere experiences a lesser decrease (Santa Maria 1902), or even an increase in precipitation (e.g. for Agung in 1963 and to a lesser extent Novarupta in 1912). This is most likely related to the ITCZ shifts found in Figure S3.4.

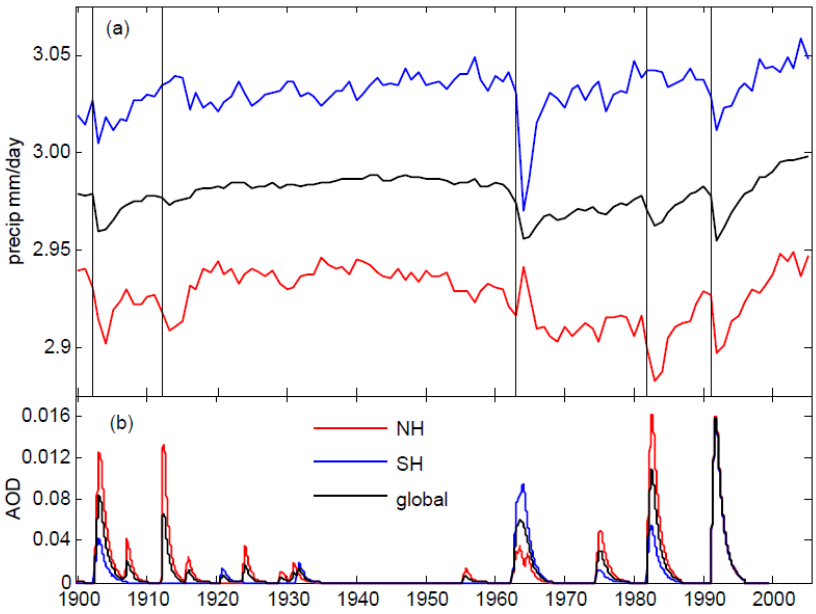

Figure S3.5: a) CMIP5 multi model mean time series of twentieth century precipitation for the globe (black), the northern hemisphere (0 to 90°N) (red) and the southern hemisphere (0 to 90°S) (blue). Black vertical lines denote timing of eruptions. b) Aerosol optical depth (AOD) based on *Crowley et al.* [2008]'s data for the same regions as in (a) in order to show towards which hemisphere volcanic aerosols were biased following each eruption.

Figure S3.6 shows the average precipitation response to eruptions for the extratropics (not shown in main text due to concerns about the quality of satellite retrievals over high latitudes) and dry tropical land regions (noisy; compare I13). The CMIP5 multi model mean exhibits a significant decrease in precipitation in both seasons for the northern hemisphere extratropical land regions (see Figure 3.2, body of paper), and both northern and southern hemisphere extratropical ocean regions, consistent with the findings for HadCM3 in I13. The

southern hemisphere extratropical land regions also undergo a significant decrease in the CMIP5 multi model mean despite the small land area involved (not shown). The multi model mean response over the dry tropical land regions does not show the same increase in precipitation as occurs over the dry tropical ocean regions, consistent with findings for HadCM3 in I13. Instead it exhibits an insignificant decrease in year 1 in NDJFMA and a significant decrease in year 0 MJJASO followed by a significant increase.

Observed results using GPCP over all these regions are generally noisy primarily due to the short record containing only two eruptions. Nevertheless, there is a prolonged significant decrease in precipitation over the southern hemisphere extratropical oceans in NDJFMA and an insignificant noisy decrease over both the northern and southern extratropical oceans in MJJASO in agreement with model expectations. One should bear in mind, however, that GPCP has large biases over extratropical oceans in winter [*Adler et al*., 2012]. Confidence intervals for GPCP based on CMIP5 runs tend to spread out less over time than the ones calculated using GPCP itself, and the biggest difference occurs in NDJFMA for the northern hemisphere extratropics (e).

Figure S3.7 compares regional precipitation responses to eruptions between three datasets over land areas using their original spatial coverage. Z07 and GPCC use 5 eruptions, whilst GPCP only uses the most recent 2. Also shown are the CMIP5 multi model means masked to replicate the spatial and temporal coverage of each dataset. The main features of the precipitation response can be seen in all three datasets, although absolute values and whether or not features are significant changes. Robust features include a drying response for the global mean and wet tropical regions, whilst the northern hemisphere and dry tropics are noisy in all datasets. The CMIP5 multi model means masked to different datasets are very similar to each other, although in MJJASO the global and wet tropics response commences in year 0 rather than year 1 when masked with GPCP.

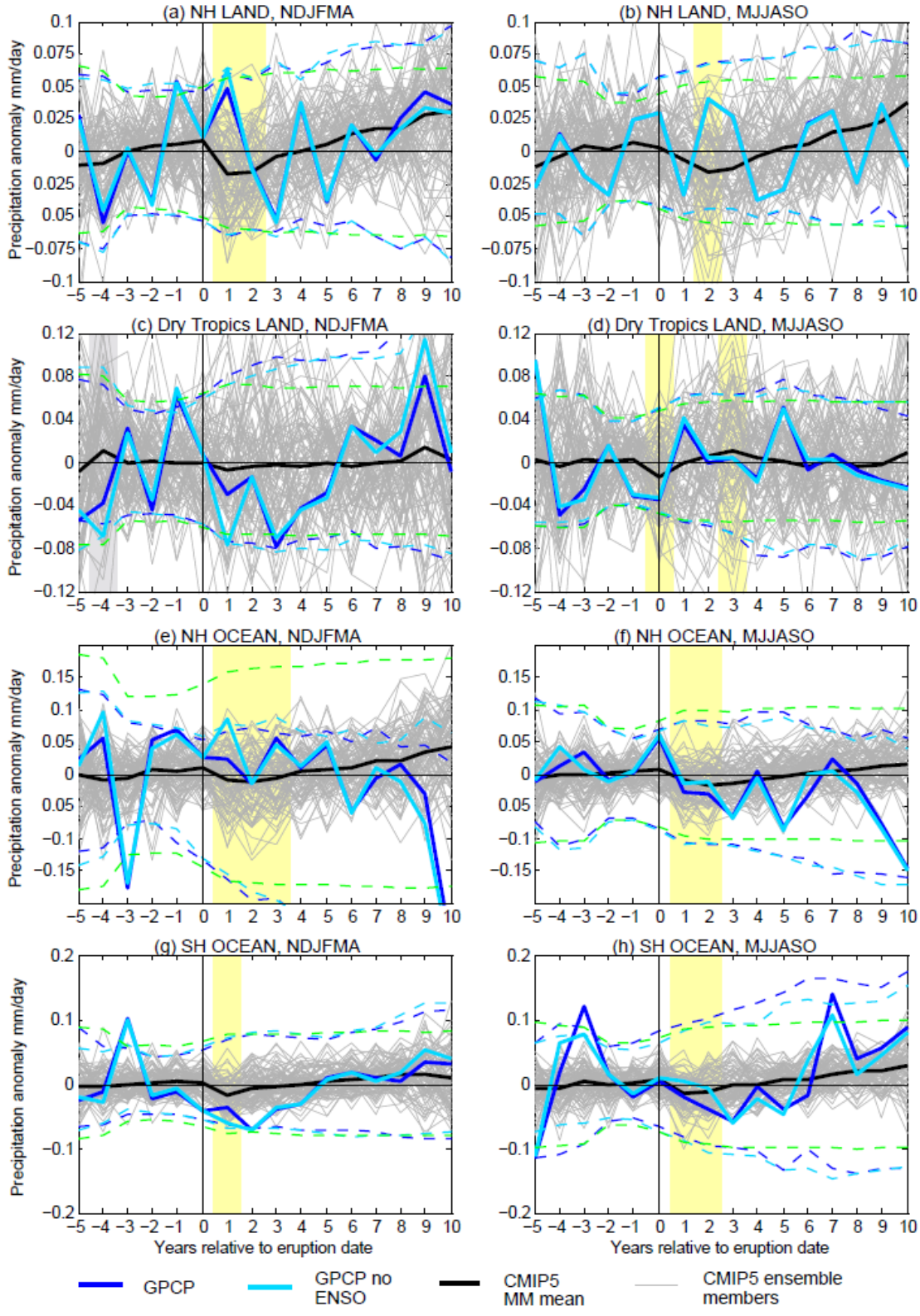

Figure S3.6: as in Figure 3.3 for (a, b) the northern hemisphere extratropical land regions (40-90°N), (c, d) dry tropical land regions, (e, f) northern hemisphere extratropical ocean regions and (g, h) southern hemisphere extratropical ocean regions. (a, c, e, g) are for the boreal cold season, (b, d, f, h) are for the warm season.

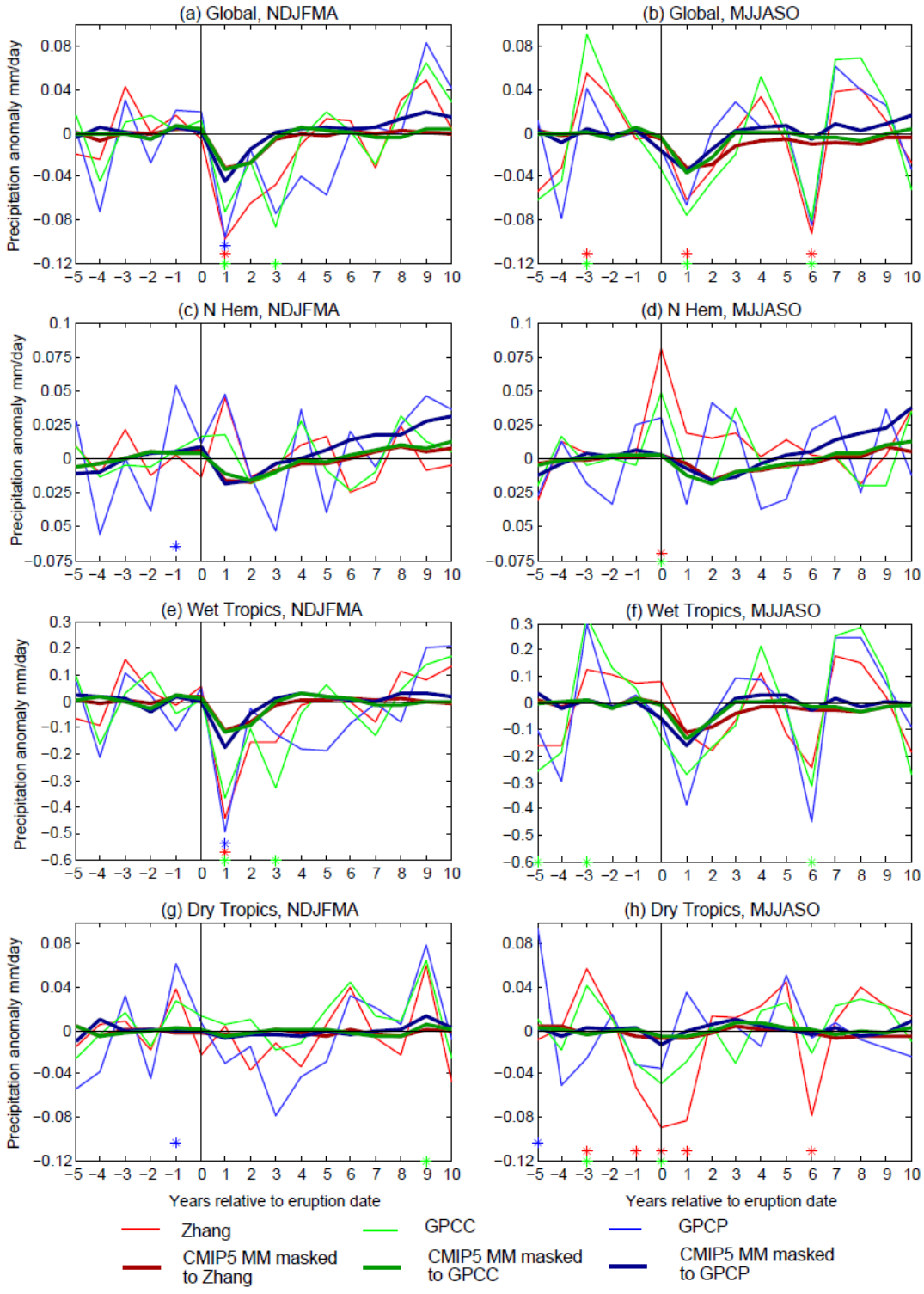

Figure S3.7: Average land precipitation response to volcanic eruptions in three observational datasets with their original spatial coverage, although GPCP is masked to include land regions only. Red is Z07, green GPCC, blue GPCP, thick dark red CMIP5 multi model mean masked according to Z07, thick dark green CMIP5 masked according to GPCC and thick dark blue, CMIP5 masked according to GPCP. Asterisks indicate where observed results are significant at the 90% level, red for Z07, green for GPCC and blue for GPCP. (a, b) Global mean, (c, d) Northern Hemisphere extratropics, (e, f) wet tropics, (g, h) dry tropics. (a, c, e, g) NDJFMA (b, d, f, h) MJJASO.

Finally, Figure S3.8 shows the effect of including the extratropics in the detection analysis when using GPCP. Including the extratropics, and keeping land and ocean as separate elements in the regression equation (light blue) (as was also done in calculating the tropics-only coefficients (dark blue)) results in almost no change compared to using only the tropics, suggesting that the tropics dominate the global results. However, if land and ocean are combined first, so that the regions fed into the equation are the wet tropics, dry tropics, northern hemisphere extratropics and southern hemisphere extratropics, coefficients become much larger for NDJFMA and smaller for MJJASO (pink). The ocean is given more weight when land and ocean are combined than when they are separate, suggesting that at least some of the discrepancy in magnitude of the response between observations and models is coming from the oceans. Further investigation through performing a detection analysis for land regions only, and ocean regions only (not shown) confirms that the ocean regions are responsible for a large part of the disagreement.

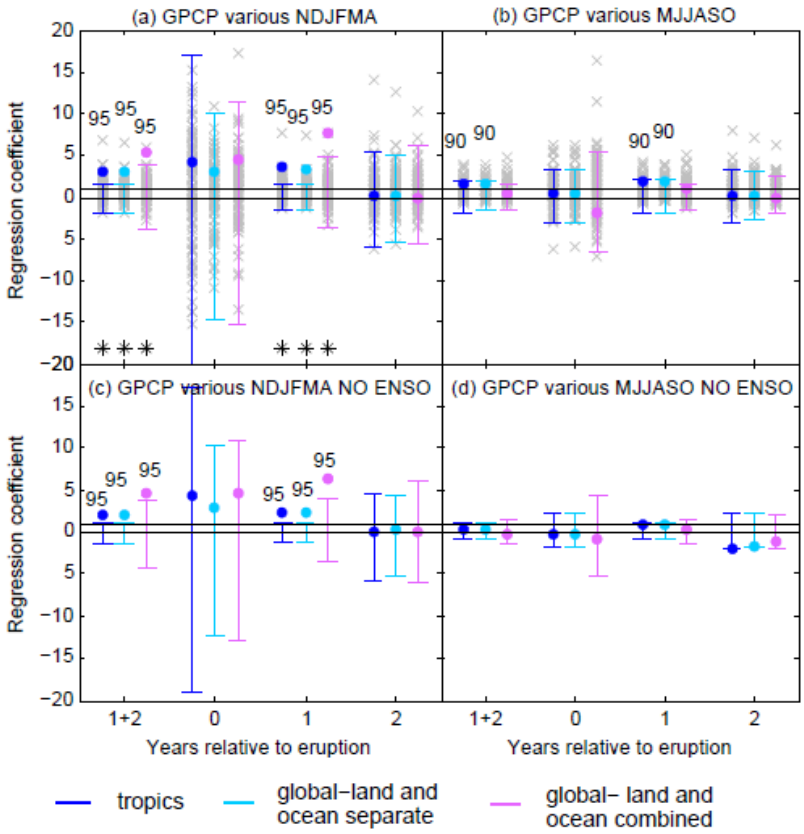

Figure S3.8: as in Figure 3.4 but using only GPCP. Dark blue denotes when the tropics only are used (regions included in the regression equation are wet tropical land regions, wet tropical ocean regions, dry tropical land regions, dry tropical ocean regions.) Light blue is for when the extratropics are included as well as the aforementioned regions, with land and ocean kept separate. Pink is as light blue but land and ocean are combined for each region before being used in the regression equation.

S3.2 Methods details

S3.2.1 Pre-eruption means

Where data availability allowed it we calculated post-eruption precipitation anomalies for each grid cell relative to a 5 year pre-eruption mean. However, when an eruption occurred too close to the beginning of a dataset to allow a full 5 year pre-eruption mean e.g. the 1902 eruption in Z07 or GPCC, or the 1982 eruption in GPCP, we used whatever years were available plus year 0 if it was not much affected by volcanic aerosols (i.e. if the eruption occurs only in the last month or after the season has finished). In the Monte Carlo analysis one eruption per cycle also had to have a short pre-eruption mean to match the analysis for the real eruptions. Finally, we required that there must be at least 2 years of data present to make any pre-eruption mean. This is only relevant to Z07 or CMIP5 masked with Z07 which have incomplete data coverage through time.

S3.2.2 Significance testing for GPCP based on CMIP5

Since GPCP has a relatively short record length (33 years), limiting the reliability of Monte Carlo based significance testing, a second set of confidence intervals were obtained using CMIP5 runs. For each region, the last 33 years of each run were combined into one long time series after converting to anomalies and rescaling each run's standard deviation to the standard deviation of GPCP. This overcomes differences in the magnitude of precipitation totals and variability between different models and the observations. Monte Carlo analysis was then performed on this new time series. (For datasets with unchanging spatial coverage through time (e.g. GPCP and CMIP5 with no observational masking), performing epoch analysis on regional mean time series is equivalent to performing it on a grid cell level first and then making spatial averages (c.f. Section 3.1)). Results were very similar to those where the multi-model mean response was subtracted from each individual simulation first before using it as an estimate of variability.

Chapter 4: The Effect of Volcanic Eruptions on Streamflow

4.1 Introduction

We have seen in the previous two chapters how volcanic eruptions affect precipitation. We now investigate whether the influence of volcanic eruptions can also be seen in observational streamflow records for major world rivers. Rivers are fundamentally important for people, including for domestic use, agriculture, industry and power generation, and for ecosystems. Therefore, understanding any impact that volcanic eruptions have on streamflow is valuable. Whereas gauge based precipitation measurements represent only a localised point, and may not exist in inaccessible areas such as mountain ranges, streamflow integrates surplus precipitation over the whole river catchment, and at the same time reduces noise associated with localised precipitation events. Whilst satellite-based precipitation records also overcome the spatial sampling limitations of gauge based measurements, records are short and are less reliable over high latitudes and complex terrain [*Adler et al*., 2012, *Hegerl et al*., 2014 and references therein]. Records for many rivers are many decades long, and also exist in high latitudes. However, streamflow does not directly reflect precipitation over an area, but rather is the difference between precipitation and evaporation and any changes in storage; for example in snow or ice, including glaciers and permafrost; groundwater; lakes and soil moisture. Human influences such as impoundment in reservoirs, extraction for irrigation or other purposes and interbasin transfers also play a role [e.g. *Nijssen et al*., 2001; *Milliman et al*., 2008].

There are few studies investigating the effect of volcanic eruptions on streamflow. *Trenberth and Dai* [2007] examined the effect of the 1963 Agung, 1982 El Chichon and 1991 Pinatubo eruptions on global streamflow using observational records. They found a significant decrease in global runoff following the Pinatubo eruption, even once the influence of ENSO had been removed, and a moderate decrease following El Chichon. There was also a noticeable runoff decrease following Agung despite an unclear precipitation signal. Simulated spatial patterns of runoff following Pinatubo from a land surface model forced

with observed precipitation matched the precipitation response pattern well, including a drying signal in the monsoon regions and southern Europe.

In response to high latitude eruptions, *Oman et al.* [2006b] found reductions in both modelled precipitation and observed streamflow in the Sahel, including for both the Nile and Niger rivers. These high latitude eruptions were associated with summer cooling over the northern hemisphere land masses, which weakens African and Indian monsoon circulations, reducing Sahelian precipitation. They further suggest that an increase in evaporation associated with reduced cloudiness would amplify the reduction in streamflow.

Finally, in response to the Toba super eruption in 73ka (100 x Pinatubo stratospheric injection of sulphur) *Timmreck et al*. [2012] found a decrease in precipitation and streamflow lasting around 2 years for the Nile, Ganges-Brahmaputra, Mekong, Krishna and Orange river basins in the climate model MPI-ESM. Precipitation and streamflow recovered quickly and were followed by anomalously high precipitation and streamflow 3-5 years after the eruption for the Nile, Ganges-Brahmaputra and to a lesser extent the Orange basins. This increased precipitation response was interpreted as the result of anomalously cold, La Nina-like sea surface temperature anomalies in the equatorial Pacific that developed a few years after the eruption. These were thought to strengthen the Indian monsoon through a shift in the active branch of the walker circulation, whilst the East Asian monsoon was unaffected.

Whilst research on the effects of volcanic eruptions on streamflow is limited, there has been more extensive work on the possible response of streamflow to greenhouse gas forcing, and on past streamflow trends and their causes. Observational studies disagree on whether global streamflow has increased over the last century, with trends sensitive to time period used, river basins included in the study, any gap filling techniques and choice of driving precipitation dataset for studies using land surface models [e.g. *Alkama et al*., 2013; *Milliman et al*., 2008; *Gerten et al*., 2008; *Labat et al*,. 2004; *Piao et al*., 2007 and *Gedney et al*., 2006]. The following discussion is based on results of land surface models driven with observed climate and other factors (e.g. CO_2, land use) unless specified otherwise. Precipitation is the main driver of global runoff trends [*Piao et al*., 2007; *Gerten et al*., 2008]

and inter-annual variability [*Gedney et al*. 2006], whilst spatially, runoff trends match precipitation trends in most places [*Milly et al*., 2005 (GCM based), *Milliman et al*., 2008 (observations), *Piao et al*., 2007, *Dai et al*., 2009 (observations)]. Land use changes, particularly deforestation are the second most important driver of global runoff trends [*Piao et al*., 2007, *Gerten et al*., 2008], and the primary driver in the tropics [*Gerten et al*., 2008]. Increased CO_2 levels also affect runoff by inducing stomatal closure, reducing transpiration, but at the same time cause structural changes such as increased leaf area index, which increase transpiration. The net effect on runoff is study dependent [*Piao et al*., 2007; *Gerten et al*., 2008]. Increasing temperatures tend to decrease runoff through increased evapotranspiration. Irrigation can cause both regional increases or decreases in streamflow depending on whether the source is fluvial or fossil groundwater, but globally its influence is negligible [*Gerten et al*., 2008]. In the Arctic, particularly Siberia, observed runoff has increased more than expected from observed precipitation trends, possibly due to increased melting of snow and permafrost under warmer temperatures [*Dai et al*. 2009; *Adam and Lettenmaier* 2008]. Finally, 'deficit rivers', generally located in dry regions, have undergone greater decreases in observed streamflow than expected from observed precipitation trends due to human consumption, evaporation from reservoirs and inter-basin transfers [*Milliman et al*., 2008]

Multi-model studies generally predict an increase in global runoff over the next century [e.g. *Alkama et al*., 2013; *Nohara et al*., 2006, but not *Arnell and Gosling*, 2013], with increases in high northern latitudes and southern Asia, and decreasing runoff in southern Europe, the Middle East, the Mediterranean coast of Africa and southern North America. Consensus between models is less good over South America and parts of Africa [*Collins et al*., 2013 see Fig 12.24, *Milly et al*., 2005; *Nohara et al*., 2006; *Arnell et al*., 2013, *Alkama et al*., 2013]. Global warming is also expected to affect the annual cycle of discharge for some rivers e.g. causing an earlier spring melt peak for cold snow dominated basins [e.g. *Arora and Boer* 2001; *Nohara et al*., 2006; *Arnell* 2003; *Arnell and Gosling* 2013; *Nijssen et al*., 2001; *Falloon and Betts* 2006], whilst an increased proportion of rain compared to snow in winter can increase winter flow and reduce the spring melt peak in others [*Nijssen et al*., 2001].

Overall, research into the effects of volcanic eruptions on streamflow is limited compared to research examining the influence of other factors and compared to research on the precipitation response to eruptions. In this chapter the streamflow response to volcanic eruptions is investigated for 50 large drainage basins spread across the world. The analysis builds on previous studies by examining the average streamflow response across multiple eruptions and examining many rivers, both individually and in combination with other nearby rivers undergoing the same sign of precipitation response, in order to reduce noise. Significance of results is then tested using a Monte Carlo technique.

4.2 Data

Streamflow data were obtained from the *Dai et al*. [2009] dataset, a version of which was also used by *Trenberth and Dai* [2007] for their research into the effects of volcanic eruptions on global streamflow. This dataset contains monthly data from the furthest downstream stations for the world's largest 925 ocean-draining rivers, together covering 80% of the ocean-draining land area, and accounting for 73% of global runoff. Data are included from various sources (see *Dai et al*. [2009] for details). There are two versions of this dataset; one with no infilling of missing data, except with scaled data from neighbouring stations for a limited number of rivers; and the other where all additional gaps between 1948 to 2004 are infilled through linear regression with streamflow simulated by a land surface model forced with observed precipitation and other meteorological variables [see *Dai et al*. 2009]. Here the non-infilled version is used, which extends further back in time than the infilled version for many rivers, and even into the 19th century for some. The average record length between 1900 and 2006 for the largest 10, 50 and 100 rivers respectively is to 79.9, 58.9 and 54.2 years [*Dai et al*. 2009].

Large river basins with data for at least 2 eruptions and at least 40 years of continuous data with no major gaps were chosen for analysis. These are shown in Figure 4.1 and detailed in Table S4.1. Since data for the Nile were only available between 1973 and 1984 in the *Dai et al*. [2009] dataset, Nile data from the RIVDIS dataset [*Vorosmarty et al*., 1998] were used instead, covering the period 1869-1984, although a long record was only available for a

station near the Aswan dam, which is a considerable distance from the river mouth. Overall, data for 50 rivers were use. Details including location of gauging station, annual mean discharge, basin size, record lengths, flow regulation indices and notes on any inhomogeneities are detailed in Table S4.1.

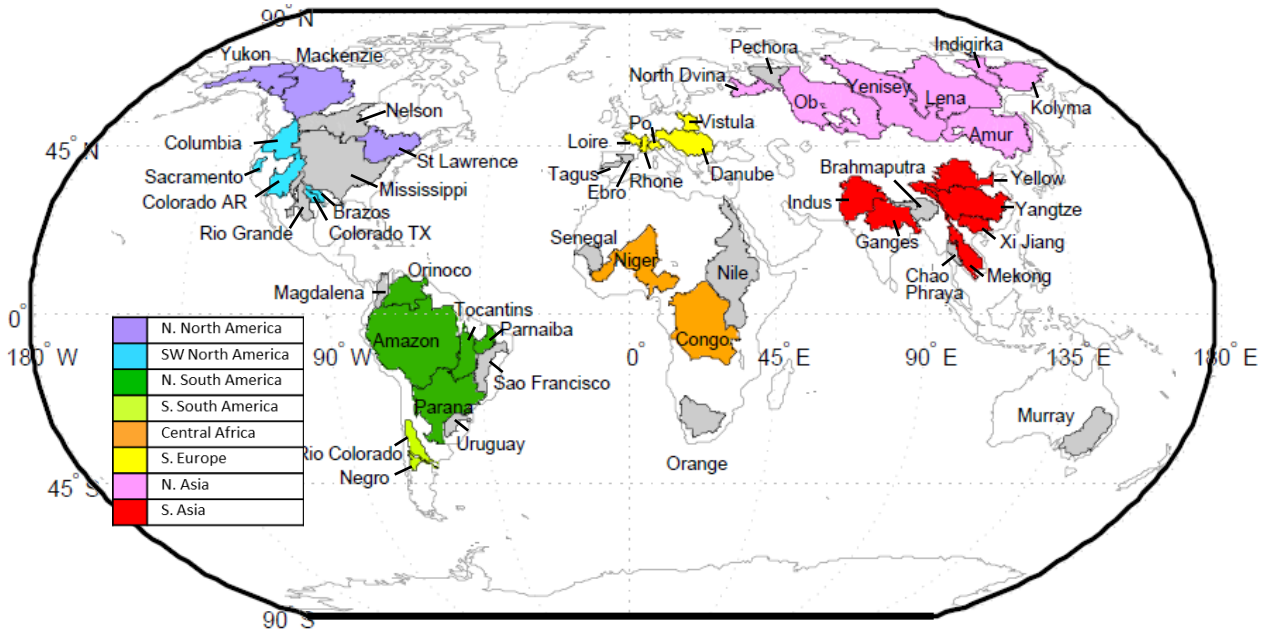

Figure 4.1: Drainage basins used in this study. Colours indicate the region to which basins are allocated for the regional analysis described in Section 4.3.2.

Dams have been found to affect seasonality of streamflow, for instance by increasing winter low flow and reducing spring or summer peak flow in high latitude basins that are influenced by storage in snow and ice [e.g. *Adam and Lettenmaier*, 2008]. Nevertheless, for most rivers dams seem to have little influence on annual flow compared to climate variations [*Dai et al*., 2009; *Milliman et al*., 2008; Adam and *Lettenmaier*, 2008]. However, there are river basins, particularly in dry regions, with very high flow regulation indexes (see Table S4.1 for definition of flow regulation index) and high levels of irrigation, or from which water has been transferred to neighbouring basins, for which anthropogenic influences have caused a significant decrease in flow [*Milliman et al*., 2008]. Since annual flow is used here, rather than seasonal, the influence of dams should not be problematic for most rivers. Nevertheless, the monthly and annual time series of flow for each river have been examined for possible dam related inhomogeneities, and notes added to Table S4.1. Where monthly flow regimes

undergo a discontinuity over time but annual variability and mean discharge do not, this was not considered problematic. However, where annual variability changes drastically post-dam construction such that streamflow variations no longer reflect climate variability, then this is an issue. The most extreme case of this for the rivers used here is the Nile post-Aswan Dam construction (Figure 4.2). In this case post-Aswan dam data were not used (i.e. 1960 onwards). Other rivers did not show such an extreme change, although some data were also excluded from the Sao Francisco. An inhomogeneity that occurs during a period in which there are no eruptions will not affect the average volcanic response, but will affect confidence intervals obtained through Monte Carlo analysis (detailed in Section 4.3.1). Finally, the construction of a large reservoir at the time of an eruption could also be problematic if it causes a temporary reduction in flow whilst the reservoir fills. Here regional results in which several rivers are combined (described in Section 4.3.2) were repeated excluding highly regulated rivers. It was assumed that irrigation would have less of a confounding influence on results since it would affect long terms trends and intra-annual variability more than interannual variability.

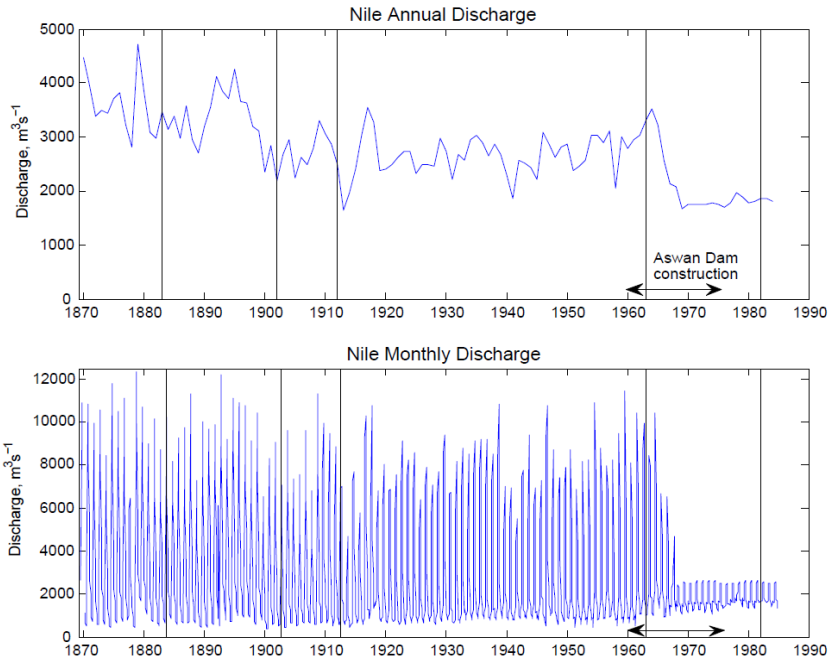

Figure 4.2: Annual (top) and monthly (bottom) discharge for the Nile River for a station near the Aswan Dam. Vertical lines denote timing of eruptions. Horizontal arrow indicates the time period over which the dam was built: construction commenced in January 1960, the first dam construction phase was finished in 1964 and the reservoir started filling, the High Dam was completed in July 1970 and the reservoir finished filling in 1976. There is a clear change in flow regime before and after dam construction in both monthly and annual data.

4.3 Methods

4.3.1 Epoch analysis

Epoch analysis (i.e. averaging across multiple eruptions) was used as described in the previous chapters. For each river and eruption, anomalies for post eruption years were calculated relative to a 5 year pre-eruption mean. Where less than 5 years of data were available to make a pre-eruption mean, the available years were used, down to a minimum of 2. Where only 1 year of data was present, year 0 was also included to make up the pre-eruption mean. Post-eruption anomalies were calculated for every year after the eruption until year 7 to avoid complications of overlap with the following eruption. Results were then averaged across all eruptions for a given river, up to a maximum of 6 eruptions (the most recent 6 in Table 2.1 Chapter 2). The analysis is based on annual data as described in previous chapters, i.e. year 1 is defined as starting 3 months after the eruption date (see also Table 2.1, Chapter 2). Using annual data minimises the effects of dams (see above) and means that each year will contain both snow building and melt phases. However, for eruptions for which year 1 starts in winter, the discharge for one year will reflect some of the previous year's precipitation, causing a slightly delayed response. Where standardised results are presented, epoch analysis results for a given river are divided by its standard deviation based on a time series of water years (i.e. October through to September). This makes results for rivers with large differences in mean flow comparable.

A Monte Carlo technique was again used to test significance. For each river the analysis was repeated 10,000 times choosing the same number of random eruption years as there are real eruptions. This number varies between different rivers. Where a real eruption has a short pre-eruption mean, a short pre-eruption mean was also applied for the equivalent eruption in the Monte Carlo analysis. Where there were missing values in either the post-eruption years or the pre-eruption mean for the real eruptions, the equivalent years were also assigned as missing values for the equivalent eruption in the Monte Carlo. The number of eruptions with data for each year relative to year 0 was then counted, and where the Monte Carlo iteration did not have enough data for a given year, that iteration was not used for that year. Overlap

between random eruption time periods was permitted. Relatively complete continuous parts of the time series for each river were used in the Monte Carlo. Where there were two long continuous parts of a river record with a substantial gap in the middle, random eruptions were not chosen in the gap. The 10th-90th percentiles of the results for each year were calculated and yield the 10-90% range of the null hypothesis of no change in river flow. Results outside this range are considered significant. The 10-90% range is chosen because river data is noisy, but the 5-95% range is also shown for comparison in some plots.

4.3.2 Regional analysis

Since streamflow at the level of the individual basin is noisy, regional results were also calculated by combining drainage basins that are geographically close to each other and that undergo the same sign of CMIP5 multi-model mean simulated precipitation response to eruptions (Figure 4.1 and 4.5, Table S4.1). The CMIP5 response was used to define regions rather than the observed response (Figure 4.6) both to avoid circularity, and because the latter is the average over only 5 eruptions and is noisy, whilst the CMIP5 response is the average over 686 eruptions (98 runs x 7 eruptions), allowing the volcanic signal to be isolated much more effectively. These regional streamflow results were calculated in two ways, firstly in absolute values of river flow (m^3s^{-1}), where epoch analysis is performed on each individual river in a particular region and then the sum of the results is calculated across all the rivers. This effectively integrates streamflow over the region, and gives more weight to large rivers. The second method involves standardising the epoch results for each river, before averaging across them. This gives an indication of the behaviour of the average river in that region, and avoids results being dominated by large rivers, such as the Amazon.

Performing Monte Carlo analysis for regional results was more complicated than for individual rivers due to varying record lengths for different rivers covering different numbers of eruptions. This precluded performing the analysis on a regional mean since variability would change over time. Instead, for each Monte Carlo iteration the average response across the random eruptions was calculated for each river first and then averaged or added across the rivers depending on whether the absolute or standardised version of the analysis was

being performed. For each river, the same number of random eruptions was chosen as the number of real eruptions the river has data for. Where, for example, several rivers in a region have data for the same three real eruptions, in the Monte Carlo analysis three random eruptions for which all rivers had data were chosen. If one of these rivers has a much shorter record than the others, but still covers the most recent 3 eruptions (e.g. one river extends back to 1956 and the others extend back to 1920), then the shorter river limits the range of years from which a random eruption can be chosen. Where a river severely limited this range due to a short record or a lot of missing data, it was not included in the regional analysis. If, for example, one river had data for 5 eruptions and the rest in the same region had data for 3, then 3 random eruptions were chosen from the timespan common to all the rivers and the remaining 2 were chosen from anywhere in the timespan of the river with the long record. If this corresponds to when the other rivers also have data then this data for the other rivers was ignored.

4.3.3 ENSO and the NAO

ENSO also has an impact on streamflow for some rivers. Figure 4.3 indicates correlation coefficients between ENSO (using the cold tongue index (CTI) which extends back to 1845, as in previous chapters) and streamflow based on water years for all basins used in the analysis, indicating where the correlation is significant. The 3 years following an eruption (and year 0 where more than a couple of months were volcanically influenced) were excluded when calculating the coefficients to avoid confusion between the volcanic and ENSO signals. Wherever $p < 0.1$, the influence of ENSO was removed from the streamflow records through regression. The spatial pattern of the influence of ENSO on streamflow generally looks much as expected from correlations with instrumental precipitation records using water years (using GPCC, a 2.5° gridded gauge based dataset, see Section 2.2.1 (not shown)).

Figure 4.4 shows correlation coefficients between the NAO (for December through to March (DJFM)) and streamflow (in water years) for non-volcanically influenced years (as for ENSO). The Hurrell station based index was used for the NAO [*Hurrell et al*., 2013] and is

based on the difference of normalised sea level pressure between Lisbon, Portugal and Stykkisholmur/Reykjavik in Iceland. It extends back to 1864 thereby covering the time period of all the river records used in the analysis (apart from the Loire that starts in 1863).

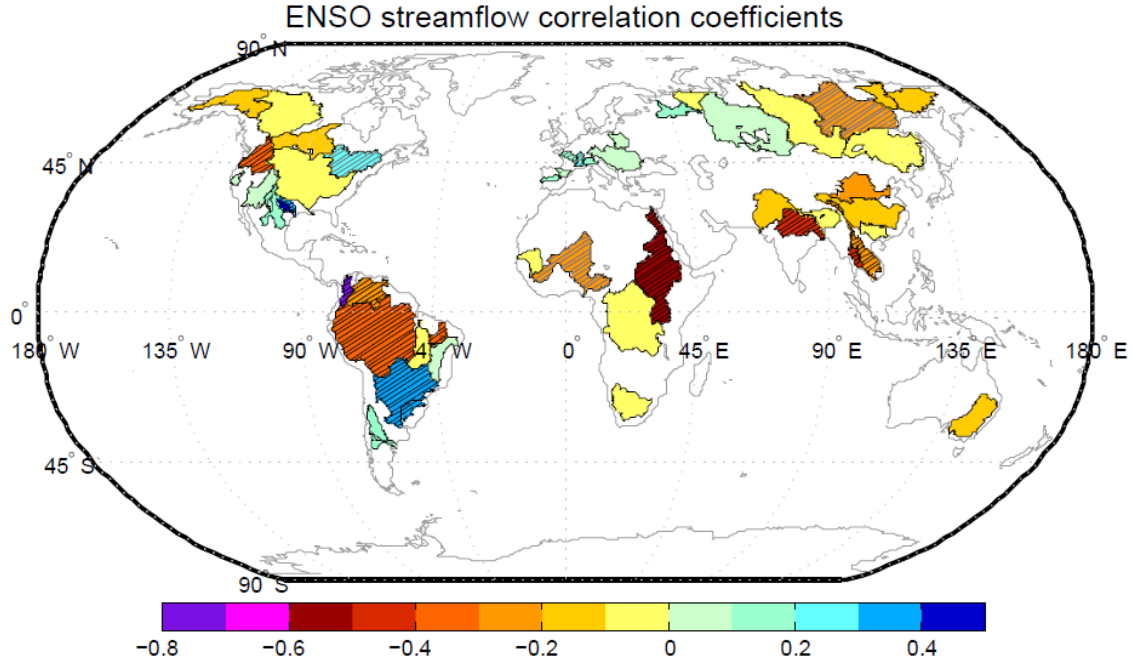

Figure 4.3 Correlation coefficients between ENSO and streamflow using water years. Hatching indicates a significant relationship, black hatching at the 95% level and grey the 90% level. Note that the length of time series used for the correlation is different for each river depending on its record length (see Table S4.1).

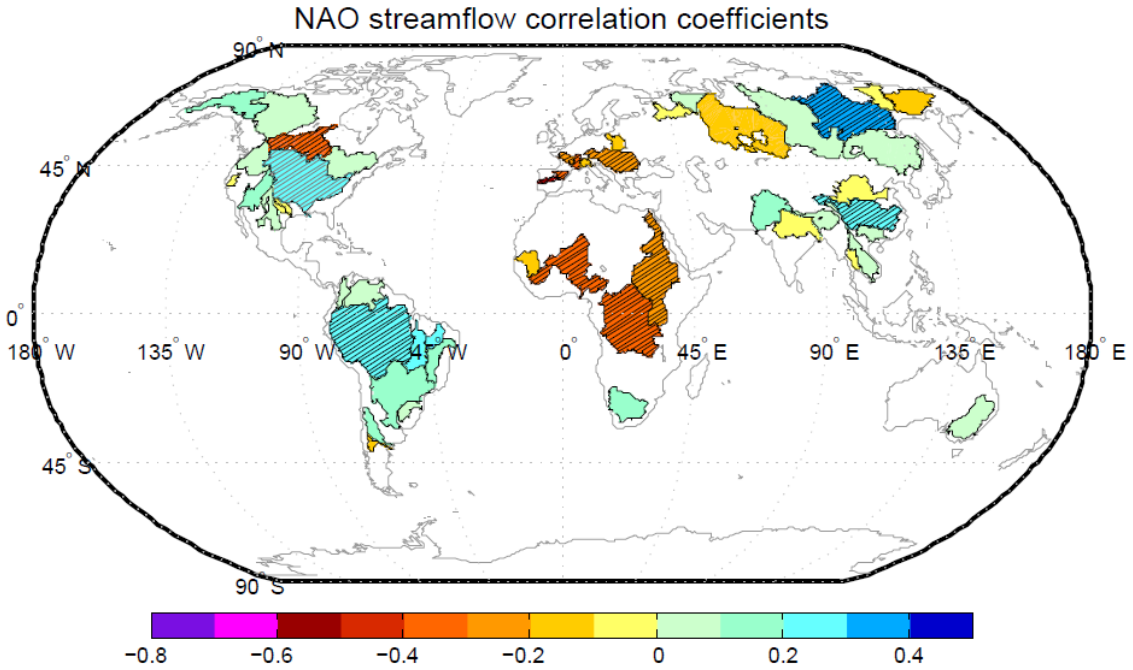

Figure 4.4 as for Figure 4.3 but for the NAO in DJFM correlated against water years streamflow

The influence of the NAO was not regressed out of the streamflow records, because a positive phase of the NAO is thought to be part of the observed climate response to volcanic eruptions [e.g. *Robock and Mao*, 1992, 1995]. Streamflow for basins in southern Europe is significantly negatively correlated with the NAO, as expected from patterns of correlation between observed water years precipitation (using GPCC) and DJFM NAO (not shown). Elsewhere, correlation coefficients for streamflow with the NAO are similar to those for precipitation, although significance is exaggerated for streamflow, perhaps because it integrates over a larger area, improving signal to noise ratios. Although unexpected, the significant negative correlations between streamflow and the NAO in the Central African basins agrees with findings for austral summer precipitation for southern Africa in *McHugh and Rogers* [2001]. The significant positive correlation of the NAO with Amazon streamflow is also unexpected, but the time series do appear well correlated (not shown), although more investigation would be required to explore whether there is a plausible physical mechanism

4.4 Results

Figure 4.5 shows the annual mean CMIP5 multi model mean precipitation response averaged across 7 eruptions (1861, 1883, 1902, 1912, 1963, 1982, 1991) with the drainage basins used in this analysis overlaid in order to give an indication of where a volcanic streamflow response might be expected to exist and in which direction. The CMIP5 runs used are the historical 'ALL' forcing runs detailed in Chapter 3 Table S3.1 (i.e. 98 individual runs from 19 models). The precipitation response over land is strongest in the first year following the eruptions and has mostly faded away by year 3. A significant decrease in precipitation can be seen over the Amazon and neighbouring basins in years 1 and 2, over central African basins, including the Congo, Nile and Niger in year 1, which has mostly ceased by year 2, over northern Asian basins in years 1-3, SE Asian basins in year 1 and some northern North American basins in years 1, 2 and to a certain extent 3. In contrast, rivers in southern Europe, southern South America and SW North America become significantly wetter following eruptions.

The observed precipitation response averaged across 5 eruptions using the GPCC dataset (see Section 2.2.1) is shown for comparison (Figure 4.6). Over African, South American and SW North American basins the observed precipitation response largely matches the CMIP5 response, although the area of drying extends further south over Africa in the observations. The northern North America and high latitude Asian response is more mixed (note the latter area is largely interpolated), whilst a large portion of SE Asia gets wetter rather than drier.

However, streamflow is not solely determined by precipitation, but is rather precipitation minus evaporation plus changes in storage. Figure 4.7 shows the precipitation (P), evaporation (E) and P-E response for year 1 following the most recent 6 eruptions in Table 2.1 using an ensemble of the 10 historical 'ALL' forcing HadCM3 runs in Table S3.1 from the CMIP5 archive. The precipitation response in HadCM3 (Fig 4.4a) appears similar to that in the CMIP5 multi model mean (Fig 4.3). The response is strongest in year 1 and fades away thereafter, largely disappearing by year 2 over South America and Africa, and year 3 elsewhere over land (not shown). Evaporation decreases over most land regions following eruptions consistent with a reduction in incoming solar radiation due to reflective sulphate aerosols. However, there is increased evaporation over the Middle East, Sahara, SW North America and Southern South America, all of which are dry regions that undergo a post-volcanic increase in precipitation, increasing the availability of moisture for evaporation. The evaporation response fades away by year 4 (not shown). The response of P-E should be most relevant for the post-volcanic streamflow response. It appears to be dominated by precipitation (pattern correlation = 0.91), although in some areas the P-E response is less clear than the precipitation response (e.g. northern Asia, SE Asia), or has reduced in magnitude (e.g. over the African drainage basins and the Amazon) and in a few places has changed sign (e.g. over the North Dvina, Rio Colorado, Kolyma and Murray-Darling). This may make the response of streamflow over these regions less clear than the precipitation response alone might suggest. However as the areas that dry or get wetter following eruptions are similar overall when P is used rather than P-E, we use P to define regions for simplicity.

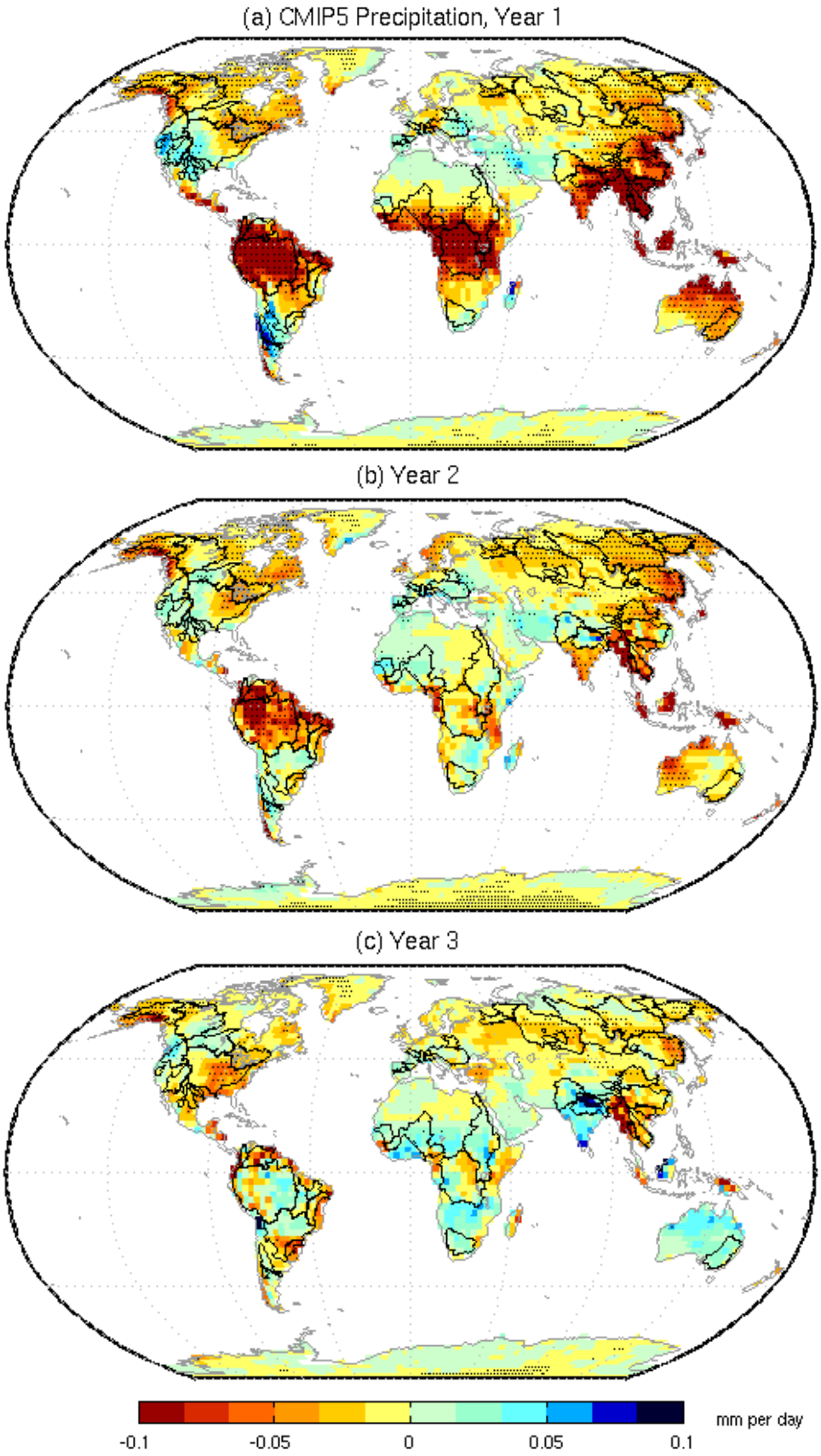

Figure 4.5 CMIP5 multi model mean precipitation response averaged across 7 eruptions for years 1-3 after the eruptions. Drainage basins used in the analysis are overlaid. Stippling indicates significance at the 90% level using a Monte Carlo technique.

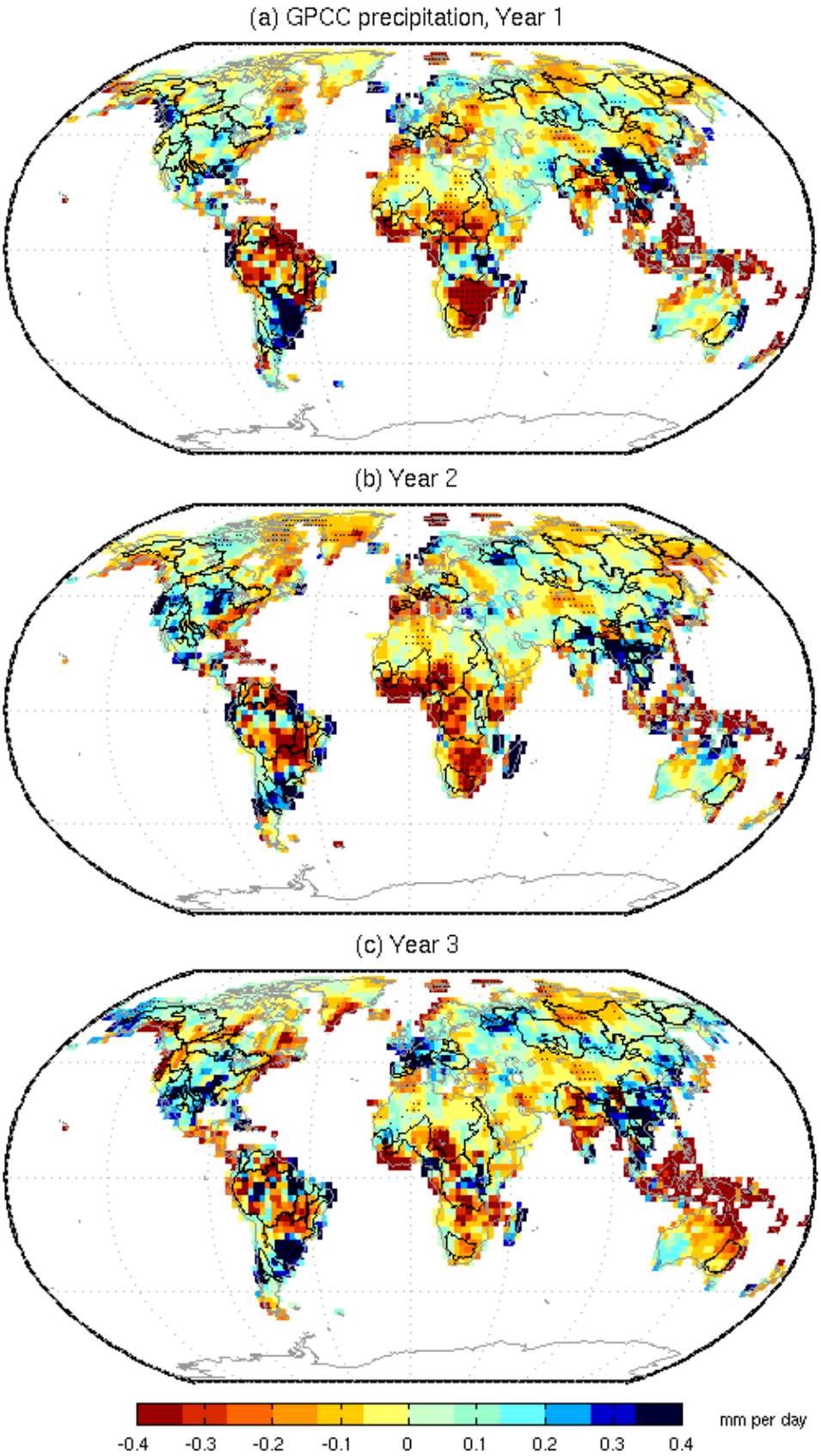

Figure 4.6: Observed precipitation response averaged across 5 eruptions using the GPCC dataset for years 1-3. Drainage basins used in the analysis are overlaid. Stippling indicates significance at the 90% level using a Monte Carlo technique. Note that data over the high latitude Asian basins are largely interpolated. Note different colour scale to Figure 4.5.

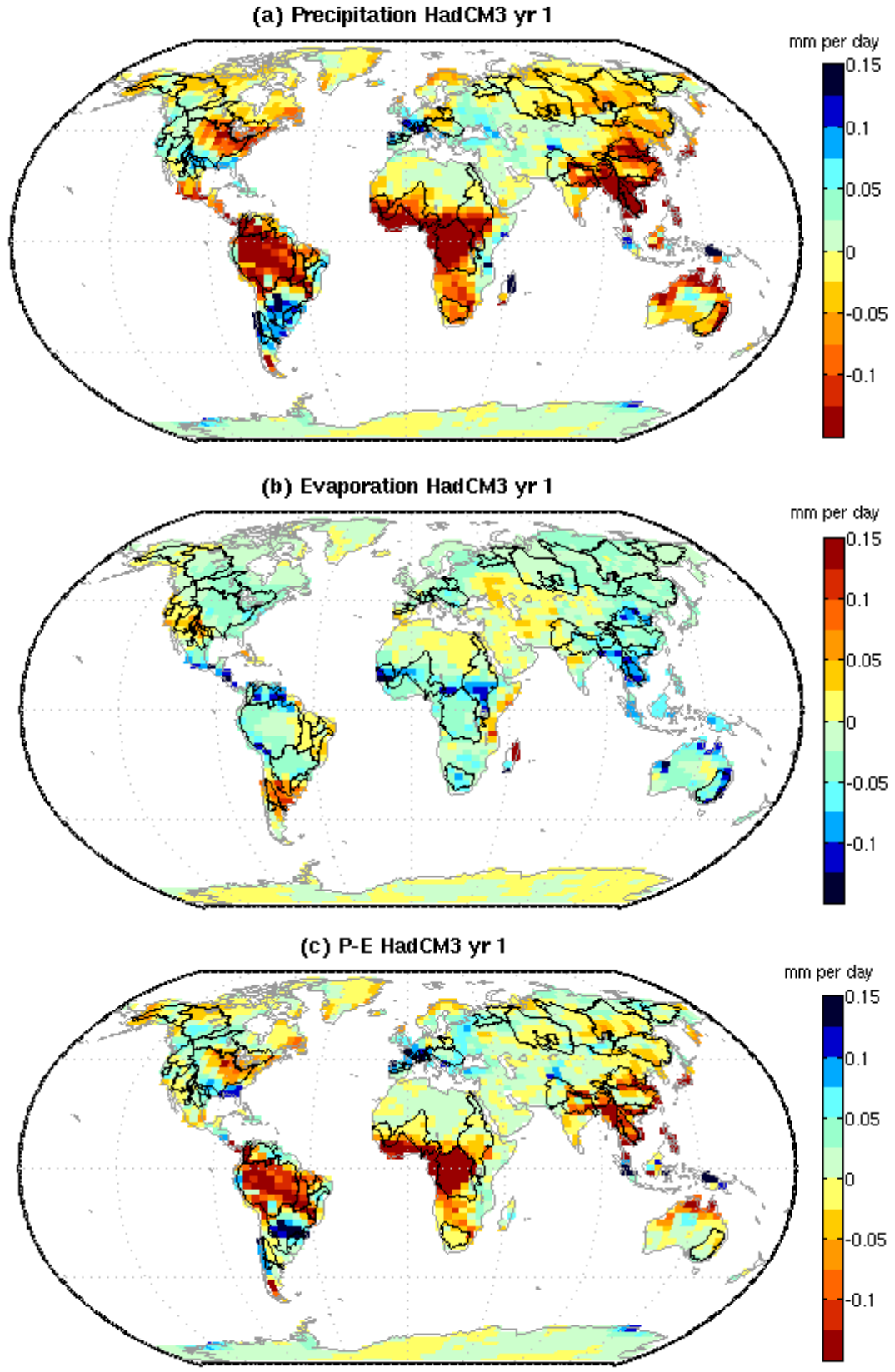

Figure 4.7: Response of a) precipitation, b) evaporation and c) precipitation minus evaporation for the first year following 6 volcanic eruptions in an ensemble of 10 HadCM3 runs. Note that the colour scale for evaporation is inverted.

Figure 4.8 shows the response of streamflow for each basin averaged across multiple eruptions for years 1-3 following the eruptions. (The eruptions used for each river are indicated in Table S4.1). Results are standardised and the influence of ENSO is removed for rivers with which it is significantly correlated as described in sections 4.3.2 and 4.3.3 respectively. Whilst streamflow might be expected to largely reflect the observed precipitation response (Figure 4.6), it should be pointed out that results for each river basin are based on different combinations of eruptions depending on data availability and so may be less consistent than expected. Rivers in central Africa experience decreased streamflow following eruptions as expected from the modelled and observed precipitation response patterns and HadCM3 simulated P-E. Northern Asian rivers tend to undergo a weak decrease in flow in year 2 and a variable response in other years, whilst Southern Asian rivers also undergo mixed response. This could be partly due to a mixed P-E and observed precipitation response over these regions. In South America the Amazon, Tocantins and Parnaiba experience a decrease in runoff lasting 2 years, whilst more southerly basins experienced increased runoff as expected from both modelled and observed P and HadCM3 simulated P-E. North American rivers undergo a mixed response, whilst over southern Europe there is a decrease in streamflow in years 1 and 2. Whilst this southern European response is the opposite of the CMIP5 and HadCM3 precipitation response, it matches the observed precipitation response and is consistent with a positive NAO response (Figure 4.4), which has been found in observational studies but is not well captured by climate models [e.g. *Stenchikov et al*., 2006; *Driscoll et al*. 2012, *Charlton Perez et al*. 2013]. Figure 4.S1 shows that if the influence of ENSO is not removed, overall patterns of basins that get wetter or drier are broadly the same, but the response of some individual basins switches sign or changes magnitude.

Timmreck et al., [2012] found a noticeable overshoot in streamflow in years 3-5 following the initial post-eruption decrease for several catchments in Africa, tropical Asia and Australia, including for the Nile, Ganges-Brahmaputra and Orange in model simulations of the very large Toba eruption in 73ka. It is not clear whether this overshoot can also be seen for individual rivers in these regions in the data examined here due to the noisy nature of

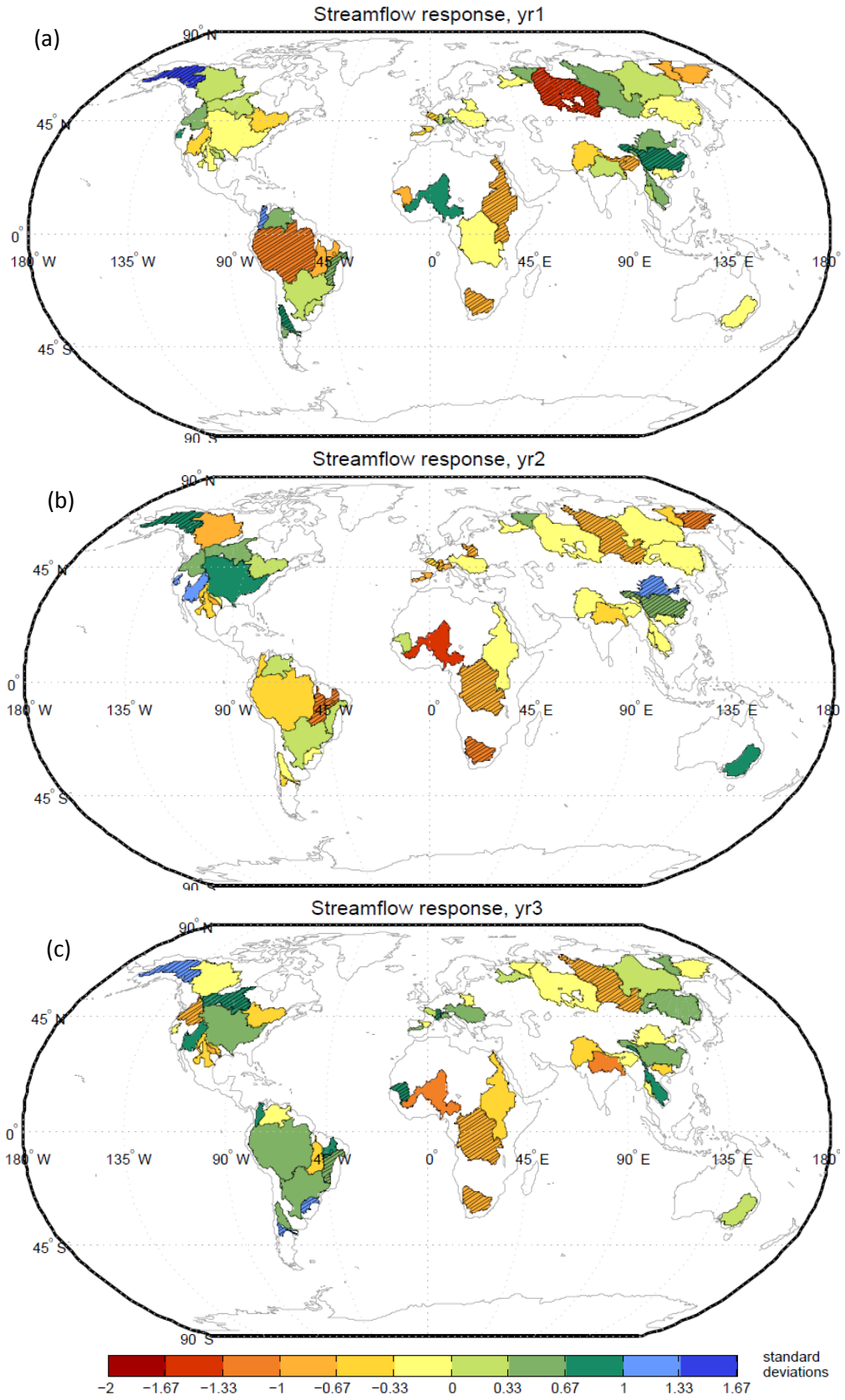

Figure 4.8 Average streamflow response across multiple eruptions for individual rivers for years 1-3, expressed in standard deviations. Hatching indicates where results are outside of the 10-90% range of natural variability. The influence of ENSO is removed for rivers with which it correlates significantly (see Figure 4.3).

results (not shown), although the results suggest a possible delayed peak in streamflow for some rivers e.g. in year 6 for the Orange, year 7 for the Niger, year 4 for the Senegal and year 8 for the Brahmaputra.

Figure 4.9 shows the response of the Amazon, Congo and Nile to volcanic eruptions. These are all rivers undergoing a significant streamflow response in the direction expected from the CMIP5 simulated and observed precipitation response. The Amazon undergoes a significant decrease in year 1 and has returned to normal by year 3. The Nile also responds in year 1 and takes until year 4 to recover. For both these rivers the response is larger if the influence of ENSO is not removed. Finally the Congo responds more slowly, reaching its minimum in year 2 and returning to normal by year 5

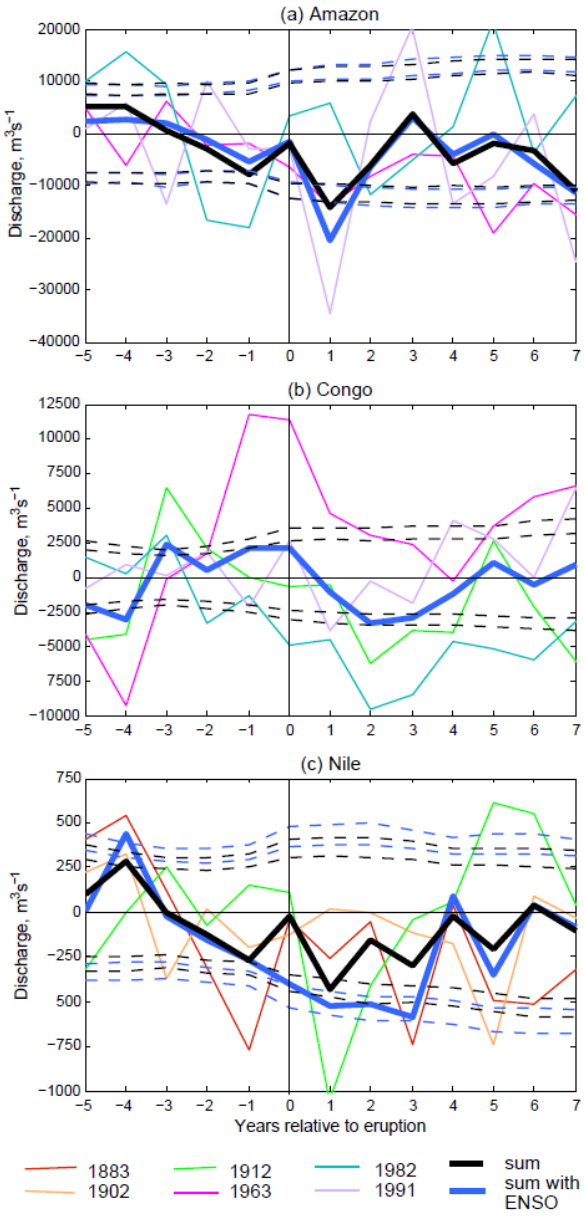

Figure 4.9: Response of a) the Amazon, b) the Congo and c) the Nile rivers to volcanic eruptions. Thick black line shows the average response across all eruptions for each river, thin lines are the response to individual eruptions. Thick blue line is the average across all eruptions but without removing the influence of ENSO (as the Congo is not significantly correlated with ENSO, ENSO is not regressed out). Dashed lines indicate confidence intervals for the average response, inner lines 10-90%, outer lines 5-95%, black without ENSO, blue with ENSO. Vertical black line indicates timing of eruptions.

Streamflow generally responds to volcanoes on roughly the same timescale as precipitation. Due to the noisy nature of results, it is not possible to establish whether there is a delayed response for some rivers. A delayed response might occur where there is storage in snow and ice and behind reservoirs. It also takes time for precipitation to be transferred to the river mouth e.g. 3-4 months for the Amazon, but only one month or less for the Brahmaputra, Ganges, Mississippi and Mekong [*Dai and Trenberth*, 2002; *Marengo et al*., 2005].

The overall number of rivers in Figure 4.8 that undergo a significant response appears limited. Streamflow data are noisy and record lengths are often fairly short, encompassing a small sample of eruptions. Table 4.1 shows the number of rivers undergoing a significant response compared to the number expected by chance. Since the 10-90th percentiles are used to assess significance, 20% of rivers would be expected to undergo a significant response by chance. Rivers are also grouped according to level of human influence and by size of drainage basin in order to see whether this affects the likelihood of significance. When all rivers are considered the number of rivers with significant results is close to or just slightly above that expected by chance (22% in years 1 and 3 and 26% in year 2). When rivers are split into more natural or humanly influenced groups, using a regulation index of 20% as a cut-off between the two, the less regulated group have a higher percentage of significant results in years 1, 2 and 1+2 combined than expected by chance, reaching a maximum of 34.5% in year 2. The highly regulated rivers have fewer significant results than expected by chance in years 1 and 2, but more than expected in year 3. This could either be due to noise, or a more delayed response through the influence of reservoirs. Finally, a greater proportion of larger basins undergo a significant response compared to small basins. This could be because they integrate precipitation over a larger area, reducing noise. Repeating the analysis without removing the influence of ENSO makes little difference to the proportion of basins with significant results. Overall, the clearest results occur in the more natural and larger rivers, which increases confidence that river flow is indeed impacted by volcanic eruptions.

However, the approach of counting the number of rivers with significant results is not ideal for a number of reasons. Firstly, based on the precipitation response patterns we do not expect all rivers to undergo a response to volcanic eruptions. Secondly, spatial

autocorrelation is a problem, especially where many small basins are clustered into a relatively small space, such as in Europe. Thirdly, not all basins are equal; smaller basins are likely to have smaller signal to noise ratios, reducing the chance of significant results. This is also the case for rivers with data for fewer eruptions.

Table 4.1: Number of basins with significant responses for years 1 to 3 and years 1 and 2 combined following eruptions.[a]

Basin type	yr1	yr2	yr3	yrs 1+2	Number expected by chance
all (50)	11 (22%)	13 (26%)	11 (22%)	13 (26%)	10 (20%)
natural (29)	8 (27.6%)	10 (34.5%)	5 (17.2%)	8 (27.6%)	5.8 (20%)
human (17)	2 (11.8%)	2 (11.8%)	6 (35.3%)	4 (23.5%)	3.4 (20%)
big + medium (28)	8 (28.6%)	8 (28.6%)	7 (25%)	10 (35.7)%	5.6 (20%)
small (22)	3 (13.6%)	5 (22.7%)	4 (18.2%)	3 (13.6%)	4.4 (20%)
Regions standardised (8)	3 (37.5%)	3(37.5%)	1 (12.5%)		1.6 (20%)
Regions absolute (8)	2 (25%)	2 (25%)	1 (12.5%)		1.6 (20%)

[a] Significance is assessed using the 10-90% confidence intervals from a Monte Carlo technique. Numbers in brackets are percentages; 20% of rivers would be expected to have significant results by chance. Pink text indicates where more than 20% of rivers are significant; yellow highlighting more than 30%. 'All' denotes all 50 rivers, 'natural' represents rivers with regulation index <20%, 'human' is rivers with regulation indexes >20%, 'big' rivers are those with basin areas represented by the gauging station over 800,000 km^2, 'medium' those between 500,000 and 800,000 km^2 and 'small' less than 500,000 km^2. Rows with 'regions' in the heading represent the number of regions undergoing a significant response (out of 8) for the 'standardised' and 'absolute' versions of the regional analysis. Regional results are based on the black lines in Figure 4.10 and 4.11. Numbers in brackets under 'basin type' are the number of rivers that fall into each category (or the total number of regions for the last 2 rows). 'Expected by chance' is the number of rivers (or regions) expected to be significant by chance for each category.

To address this and to improve signal to noise ratios, neighbouring basins undergoing the same sign of CMIP5 multi-model mean simulated precipitation response were combined as described in Section 4.3.2 and shown in Figure 4.1. Figure 4.10 shows results for the standardised version of the analysis, in which each river has a standard deviation of 1 and a mean of 0, and the average response is taken across the epoch analysis results for them all. Results for many of the regions are significant, albeit at the 80% level. Rivers in northern South America, central Africa and in High latitude Asia undergo a significant decrease in

discharge at the 80% level (90% for northern South America) as expected from the CMIP5 precipitation response. Results for northern South America were repeated without the Parana since it has a higher regulation index (28%) than the other rivers, whilst in HadCM3 precipitation increases over its basin post-eruption. This resulted in a larger average decrease in flow over the region, although levels of significance were the same. Rivers in southern South America undergo a marginally significant increase in flow in years 1 and 3, whilst south-western North American rivers undergo a significant increase in streamflow in year 2 when small basins are excluded, and an insignificant increase when they are not, again consistent with the sign of the modelled precipitation response. Over Europe streamflow decreases in years 1 and 2 and then increases in years 3-5. This initial decrease is consistent with a positive NAO-like pattern as discussed above. Over southern Asia there is a weak increase in streamflow but this is not clear and is sensitive to the choice of rivers included (not shown). Excluding the more humanly influenced rivers does not make the results for southern Asia any clearer. Finally, over northern North America results are noisy and insignificant. Table 4.1 shows that a higher proportion of results are significant when rivers are grouped into regions in this way rather than analysed individually (37.5% based on the black lines in Figure 4.10 in years 1 and 2) which is also higher than expected by chance.

Using absolute values (i.e. not standardised) and taking the sum across the epoch results for all the rivers in a region effectively integrates streamflow over that region. However, where one river has particularly high discharge it dominates results. Results using absolute values are generally similar to the standardised versions (Figure 4.11). There is still a significant drying response over central Africa and northern South America and a significant increase in streamflow in southern South America and SW North America. Over northern North America the response remains insignificant. Excluding the Parana makes little difference to results in northern South America since it is small compared to the Amazon, which by far dominates the response in this region. Limiting the analysis to only big basins in SW North America does not make much difference to the overall shape of the response, but renders it slightly insignificant. Over northern Asia the response is still a decrease, but is no longer significant and appears noisier. Southern Asia undergoes a significant increase in streamflow

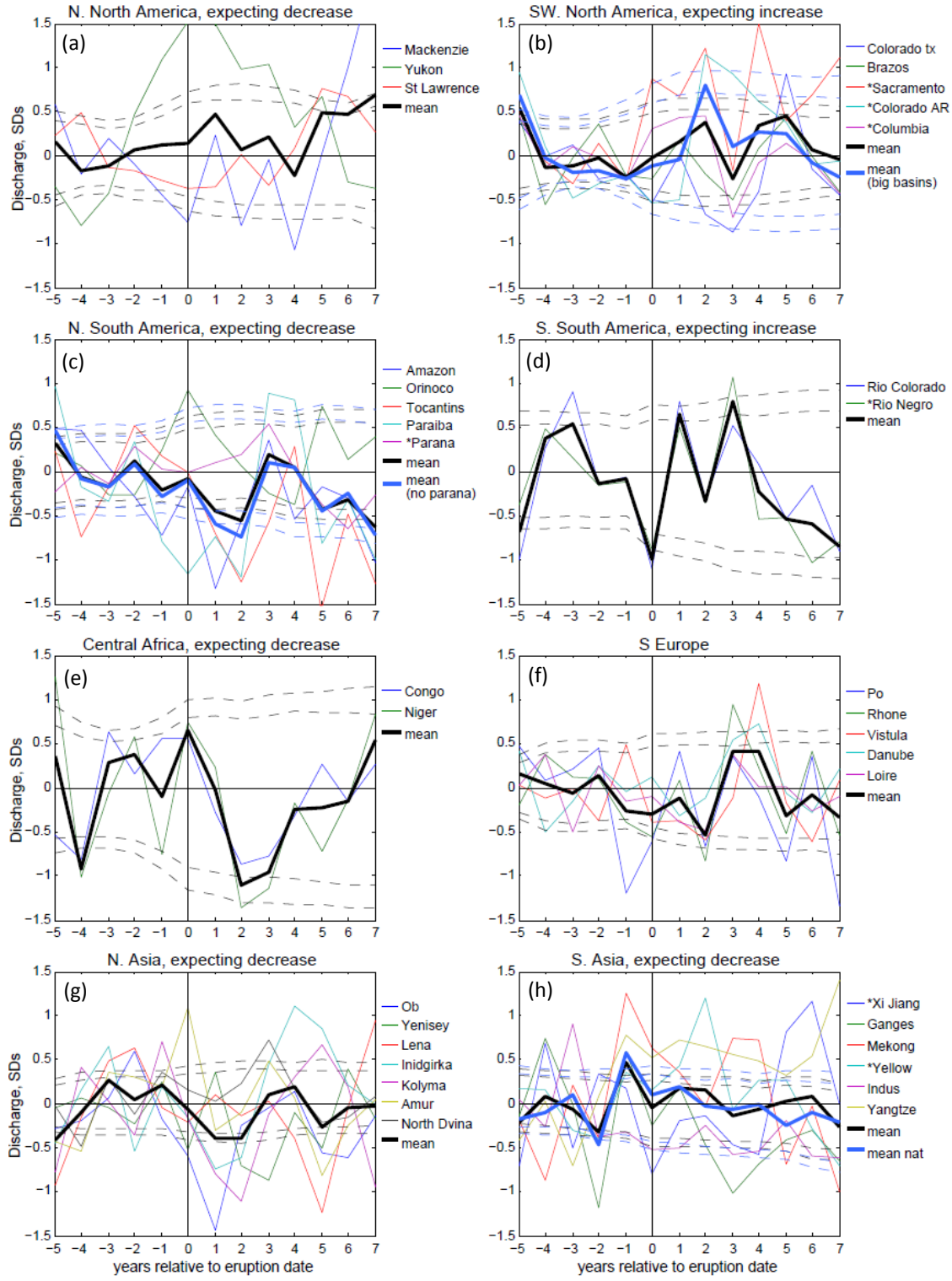

Figure 4.10 Average streamflow response across multiple eruptions for the regions shown in Figure 4.1. Results for individual rivers are standardised (thin lines) before taking the mean across a region (thick black line). For south-western North America (b) the thick blue line indicates results using only large basins (Columbia and Colorado AR), for northern South America (c) it represents results excluding the Parana, and for southern Asia (h) it represents rivers with regulation indexes below 20%. Dashed lines indicate confidence intervals for the average responses, inner lines 10-90%, and outer lines 5-95%. Asterisks in the legends denote rivers with higher human influence, i.e. flow regulation indexes above 20%. Units are standard deviations.

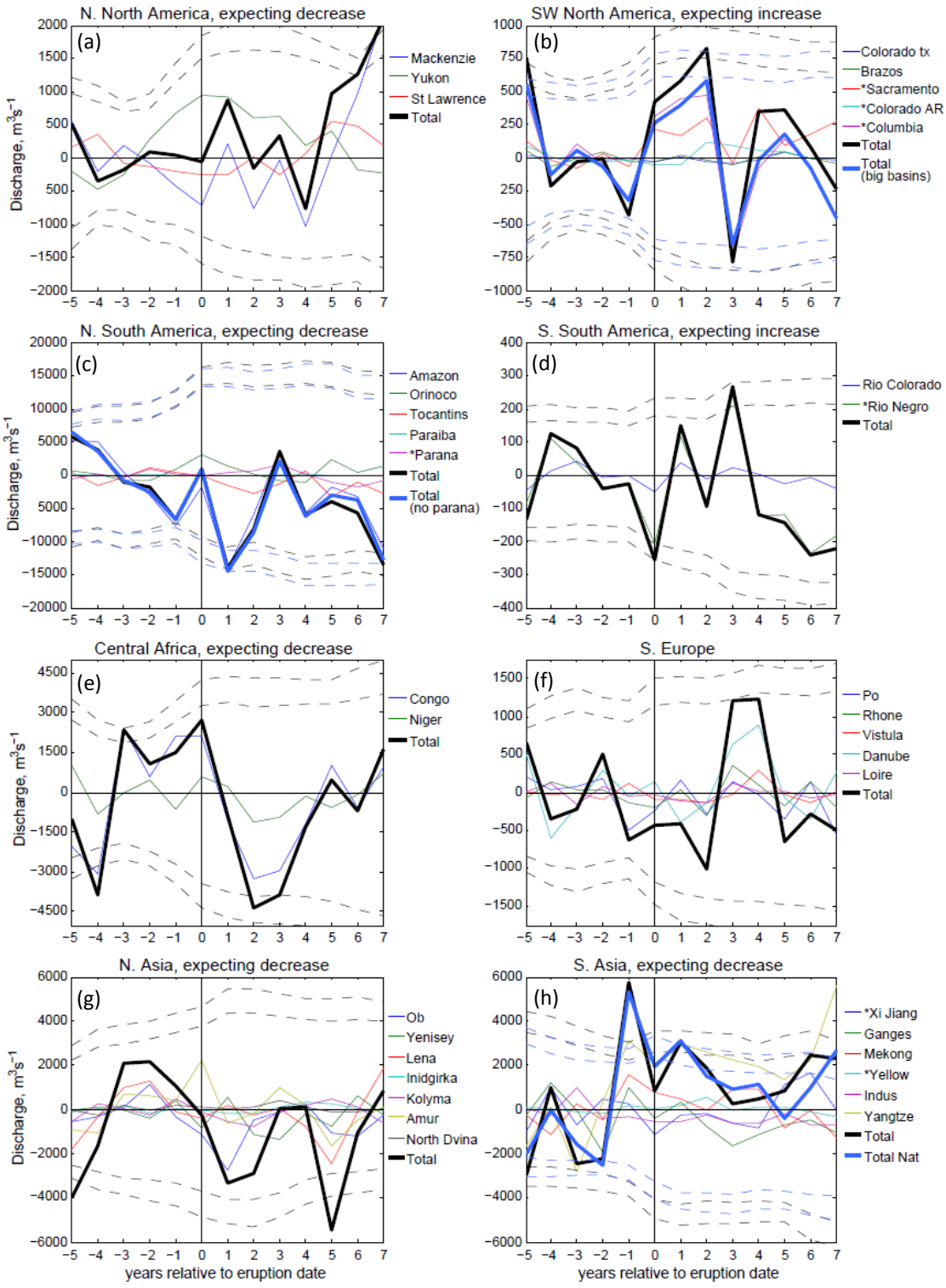

Figure 4.11 As for Figure 4.10, but using absolute values, where thick black and blue lines represent the sum of results for individual rivers in a region.

in year 1, although again results are noisy. Results for southern Asia do not change much when only natural rivers are considered, although are significant at a higher level in year 1. The proportion of regions undergoing a significant response is slightly higher than expected by chance (25% in years 1 and 2), although less than for the standardised regional analysis, possible because there were a number of occasions where results were very close to, but not quite beyond the confidence interval.

In chapters 2 and 3 it was found that precipitation in wet tropical regions decreases following eruptions. We investigate whether this is also the case for streamflow. Figure 4.12 shows the tropics divided into wet, intermediate and dry thirds based on GPCC climatology and indicates the 10 drainage basins used to represent the wet regions. The basins chosen are those that overlap with the wettest third of grid cells. The Ganges and Yangtze only overlap the wettest third by a small amount, but results are insensitive to their exclusion. Some basins in the wet regions could not be included in the analysis due to short or incomplete records that limited the range of random years that could be chosen for the Monte Carlo analysis. Results are shown in both standardised (Figure 4.13a) and absolute versions (Figure 4.13b), and with and without the influence of ENSO removed for rivers with which it has a significant relationship (Figure 4.3).

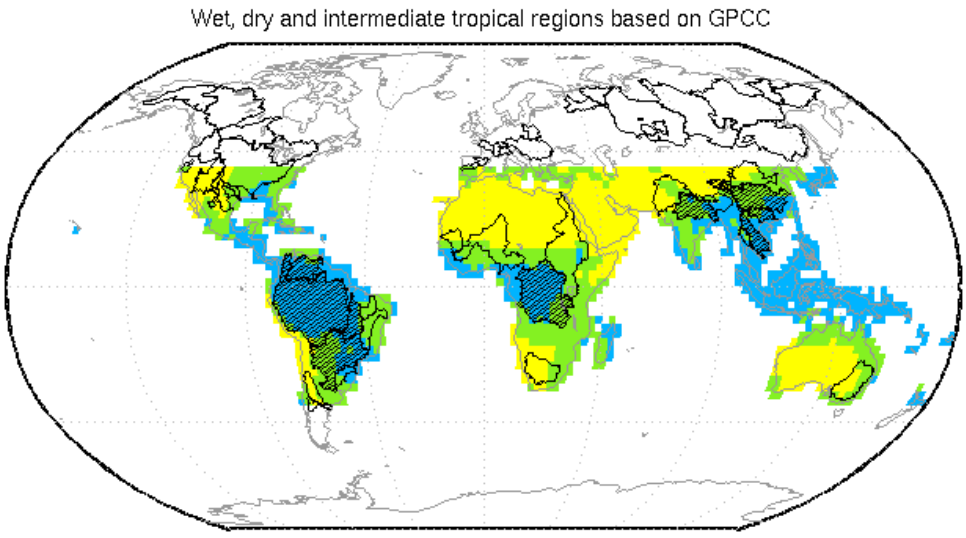

Figure 4.12 Wet (blue), intermediate (green) and dry (yellow) tropical regions based on GPCC climatology with drainage basins overlaid. Hatching indicates the basins used to calculate results for the wet regions.

For the standardised results a significant decrease in streamflow can be seen both with and without ENSO removed, although the timing differs slightly. In both cases there is also a significant peak in year -1 and 0. For the analysis using absolute values a significant decrease in streamflow can also be seen, and the pre-eruption peak is less noticeable and insignificant. If the influence of ENSO is not removed, then the decrease in streamflow is larger and more highly significant. Finally results were repeated excluding the Amazon, since it is large enough to dominate the results. Streamflow in the wet regions undergoes a smaller, insignificant decrease with the Amazon excluded, and the pre-eruption peak has become larger and highly significant. This pre-eruption peak in year -1 for both the absolute

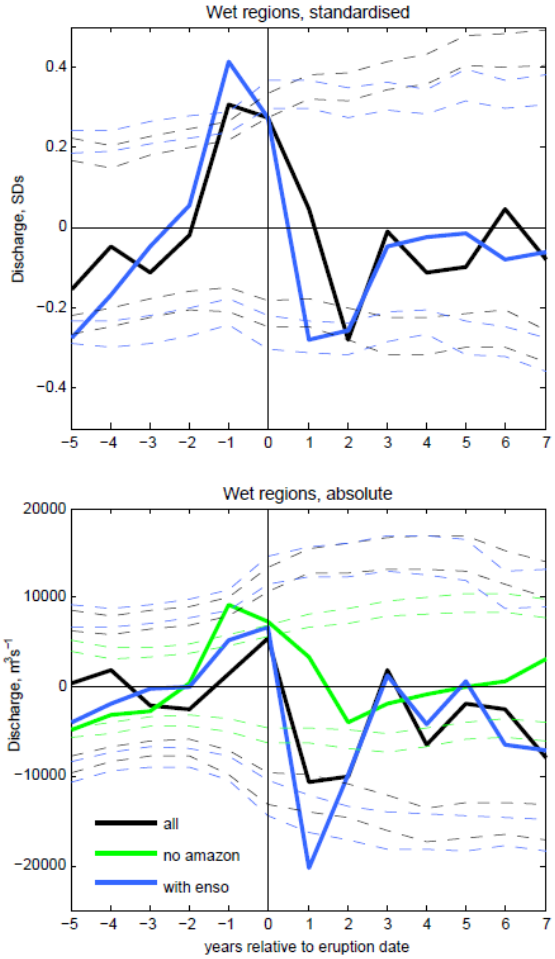

Figure 4.13 Streamflow response of rivers in the wet tropical regions (see Fig. 4.12) to multiple volcanic eruptions. a) Mean of standardised response of individual rivers, b) sum of response of individual rivers in absolute values. Thick black line represent the mean (a) or total (b) response for all rivers in the wet regions, with the influence of ENSO removed from rivers that have a significant relationship with it ($p<0.1$). Thick blue line is the same but without removing ENSO. Thick green line is the equivalent of the black line but excluding the Amazon. Dashed lines are confidence intervals, colours indicating the mean or total to which they correspond; inside lines indicate the 10-90% range, outside lines 5-95%.

and standardised versions of the analysis originates from most of the rivers having positive anomalies in this year, with the largest contributions from the Congo, Mekong and Yangtze in year -1, whilst these same rivers plus the Magdalena and Orinoco contribute to the high discharge in year 0. Repeating the wet regions results with only the more natural rivers made little difference, although there are only 2 rivers with a regulation index of more than 20% (the Xi Jiang and Parana) and their indexes are still relatively low compared to some other rivers at around 30%. We do not show the equivalent for dry regions because there are few major rivers in the driest regions, and those that exist tend to be very highly regulated, whilst parts of the basins that overlap with wetter regions are likely to be overrepresented.

4.5 Conclusions

In this chapter the response of 50 major world rivers to volcanic eruptions was investigated using instrumental records. The streamflow response was compared to the CMIP5 simulated precipitation (P), HadCM3 simulated P and P-E response, and observed precipitation response. Changes in P-E were dominated by changes in precipitation. The number of rivers undergoing a significant response was close to but slightly above that expected by chance, as might be expected due to short, noisy records with a limited sample of eruptions. These included the Amazon, Congo, Nile, Orange, Ob, Yenisey and Yangtze. When only larger basins or those less influenced by dams were considered, the proportion of basins with a significant response increased slightly. Regional analyses were also performed in which neighbouring basins undergoing the same sign of CMIP5 multi-model mean precipitation response to volcanic eruptions were combined to improve signal to noise ratios. A significant decrease in streamflow could be seen for northern South America, Central Africa, and less robustly for high latitude Asia, along with a significant increase in streamflow in southern South America and SW North America as expected from CMIP5 precipitation response patterns. The response tended to occur within years 1-3 after the eruption. A decrease in streamflow could also be seen in southern Europe, consistent with a positive phase of the NAO which has been found following tropical eruptions in observational studies [e.g. *Robock and Mao*, 1992, 1995] but does not appear to be well captured by climate models [e.g. *Stenchikov et al*., 2006; *Driscoll et al*. 2012, *Charlton Perez et al*. 2013] . Finally,

streamflow was found to decrease significantly across the wet tropical regions following eruptions, in agreement with reduced land precipitation over this area found in chapters 2 and 3. The Amazon dominated results based on absolute values. In conclusion, the observations show evidence that global streamflow indeed shows significant responses following volcanic eruptions, albeit with a low signal to noise ratio.

In terms of human impact, for most of the regional results and for many individual rivers the streamflow response was within 1 standard deviation of natural variability, although for Central Africa and for some individual rivers e.g. the Amazon, Niger, Orange, Ganges, Yellow, Ob and Yukon the response was larger, and is therefore more likely to be felt. For a larger eruption these effects might be expected to be bigger and have more impact.

Chapter S4: Supplementary Material

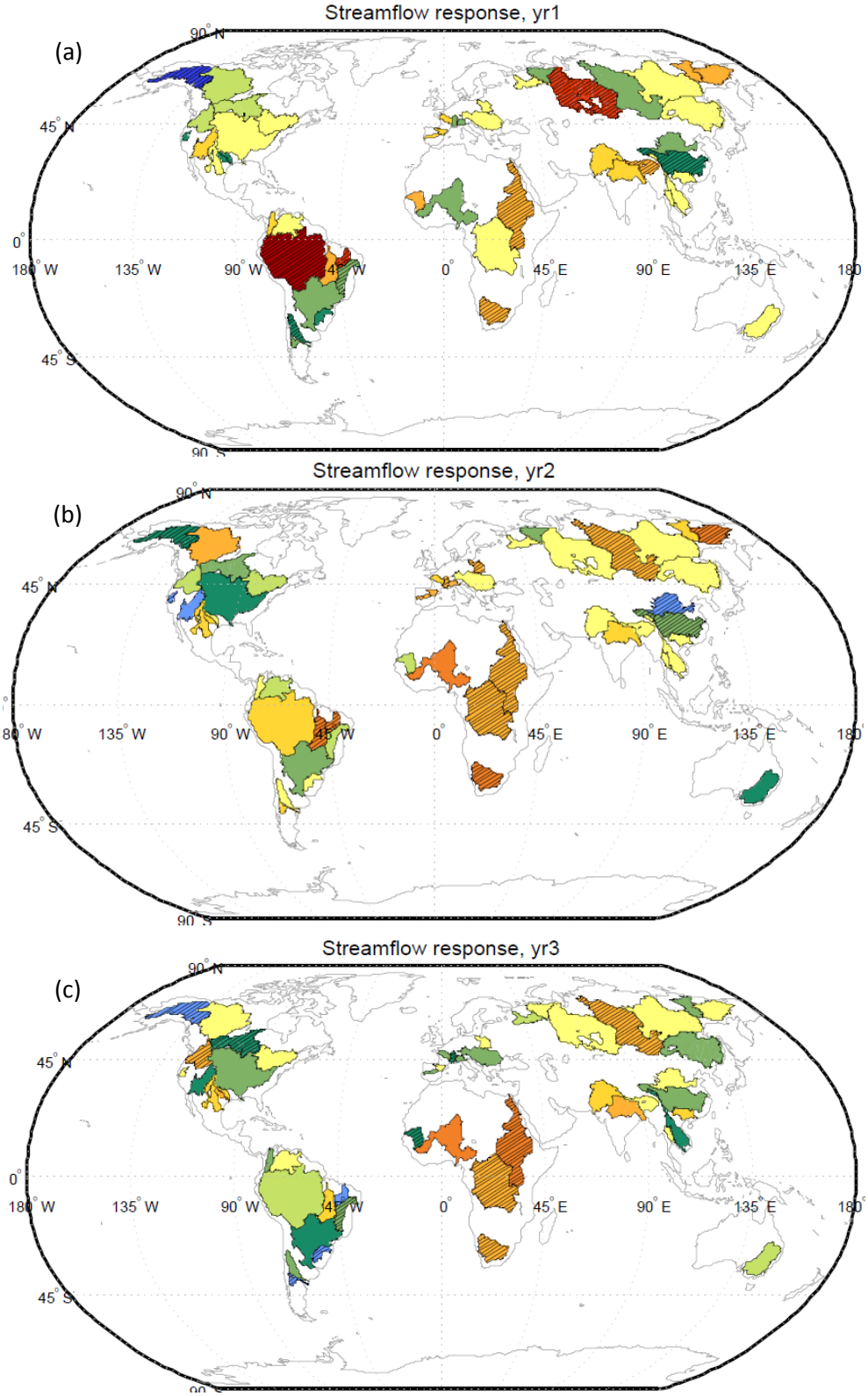

Figure S4.1 as in Figure 4.8 but without removing the influence of ENSO.

Table S4.1: Details of the rivers used in the analysis[a]

River name	Region assigned to (see Fig 1)	Station location (lat°N lon°E)	Annual mean discharge at station (km^3yr^{-1}) (*and as % of flow at mouth*)	Drainage area at station (10^3km^2) (*and as % of area at mouth*)	Start Year of record	End Year	No. years data	Eruptions covered	Regulation Index[b] (live dam capacity as % of annual discharge)	Notes (actual data range used and any inhomogeneities)
North America										
Mackenzie	N. North America	67.46 °N, -133.74 °E	283.4 *(99.3%)*	1660 *(96.9%)*	1943	2006	46.58	1982, 1991	12	Used from 1964, little data beforehand
Saint Lawrence	N. North America	45 °N, -74.74 °E	224.7 *(62.3%)*	773.9 *(61.1%)*	1900	2006	106.75	1902, 1912, 1963, 1982, 1991	11	
Yukon	N. North America	61.93 °N, -162.88 °E	227.5 *(95.8%)*	831.4 *(97.6%)*	1956	2006	50	1963, 1982, 1991	0.05	
Columbia	SW North America	45.61 °N, -121.17 °E	164.9 *(68.3%)*	613.8 *(84.8%)*	1878	2006	128.25	1883, 1902, 1912, 1963, 1982, 1991	24	
Colorado AR	SW North America	36.02 °N, -114.74 °E	12.4 *(108.6%)*	444.7 *(55%)*	1934	2006	72.5	1963, 1982, 1991	280	Abnormally high flow around early 1980 to mid-1980s.
Brazos	SW North America	29.58 °N, -95.76 °E	6.7 *(94.4%)*	116.6 *(93.3%)*	1903	2006	87.5	1963, 1982, 1991		Used from 1922, large gap before
Coloroado TX	SW North America	29.31 °N, -96.1 °E	2.6 *(100%)*	108.8 *(89.9%)*	1919	2006	74.67	1963, 1982, 1991		Used from 1938, large gap before
Sacramento	SW North America	38.46 °N, -121.5 °E	21.5 *(30.3%)*	60.9 *(31.5%)*	1948	2006	57	1963, 1982, 1991	49	Used up until 2004- missing data afterwards
Nelson	-	54.77 °N, -97.92 °E	69.6 *(55.6%)*	997 *(95.2%)*	1915	2006	71.25	1963, 1982, 1991	90	Used from 1947, very incomplete beforehand
Mississippi	-	32.31 °N, -90.91 °E	537.3 *(87.9%)*	2896 *(90.4%)*	1928	2006	79	1963, 1982, 1991	15.5	
Rio Grande	-	25.88 °N, -97.45 °E	1.5 *(100%)*	456.7 *(56.7%)*	1934	2000	67	1963, 1982, 1991	49	Steep downward trend of discharge in until mid-1950s and low flow thereafter

[a] Rivers with regulation indexes higher than 20% or with inhomogeneities noted are highlighted pink.

[b] From *Nilsson et al.* [2005]. The flow regulation index is the amount of water that can be held in all the dams in a river, expressed as a percentage of annual mean discharge. It uses the dams' 'live capacity', i.e. excluding bottom water that cannot be released, rather than gross capacity.

River	Region	Location	Annual discharge	Drainage basin area	Start year	End year	No. yrs data	Eruptions	Regulation index	Notes
South America										
Amazon	N. South America	-1.95 °N, -55.51 °E	5389.5 *(80.2%)*	4618.8 *(78.9%)*	1928	2006	79	1963, 1982, 1991	3	
Orinoco	N. South America	8.15 °N, -63.6 °E	980.1 *(87.2%)*	836 *(80.5%)*	1923	1999	75.75	1963, 1982, 1991	3	Limited data for first 2 years, used from 1925 onwards
Tocantins	N. South America	-3.76 °N, -49.67 °E	357.7 *(69.7%)*	742.3 *(96.5%)*	1956	2006	49.42	1982, 1991		Used from 1965 onwards, incomplete record beforehand
Parnaiba	N. South America	-3.46 °N, -42.37 °E	24.0 *(92.3%)*	282 *(85.2%)*	1963	2006	43.25	1982, 1991	10	Used from1965, incomplete beforehand
Parana	N. South America	-32.67 °N, -60.71 °E	476.6 *(83.8%)*	2346 *(88.2%)*	1905	2006	101.25	1912, 1963, 1982, 1991	28	
Rio Colorado	S. South America	-38.82 °N, -64.95 °E	4.2 *(100%)*	22.3 *(100%)*	1918	2000	82.5	1963, 1982, 1991		
Negro	S. South America	-40.45 °N, -63.72 °E	26.9 *(93.1%)*	95 *(48%)*	1927	1994	66.83	1963, 1982, 1991	140	Temporarily reduced variability of flow in early 70s, coinciding with the building of the Palmar dam. Less noticeable for annual data
Sao Francisco	-	-9.98 °N, -36.99 °E	89.4 *(98.9%)*	622.6 *(101.2%)*	1926	2006	76.42	1963, 1982, 1991	37	Noticeably lower mean annual flow before 1938, data before 1938 not used. Monthly discharge also changes noticeably in its variability after late 1990s, less obvious for annual data.
Uruguay	-	-31.4 °N, -58.03 °E	166.9 72.4*(%)*	249.3 *(70%)*	1942	2006	57.25	1963, 1982, 1991	28	Used from 1961, incomplete data before
Magdalena	-	10.25 °N, -74.92 °E	230.9 *(100%)*	257.4 *(102.2%)*	1950	2000	51	1963, 1982, 1991	1	
Africa										
Congo	Central Africa	-4.3 °N, 15.3 °E	1270.2 *(97.2%)*	3475 *(93.9%)*	1903	2000	97.08	1912, 1963, 1982, 1991	0	
Niger	Central Africa	7.8 °N, 6.77 °E	180.5 *(98.6%)*	2209.3 *(98.6%)*	1915	2006	73	1963, 1982, (1991)	15	1991 eruption is used for analysis on the Niger on its own, but not for the regional analysis. Data between 1941-1993 are used, incomplete before and after.

River	Region	Location	Annual discharge	Drainage basin area	Start year	End year	No. yrs data	Eruptions	Regulation index	Notes
Senegal	-	16.52 °N, -15.5 °E	21.7 *(100%)*	268 *(31.6%)*	1903	2000	94.67	1912, 1963, 1982	24	Unusually high flow in late 1960s and early 1970s, returning to normal afterwards.
Orange	-	-28.78 °N, 17.63 °E	6.9 *(100%)*	850.5 *(90.1%)*	1935	2001	65.17	1963, 1982, 1991	14	Change in monthly variability in last half of record, not noticeable in annual data.
Nile	-	23.96 °N, 32.9 °E			1869	1984	115.17	1883, 1902, 1912	95	Substantial decrease in variability for both annual, but especially monthly flow, along with lower mean flow after construction of the Aswan dam commenced in the 1960s. Post-Aswan dam data are therefore excluded from the analysis.
Europe										
Danube	S. Europe	45.22 °N, 28.73 °E	203.7 *(100%)*	807 *(102.4%)*	1900	2002	103	1902, 1912, 1963, 1982, 1991	4.6	
Rhone	S. Europe	43.81 °N, 4.64 °E	53.9 *(100%)*	95.6 *(96.6%)*	1920	2000	81	1963, 1982, 1991	5.5	
Loire	S. Europe	47.38 °N, -0.83 °E	27.6 *(92.9%)*	110 *(93.2%)*	1863	1999	137	1983, 1902, 1912, 1963, 1982, 1991	1.5	
Po	S. Europe	44.88 °N, 11.65 °E	47.7 *(87.3%)*	70.1 *(68.7%)*	1918	1998	80.25	1963, 1982, 1991	4	
Vistula	S. Europe	54.09 °N, 18.8 °E	32.9 *(97.1%)*	194 *(107.2%)*	1900	1994	94	1902, 1912, 1963, 1982, 1991	4	
Ebro	-	40.82 °N, 0.5 °E	14.8 *(100%)*	84.2 *(101.5%)*	1913	1999	72	1963, 1982, 1991	23	No data between 1936 and 1950
Tagus	-	39.47 °N, -8.37 °E	10.0 *(100%)*	67.5 *(92.5%)*	1913	1990	72	1963, 1982	25	
N. Eurasia										
Ob	N. Asia	66.63 °N, 66.6 °E	396.1 *(96.4%)*	2430 *(94.6%)*	1930	2006	76	1963, 1982, 1991	9	
Yenisey	N. Asia	67.43 °N, 86.48 °E	583.8 *(96.3%)*	2440 *(94.5%)*	1936	2006	69.33	1963, 1982, 1991	18	Used up until 2002, some gaps at end
Lena	N. Asia	70.68 °N, 127.39 °E	529.3 *(99.1%)*	2430 *(100.5%)*	1934	2006	71.42	1963, 1982, 1991	3	

River	Region	Location	Annual discharge	Drainage basin area	Start year	End year	No. yrs data	Eruptions	Regulation index	Notes
Indigirka	N. Asia	69.57 °N, 147.53 °E	50.4 *(92.6%)*	305 *(94.1%)*	1936	1998	62.25	1963, 1982, 1991	0	
Kolyma	N. Asia	68.73 °N, 158.72 °E	97.1 *(83.9%)*	526 *(79%)*	1927	2004	74.25	1963, 1982, 1991	5	1934-2001 used, incomplete otherwise
Amur	N. Asia	50.53 °N, 137 °E	305.9 *(88.1%)*	1730 *(59.6%)*	1900	1999	99.92	1902, 1912, 1963, 1982, 1991	9	
North Dvina	N. Asia	64.13 °N, 41.92 °E	104.4 *(94.6%)*	348 *(94.8%)*	1881	2006	124	1983, 1902, 1912, 1963, 1982, 1991	1	
Pechora	-	67.63 °N, 52.18 °E	137.8 *(96.4%)*	312 *(103.3%)*	1916	2000	73.75	1963, 1982, 1991	0	First half of record incomplete, so data used from 1950 onwards
S. Asia										
Ganges	S. Asia	24.55 °N, 88.13 °E	379.7 *(94.6%)*	951 *(99.5%)*	1949	1996	48	1963, 1982, 1991	8	
Mekong	S. Asia	15.11 °N, 105.8 °E	300.4 *(55.6%)*	545 *(70.4%)*	1923	2005	82.58	1963, 1982, 1991	3	Used from 1924
Yellow (Huang He)	S. Asia	35.23 °N, 114.92 °E	44.9 *(95.7%)*	734.1 *(82.1%)*	1934	2000	52.33	1963, 1982, 1991	51	Used from 1950, large gap in data beforehand
Xi Jiang (Pearl)	S. Asia	23.48 °N, 111.32 °E	219.7 *(81.9%)*	329.7 *(80.6%)*	1915	1986	45.67	1963, 1982	31	Used from 1941 large gap in data beforehand
Yangtze (Chang Jiang)	S. Asia	30.77 °N, 117.62 °E	905.1 *(96.4%)*	1705.4 *(95.1%)*	1900	2000	99.58	1902, 1912, 1963, 1982, 1991	12	
Indus	S. Asia	25.36 °N, 68.3 °E	88.5 *(85.6%)*	975 *(85.3%)*	1936	2000	63.75	1963, 1982, 1991	13	
Brahmaputra	-	25.18 °N, 89.67 °E	670.9 *(97.6%)*	554.5 *(95.1%)*	1956	2000	44.25	1963, 1982, 1991	8	
Chao Phraya	-	15.27 °N, 100.06 °E	23.3 *(85.3%)*	118.8 *(83.7%)*	1912	2000	86.5	1963, 1982, 1991	76	Discontinuity in annual mean flow and monthly variability from 1952 after construction of Chao Phraya dam. However, annual variability appears unchanged.
Australia										
Murray Darling	-	-34.6 °N, 142.76 °E	8.5 *(90.4%)*	991 *(96%)*	1930	2000	69.92	1963, 1982, 1991	67	

Chapter 5: Conclusions

5.1 Summary

The aim of this thesis was to investigate the effect of large explosive volcanic eruptions on the hydrological cycle. This involved using epoch analysis (i.e. averaging across multiple eruptions) to investigate the robust features of the precipitation response to eruptions from observations and quantitatively comparing them to model simulated responses, focusing on regional and seasonal scales. This included a detection analysis that builds on previous detection studies [e.g. *Gillett et al*., 2004] by specifically targeting the response to volcanic eruptions through focusing on inter-annual time scales, and by identifying key mechanisms, such as a particularly pronounced drying of wet regions after eruptions. An ensemble of last millennium HadCM3 simulations was used to identify the main robust features of the precipitation response to 18 large eruptions. The model simulated land precipitation response to 5 twentieth century eruptions was then compared to the Z07 observational dataset, and detected in that dataset. The analysis was then extended to historical runs of the CMIP5 (Coupled Model Intercomparison Project Phase 5) models to establish whether the features found in HadCM3 were consistent with other models, many of which are more modern, higher resolution and extend further into the stratosphere. This is the first multi-model study focusing on the precipitation response to volcanic eruptions and allows assessment of consistency of the response between models. CMIP5 results were compared to a satellite-gauge dataset for the most recent 2 eruptions, which includes ocean coverage. Sensitivity of results over land to using alternative datasets was assessed. Finally the streamflow response of 50 major rivers worldwide to volcanic eruptions was investigated using historical records, both individually and grouped into regions that are expected to become drier or wetter, based on the multi-model mean precipitation response. Previous studies on streamflow have not examined the average response to multiple eruptions, and have either focused on the global mean or on a small number of basins [*Trenberth and Dai*, 2007; *Oman et al*., 2006; *Timmreck et al*., 2012].

The main features of the model-simulated precipitation response to volcanic eruptions were consistent between HadCM3 and CMIP5. This included a significant reduction in global and extratropical precipitation over both land and ocean, in agreement with other studies [e.g. *Robock and Liu*, 1994; *Trenberth and Dai*, 2007; *Schneider et al.*, 2009*; Gu et al.*, 2007; *Gu and Adler*, 2011]. Furthermore, when tropical regions were split into wet and dry regions, the wet regions dried significantly following eruptions whilst dry ocean regions got significantly wetter. This is the opposite of the predicted response under global warming [*Held and Soden*, 2006; *Trenberth*, 2011*; Meehl et al*., 2007]. Monsoon regions dried following eruptions in agreement with previous studies [*Joseph and Zeng*, 2011; *Schneider et al*., 2009; *Trenberth and Dai*, 2007], whilst analysis using CMIP5 showed that the Intertropical Convergence Zone shifts away from the hemisphere with the larger concentration of volcanic aerosols in response to individual eruptions, in agreement with *Haywood et al*., [2013]. The precipitation response over ocean was longer lasting than that over land in all models (5-7 years vs. 2-3 years respectively). Further investigation using HadCM3 found that the ocean response matched the timescale of near surface air temperature. In contrast land precipitation responded more quickly than air temperature in agreement with the results of *Joseph and Zeng* [2011] using a model of intermediate complexity. It was further found that the timescale of the land precipitation response was similar to that of aerosol optical depth and a reduction of land-ocean temperature contrast, suggesting a directly forced component and possible contributions from weakening monsoons. Finally, precipitation was found to be more sensitive to changes in temperature in response to volcanic forcing (3.3 % K^{-1}) compared to greenhouse gas forcing (1.5 % K^{-1}) or internal variability (2.0 % K^{-1}).

Many of these model-simulated features are also seen in observational data. This includes a reduction in land precipitation for the global mean and wet tropical regions, which is significant in the cold season. Epoch analysis was also performed on observed ocean precipitation data for the first time, but results were noisy due to a short record length encompassing only 2 eruptions, and only follow the modelled response in the cold season. The record was too noisy to confirm whether the long ocean precipitation response seen

in models also occurs in the observations. Although observed spatial response patterns were only marginally significant, monsoon regions dry in the observations, in agreement with the model results, with the exception of SE Asia. A precipitation pattern resembling the positive phase of the NAO could be seen in the cold season [see also *Fischer et al.*, 2007], although this was not convincingly captured by any model [see also *Driscoll et al.*, 2012 and *Charlton-Perez et al.*, 2013]. Land precipitation response features were robust to choice of dataset. Detection analyses found that the influence of volcanic forcing on precipitation was detectable against internal variability in all observational datasets in the cold season, in year 1 and 1+2 combined, including when using the Global Precipitation Climatology Project satellite-gauge dataset (GPCP) which includes ocean coverage. In contrast, the response was only marginally detectable in the warm season. The magnitude of the response was underestimated in the cold season by both HadCM3 and the CMIP5 models despite model improvements relative to HadCM3, and this originated from the wet tropical regions. Removing the influence of ENSO generally brought the models and observations into closer agreement, although rendered some results insignificant in the warm season.

Finally, the number of rivers undergoing a significant streamflow response following eruptions was close to but slightly above that expected by chance. Rivers undergoing a significant reduction in streamflow included the Amazon, Congo, Nile, Orange, Ob and Yenisey. However, relatively short records with a limited sample of eruptions results in poor signal to noise ratios. When neighbouring basins undergoing the same sign of CMIP5 multi-model mean predicted precipitation response were combined into regions, the streamflow response often better reflected the modelled precipitation response over the region. For example, streamflow decreased significantly in northern South America, Central Africa and less robustly in high latitude Asia and increased significantly in southern South America and SW North America. Over Southern Europe streamflow decreased matching the observed precipitation response rather than the modelled one, reflecting a positive NAO pattern. Streamflow also decreased significantly following eruptions over the wet tropics as a whole, although the Amazon dominated results when

using absolute rather than standardised values, and the post-eruption decrease in streamflow became insignificant following its removal.

5.2 Challenges and limitations

The main challenge in this research has been the noisy nature of both precipitation and streamflow, combined with a small sample of eruptions in the twentieth century for which instrumental data exists. This is particularly the case over oceans, for which data span only 2 eruptions. In addition, poor data coverage over land at the beginning of the 20th century and again after 1990 means that some land regions have data for only a couple of eruptions or are interpolated (see Figure 5.1). Some of the areas that are data sparse for early eruptions undergo the largest post-volcanic reduction in land precipitation, for example, over wet tropical regions. Furthermore, the fact that 3 of 5 twentieth century eruptions were followed by El Nino events, whilst the 1902 eruption occurred half way through one, leads to possible confusion of the volcanic and ENSO signals. All these factors make it more difficult to confidently identify robust precipitation response features in observational data, particularly when examining spatial response patterns, which have poorer signal to noise ratios than spatial averages. Nevertheless a combination of significance testing, removing the influence of ENSO, and analysing the observations in conjunction with climate models increases confidence in results particularly where models and observations agree. An example is the reduction in land precipitation both globally and in wet tropical regions and ocean precipitation in these same places in the boreal cold season. Another example is the drying of African and South American monsoon regions. For some regions the model ensemble mean and observations do not agree on the sign of the response, but the observed response is within the ensemble envelope (e.g. NH land and wet tropical ocean regions in MJJASO for GPCP vs CMIP5; Fig 3.3, S3.6). In such a case, the spread between ensemble members indicates that the observed change is a plausible combination of response to the eruption and climate variability. However in some regions the observations are also outside of the ensemble envelope as well as of opposite sign (e.g. global ocean in MJJASO for GPCP vs CMIP5 (Fig 3.3), NH land for Z07 vs HadCM3 (Fig 2.9)), suggesting that the model

either misses the response or underestimates the variability (see discussion in Section 5.3). Observational error, e.g. due to missing values and noisy records, may also contribute to this model data difference. It is difficult to pinpoint the cause for such discrepancies. Note that the methods applied account for entire gridboxes missing in observations by removing them from models as well, but do not account for sparse sampling of changes within gridboxes.

Despite integrating surplus or deficits in precipitation over an area, streamflow results also appeared noisy at the scale of the individual drainage basin and were significant for only marginally more drainage basins than expected by chance. Streamflow is affected by many factors besides precipitation, including evaporation, storage of water in snow, ice, lakes and behind dams, extraction for irrigation and land use changes. If we partially circumvent the interference of human infrastructure by focusing on river basins that are not strongly affected by dams we find an increase in the proportion of rivers undergoing a significant response. Nevertheless, data for more eruptions would be required to be confident in the response of individual rivers to eruptions. Signal to noise ratios improved when rivers were combined into regions and the fact that the direction of response often matched modelled expectations of precipitation response increases confidence that the influence of volcanism can indeed be seen.

Further limitations include inherent problems with precipitation datasets e.g. for gauge datasets: exaggerated variability where few stations exist in a given grid cell (as discussed above); lack of stations in inaccessible areas such as mountainous regions, high latitude regions and deserts; problems with wind-induced undercatch particularly for snow; wetting and evaporation losses; and inhomogeneities associated with changes in measuring techniques and stations coming into and out of action [e.g. *Becker et al.*, 2013; *Hegerl et al*., 2014 and references in both; *Zhang et al*., 2007 supplement]. For satellite-based precipitation measurements biases exist in high latitudes in winter, particularly over oceans, whilst record lengths are short [*Adler et al.*, 2012]. At the beginning of the record (1979-1987) GPCP is based only on infrared radiation measurements, which relate cold cloud top area to precipitation. A microwave sensor was introduced from 1987

onwards, improving accuracy, but introducing a possible inhomogeneity [*Adler et al*., 2003]. However, since this study focuses on interannual variability, such inhomogeneities are not as problematic as they would be for trend analysis.

Whilst climate models are helpful in determining the noise-free precipitation response to volcanic forcing by averaging across many realizations, and are useful in performing experiments to elucidate mechanisms, they are not perfect representations of reality and may not simulate the precipitation response to volcanoes correctly. Climate models have some systematic biases in simulating climatological precipitation e.g. insufficient precipitation in the equatorial West Pacific, too much in the convergence zones south of the equator in the Atlantic and Eastern Pacific, an overly zonal South Pacific Convergence zone, overly frequent light rainfall events, and errors in the timing of the diurnal cycle of rainfall and convection over land [*Flato et al*., 2013]. These latter two are unlikely to be problematic for the analysis presented here since half year seasons are used. Furthermore, errors in the location of features such as convergence zones are taken into account by defining wet and dry regions for each model and observational dataset separately. It is possible that where the magnitude of climatological precipitation is incorrect, the magnitude of the precipitation response to eruptions could also be incorrect, but it may well still react in the right direction In addition, volcanic aerosol forcing datasets and the way they are incorporated in climate models are simplifications of reality and could result in errors. Furthermore, different models use different forcing datasets which sometimes disagree on the magnitude of eruptions (e.g. see Figure 1.1). Examples of possible model problems in simulating the precipitation response to volcanoes identified here include the lack of NAO response and the apparent underestimate of precipitation response in the cold season. However, since the observed response is noisy, it is difficult to obtain a reliable fingerprint of the precipitation response to volcanic forcing against which to evaluate models.

Other possible limitations of this research include: possible incomplete removal of the ENSO signal from observations, especially using the short GPCP record; inconsistent non-volcanic forcings in the HadCM3 ensemble used in Chapter 2 (however, sensitivity

tests suggested that this did not make a difference to results); and ignoring differences in seasonal timing of eruptions. The latter is not expected to be a problem for eruptions of Pinatubo size (see discussion in Chapter 2, Section 2.3.1). Ideally we would have analysed eruptions whose aerosol clouds were biased towards either hemisphere separately and not included a high latitude eruption as this all makes a difference to the precipitation response, but due to the small sample of eruptions with observational records this was not possible.

5.3 Wider implications

In terms of human impact, whilst the global mean precipitation decrease following eruptions is only a couple of percent of climatological rainfall, on regional levels the response is bigger. Examples include a decrease of 5-12.5% in some monsoon regions and an increase of more than 15% in some dry regions (Figure 2.4) (although this latter will appear inflated due to very low mean precipitation). The extent to which these changes are likely to affect people depends on the location e.g. whether it is populated, the extent to which the population is reliant on agriculture, whether it is a water-stressed area and how much rainfall normally varies. For instance, regarding the c. 10% decrease in the monsoon regions, over central Africa this may well not pose much of a challenge as freshwater withdrawals are less than 1% of freshwater availability (WRI, http://www.fao.org/nr/water/aquastat/data/query/index. html), whilst the South American monsoon region is largely rainforest. In contrast, India and Pakistan use a higher percentage of their available freshwater (34 and 74% respectively (WRI)), whilst the interannual standard deviation of the Indian monsoon is itself 10% [e.g. *Joseph et al*., 2013], and so a 10% decrease in rainfall might have more impact. The highly water stressed areas in northern Africa and the Middle East are actually areas expected to experience increased precipitation following eruptions. Impacts on the mid and high latitudes are likely small because precipitation changes are only a small percentage of climatological rainfall. Having said this *Trenberth and Dai* [2007] find widespread moderate to severe drought in many regions worldwide following the Pinatubo eruption, although the coinciding El Nino event will have exacerbated this by shifting precipitation

offshore [*Trenberth and Dai*, 2007]. The streamflow response of most rivers was within one standard deviation of natural variability, although was bigger for some e.g. the Niger, Orange, Amazon and Yellow. Again the human impact depends on the factors mentioned above. Following larger eruptions the hydrological cycle response is likely to be bigger and have more impact (e.g. see *Timmreck et al*., 2012 for the precipitation and streamflow response to the Toba super-eruption), although will not necessarily vary linearly with magnitude e.g. due to coagulation of aerosols which decreases their effectiveness at reflecting shortwave radiation per unit mass [*Timmreck et al*, 2009].

The results presented here are also relevant to people in terms of predicting the precipitation response to future eruptions. Based on the historical record it is likely that such an eruption will occur in the next few decades [*Crowley et al*., 2008]. Whilst our findings represent the average response to eruptions, precipitation and streamflow can deviate from this average response following individual eruptions. For instance, at the global mean and wet tropical regions scale some ensemble members show an increase in precipitation rather than a decrease (e.g. see Figure 3.3). Therefore, assuming climate models are a reasonable representation of reality, precipitation might be expected to increase in these areas following some eruptions. However, it is the local scale over land that is most relevant for human impacts. Figure 5.1 shows the observed precipitation response to individual twentieth century eruptions, thereby giving a rough indication of how consistent the response is between eruptions. Over many areas e.g. North America and Australia in winter, precipitation differs considerably between eruptions, whereas in others e.g. Southern Africa and southern Europe in winter, it is more consistent. In order to explore predictability at the local scale more formally Figure 5.2 (a, b) indicates the grid squares for which the precipitation response is consistent in sign 60% of the time in response to 50 eruptions, using the HadCM3 CMIP5 historical runs (10 ensemble members, 5 eruptions (Table S3.1)), and for 7 out of 10 ensemble members for each of the twentieth century eruptions separately (c-l). Using a criterion of 60% for Fig 5.2a and b seems low, but very few grid cells pass a 70% criterion. Over many land regions in (a-b) the precipitation response is small compared to variability with individual realizations

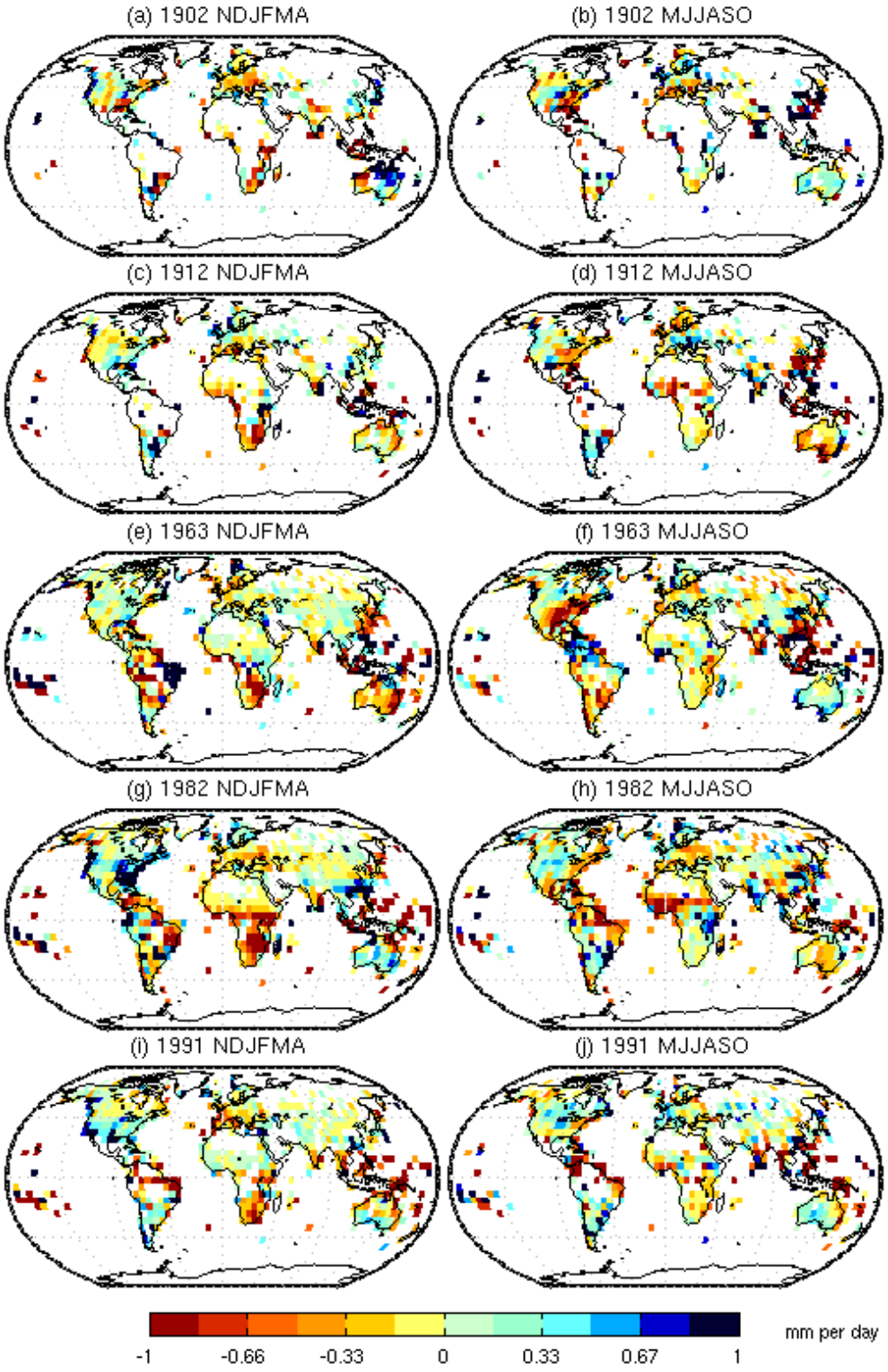

Figure 5.1: The precipitation response to individual twentieth century eruptions in the Z07 dataset for years 1 and 2 combined, illustrating levels of consistency between eruptions and indicating data coverage through time.

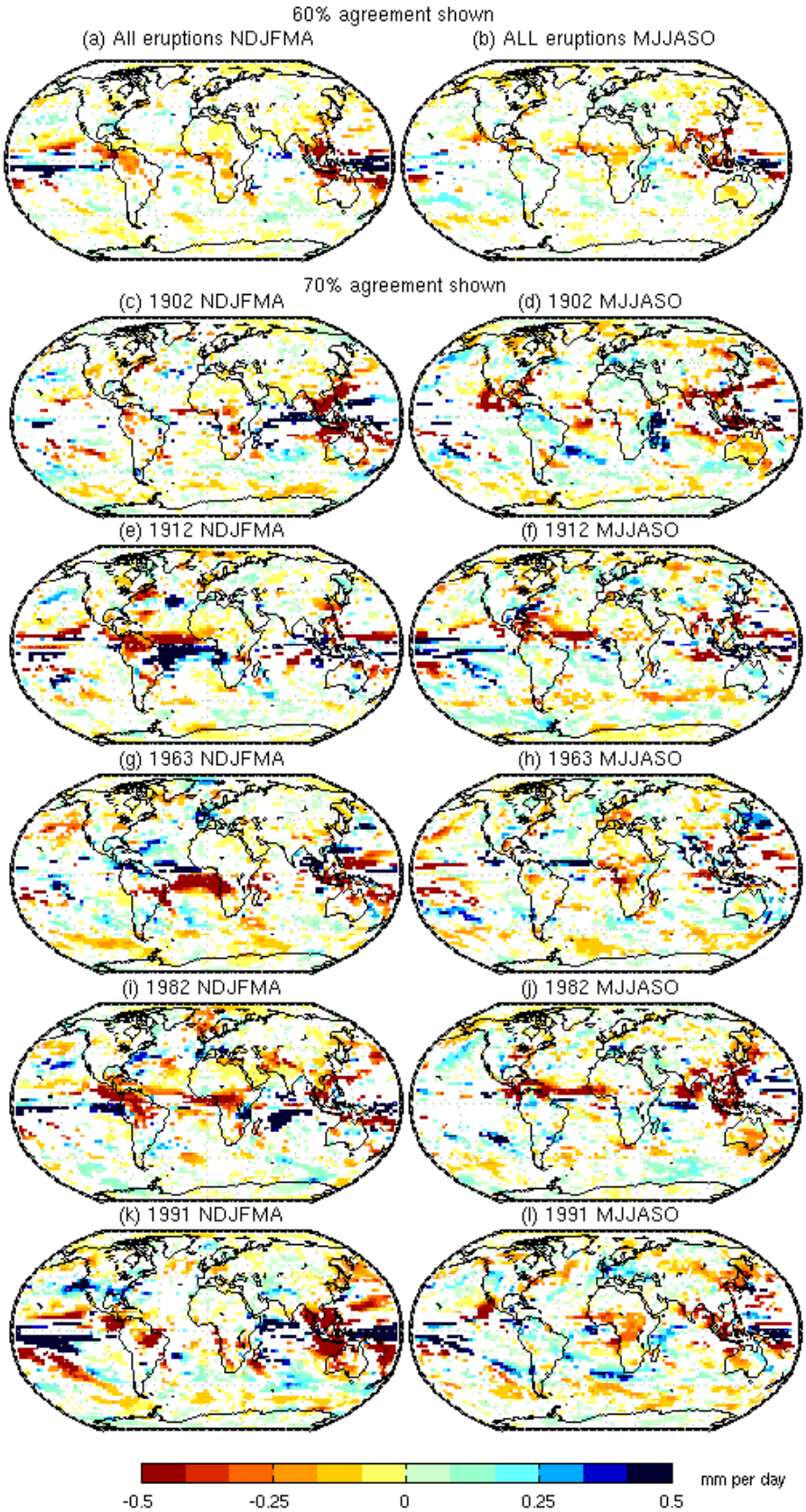

Figure 5.2: (a-b) Precipitation response to 50 eruptions for years 1 and 2 combined, simulated by HadCM3 (10 ensemble members, 5 eruptions) showing grid cells where the direction of response is consistent 60% or more of the time. (c-l) as (a-b) but for individual eruptions, indicating where 7/10 ensemble members agree on the sign.

varying widely. In contrast, the response to eruptions is more obvious in monsoon regions and near to the ITCZ, suggesting that volcanic eruptions lead to a more predictable precipitation change there. When individual twentieth century eruptions are analysed separately (c-l), the response is more consistent between ensemble members and the majority of grid cells pass a 60% predictability criterion (not shown). This suggests that knowing the latitudinal distribution of the eruption aerosol cloud can improve predictability, particularly in regions affected by ITCZ shifts. It is likely that taking into account the underlying ENSO state would improve predictability further. For streamflow, the response at the level of individual rivers (which is the scale most relevant to people) is still not that well characterised and is often not very consistent between eruptions (not shown).

The findings of this study also have implications for solar radiation management based geoengineering schemes. Although the spatial patterns of precipitation response to eruptions are broadly the opposite of the global warming response, previous studies (see discussion in Section 1.2.2) and the hydrological sensitivity analysis in Chapter 2 show that precipitation is more sensitive to short-wave forcing than to longwave forcing such as by greenhouse gases. This means that if temperature was kept constant under increasing CO_2 concentrations, precipitation would still decrease. A decrease in global precipitation is obviously undesirable, although previous studies imply that this decrease may be less than the changes that would have occurred under global warming with no geoengineering, but not in all regions [*Schmidt et al*., 2012; *Tilmes et al*., 2013; *Kravitz et al*., 2013b]. Furthermore the shifts in the position of the ITCZ found in Chapter 3 and in *Haywood et al*., [2013] in response to asymmetric forcing imply that the latitudinal distribution of geoengineering (e.g. sulphate aerosols) is important.

Finally, a key finding of this thesis was that climate models underestimate the precipitation response to eruptions in the boreal cold season. This underestimate could be for a variety of reasons. For instance *Zhang et al*. [2007] found that climate models underestimate variability compared to their observational dataset (Z07) at least in part because grid cells for which few stations exist tend to overestimate variability. GPCP also

tended to show higher variability over oceans that CMIP5 models, but not over land (not shown). Other possible reasons could include incomplete ENSO removal from the observations, inaccuracies in volcanic forcing datasets and simplifications in their implementation, and model errors in ocean heat uptake, climatology, SST response, monsoon responses, or other circulation responses to eruptions. However, if this underestimate is a real phenomenon, it implies that climate models could also underestimate the precipitation response to geoengineering schemes. Previous studies have also suggested that climate models underestimate the precipitation response to greenhouse gases [*Zhang et al*., 2007; *Polson et al*., 2013b].

5.4 Areas for future research

There are a number of ways in which the research presented here could be furthered and other wider aspects of the response of the hydrological cycle to volcanic eruptions that would benefit from further research. The most obvious research question that needs to be addressed is the causes of the model-data mismatch in the magnitude of the wet region response to volcanic eruptions. The following questions could shed light on this, but are also interesting in their own right. For instance, model experiments could be analysed to assess whether or not the choice of forcing dataset makes a discernible difference to the precipitation response and to check whether or not the seasonal timing of eruptions makes a difference. The influence of the background ENSO state at the time of eruptions on the precipitation response could be analysed further by selecting eruptions in climate model simulations that occur at a certain phase of ENSO e.g. to match the ENSO-state for the twentieth century eruptions. Furthermore, elucidating the mechanisms by which the precipitation influence comes about in models and reanalysis data can lead to improved understanding of climate dynamics and may help to identify any differences in the magnitude of the response between models and data.

Further questions that arise include the response of precipitation extremes to volcanic eruptions, whilst the effect of eruptions on drought could be examined in more detail than has been done previously, including any contribution to past mega-droughts. Related to

this the influence of eruptions on soil moisture could be investigated, as soil moisture is of importance to impacts on vegetation. However, lack of observations means that this would have to be model-based. A further interesting question relates to the ocean response to volcanic eruptions, including their influence on salinity. Salinity can be influenced by precipitation, evaporation and freshwater runoff from continents.

The streamflow response to eruptions is another area that has a lot of scope for further research. For instance observational results could be compared with climate model simulations and a detection analysis performed. It would also be interesting to see whether volcanic eruptions affect the timing of the spring melt peak for rivers with a significant contribution from snow and ice- it could be later due to cooler temperatures, or earlier in some places due to the winter warming response. However, the small sample size of eruptions in the observed record might render this unfeasible using instrumental data. It would also be interesting to look into the significant correlation between Amazon streamflow and the NAO found in Chapter 4 and see if there is a mechanism that could explain it. An examination of the time series suggests that this is not due to trends or anomalous points.

Finally, when the next big eruption occurs this will allow both the observed precipitation and streamflow response to be better constrained, particularly for the precipitation response over oceans, for which data currently exists for only 2 eruptions. This may help to clarify whether the model-simulated long response in precipitation over ocean relative to land is realistic.

References

Adam, J. C., and D. P. Lettenmaier (2008), Application of New Precipitation and Reconstructed Streamflow Products to Streamflow Trend Attribution in Northern Eurasia, *J. Clim.*, *21*(8), 1807–1828, doi:10.1175/2007JCLI1535.1.

Adams, J.B., M.E. Mann, C.M. Ammann, (2003), Proxy evidence for an El Nino-like response to volcanic forcing, *Nature.*,*426*(6964), 274-278, doi:10.1038/nature02101.

Adler, R.F. et al. (2003), The Version 2 Global Precipitation Climatology Project (GPCP) Monthly Precipitation Analysis (1979-Present), *J. Hydrometeor*., *4*(6), 1147-1167, doi: 10.1175/1525-7541(2003)004<1147:TVGPCP>2.0.CO;2.

Adler, R. F., G. Gu, and G. J. Huffman (2012), Estimating Climatological Bias Errors for the Global Precipitation Climatology Project (GPCP), *J. Appl. Meteorol. Climatol.*, *51*(1), 84–99, doi:10.1175/JAMC-D-11-052.1.

Alkama, R., L. Marchand, A. Ribes, and B. Decharme (2013), Detection of global runoff changes: results from observations and CMIP5 experiments, *Hydrol. Earth Syst. Sci.*, *17*(7), 2967–2979, doi:10.5194/hess-17-2967-2013.

Allan, R. P., and B. J. Soden (2008), Atmospheric warming and the amplification of precipitation extremes, *Science*, *321*(5895), 1481–4, doi:10.1126/science.1160787.

Allan, R. P., B. J. Soden, V. O. John, W. Ingram, and P. Good (2010), Current changes in tropical precipitation, *Environ. Res. Lett.*, *5*(2), 025205, doi:10.1088/1748-9326/5/2/025205.

Allen, M. R., and W. J. Ingram (2002), Constraints on future changes in climate and the hydrologic cycle, *Nature*, *419*(6903), 224–32, doi:10.1038/nature01092.

Ammann, C.M., G.A. Meehl, W.M. Washington, and C.S. Zender (2003), A monthly and latitudinally varying volcanic forcing dataset in simulations of 20th century climate, *Geophys. Res. Lett.*, *30*(12), doi:10.1029/2003GL016875.

Ammann, C. M., F. Joos, D. S. Schimel, B. L. Otto-Bliesner, and R. A. Tomas (2007), Solar influence on climate during the past millennium: Results from transient simulations with the NCAR Climate System Model, *Proc. Natl. Acad. Sci. U. S. A.*, *104*, 3713–3718.

Ammann, C. M., W. M. Washington, G. A. Meehl, L. Buja, and H. Teng (2010), Climate engineering through artificial enhancement of natural forcings: Magnitudes and implied consequences, *J. Geophys. Res.*, *115*(D22), D22109, doi:10.1029/2009JD012878.

Anchukaitis, K.J., B.M. Buckley, E.R. Cook, B.I. Cook, R.D. D'Arrigo, and C.M. Ammann (2010), Influence of volcanic eruptions on the climate of the Asian monsoon region. *Geophys. Res. Lett.*, *37*, L22703, doi:10.1029/2010GL044843.

Andres, R. J. and A. D. Kasgnoc (1998), A time averaged inventory of subaerial volcanic sulphur emissions. *J. Geophys. Res., 103* (D19), 25251–25261, doi: 10.1029/98JD02091

Annamalai, H., K. Hamilton, and K. R. Sperber (2007), The South Asian Summer Monsoon and Its Relationship with ENSO in the IPCC AR4 Simulations, *J.Clim.*, *20*(6), 1071–1092, doi:10.1175/JCLI4035.1.

Arnell, N. W. (2003), Effects of IPCC SRES* emissions scenarios on river runoff: a global perspective, *Hydrol. Earth Syst. Sci.*, *7*(5), 619–641, doi:10.5194/hess-7-619-2003.

Arnell, N. W., and S. N. Gosling (2013), The impacts of climate change on river flow regimes at the global scale, *J. Hydrol., 486*, 351–364, doi:10.1016/j.jhydrol.2013.02.010.

Arora, V. K., and G. J. Boer (2001), Effects of simulated climate change on the hydrology of major river basins, *J. Geophys. Res.,106*(D4), 3335-3348, doi:10.1029/2000JD900620

Bala, G., P. B. Duffy, and K. E. Taylor (2008), Impact of geoengineering schemes on the global hydrological cycle., *Proc. Natl. Acad. Sci. U. S. A.,105*(22), 7664–9, doi:10.1073/pnas.0711648105.

Balan Sarojini, B.B., P.A. Stott, E. Black, and D. Polson (2012), Fingerprints of changes in annual and seasonal precipitation from CMIP5 models over land and ocean. *Geophys. Res. Lett.,39,* L21706, doi: 10.1029/2012GL053373.

Ban-Weiss, G. A, and K. Caldeira (2010), Geoengineering as an optimization problem, *Environ. Res. Lett., 5*(3), 034009, doi:10.1088/1748-9326/5/3/034009.

Becker, A., P. Finger, A. Meyer-Christoffer, B. Rudolf, K. Schamm, U. Schneider, and M. Ziese (2013), A description of the global land-surface precipitation data products of the Global Precipitation Climatology Centre with sample applications including centennial (trend) analysis from 1901–present, *Earth Syst. Sci. Data*, *5*, 71-99, doi:10.5194/essd-5-71-2013.

Bentsen, M., et al. (2013), The Norwegian Earth System Model, NorESM1-M – Part 1: Description and basic evaluation of the physical climate, *Geosci. Model Dev., 6*(3), 687–720, doi:10.5194/gmd-6-687-2013.

Bi, D., et al. (2013), The ACCESS coupled model: Description, control climate and evaluation, *Aust. Meteorol. Ocean., 63*(1), 41–64.

Bindoff, N.L. et al., (2013) Detection and Attribution of Climate Change: from Global to Regional, in *Climate Change 2013: The Physical Science Basis. Contribution of Working Group I to the Fifth Assessment Report of the Intergovernmental Panel on Climate Change*, edited by T.F. Stocker, D. Qin, G.-K. Plattner, M. Tignor, S.K. Allen, J. Boschung, A. Nauels, Y. Xia, V. Bex and P.M. Midgley, Cambridge University Press, Cambridge, United Kingdom and New York, NY, USA.

Boucher, O. et al., (2013) Clouds and Aerosols, in *Climate Change 2013: The Physical Science Basis. Contribution of Working Group I to the Fifth Assessment Report of the Intergovernmental Panel on Climate Change*, edited by T.F. Stocker, D. Qin, G.-K. Plattner, M. Tignor, S.K. Allen, J. Boschung, A. Nauels, Y. Xia, V. Bex and P.M. Midgley, Cambridge University Press, Cambridge, United Kingdom and New York, NY, USA.

Broccoli, A. J., K. W. Dixon, T. L. Delworth, T. R. Knutson, R. J. Stouffer, and F. R. Zeng (2003), Twentieth-century temperature and precipitation trends in ensemble climate simulations including natural and anthropogenic forcing, *J. Geophys. Res.*, *108*(D24), 4798, doi:10.1029/2003JD003812.

Caldeira, K., G. Bala, and L. Cao (2013), The Science of Geoengineering, *Annu. Rev. Earth Planet. Sci.*, *41*(1), 231–256, doi:10.1146/annurev-earth-042711-105548.

Cao, L., G. Bala, and K. Caldeira (2012), Climate response to changes in atmospheric carbon dioxide and solar irradiance on the time scale of days to weeks, *Environ. Res. Lett.*, *7*(3), 034015, doi:10.1088/1748-9326/7/3/034015.

Charlton-Perez, A. J., et al. (2013), On the lack of stratospheric dynamical variability in low-top versions of the CMIP5 models, *J. Geophys. Res.*, *118*(6), 2494–2505, doi:10.1002/jgrd.50125.

Chen, D., M. A. Cane, A. Kaplan, S. E. Zebiak, and D. Huang (2004), Predictability of El Niño over the past 148 years, *Nature*, *428*(6984), 733–6, doi:10.1038/nature02439.

Chou, C., J.C.H. Chiang, C.W. Lan, C.H. Chung, Y.C. Liao and C.J. Lee (2013), increase in the range between wet and dry season precipitation. *Nat. Geosci.6*(4), 263-267, doi:10.1038/NGEO1744.

Chylek, P., J. Li, M. K. Dubey, M. Wang, and G. Lesins (2011), Observed and model simulated 20th century Arctic temperature variability: Canadian Earth System Model CanESM2, *Atmos. Chem. Phys. Discuss.*, *11*(8), 22893–22907, doi:10.5194/acpd-11-22893-2011.

Collins, M., S. Tett, and C. Cooper (2001), The internal climate variability of HadCM3, a version of the Hadley Centre coupled model without flux adjustments, *Clim. Dyn.*, *17*(1), 61-68, doi:10.1007/s003820000094.

Collins, W. J. et al. (2011), Development and evaluation of an Earth-System model – HadGEM2, *Geosci. Model Dev.*, *4*(4), 1051–1075, doi:10.5194/gmd-4-1051-2011.

Collins, M., R. et al., (2013) Long-term Climate Change: Projections, Commitments and Irreversibility, in *Climate Change 2013: The Physical Science Basis. Contribution of Working Group I to the Fifth Assessment Report of the Intergovernmental Panel on Climate Change*, edited by T.F.Stocker, D. Qin, G.-K. Plattner, M. Tignor, S.K. Allen, J. Boschung, A. Nauels, Y. Xia, V. Bex and P.M. Midgley, Cambridge University Press, Cambridge, United Kingdom and New York, NY, USA.

Crowley, T.J., G. Zielinski, B. Vinther, R. Udisti, K. Kreutz, J. Cole-Dai, and E. Castellano (2008), Volcanism and the Little Ice Age. *PAGES News, 16*(2), 22-23.

Dai, A., and K. E. Trenberth (2002), Estimates of freshwater discharge from continents: Latitudinal and seasonal variations., *J. Hydrometeorol., 3*(6), 660–687, doi: 10.1175/1525-7541(2002)003<0660:EOFDFC>2.0.CO;2

Dai, A., T. Qian, K. E. Trenberth, and J. D. Milliman (2009), Changes in Continental Freshwater Discharge from 1948 to 2004, *J. Clim., 22*(10), 2773–2792, doi:10.1175/2008JCLI2592.1.

Delworth, T. J. et al. (2006) GFDL's CM2 Global Coupled Climate Models. Part I: Formulation and Simulation Characteristics. *J. Clim.,19*(5), 643-674, doi:10.1175/JCLI3629.1

Dix, M. et al. (2013) The ACCESS coupled model: documentation of core CMIP5 simulations and initial results. *Aust. Meteorol. Ocean. 63*(1), 83-99

Donner, L. J. et al. (2011), The Dynamical Core, Physical Parameterizations, and Basic Simulation Characteristics of the Atmospheric Component AM3 of the GFDL Global Coupled Model CM3, *J. Clim., 24*(13), 3484–3519, doi:10.1175/2011JCLI3955.1.

Driscoll, S., A. Bozzo, L. J. Gray, A. Robock, and G. Stenchikov (2012), Coupled Model Intercomparison Project 5 (CMIP5) simulations of climate following volcanic eruptions, *J. Geophys. Res., 117*, D17105, doi:10.1029/2012JD017607.

Emile-Geay, J., R. Seager, M. a. Cane, E. R. Cook, and G. H. Haug (2008), Volcanoes and ENSO over the Past Millennium, *J.Clim., 21*(13), 3134–3148, doi:10.1175/2007JCLI1884.1.

Falloon, P. D., and R. A. Betts (2006), The impact of climate change on global river flow in HadGEM1 simulations, *Atmos. Sci. Lett.*, 7(3), 62–68, doi:10.1002/asl.133

Feng, J. (2013) Introduction of the CMIP5 Experiments Carried out by BNU-ESM. *Advances in Climate Change Research, 9*(4): 291-294. doi:10.3969/j.issn.1673-1719.2013.04.008

Ferraro, A. J., E. J. Highwood, and A. J. Charlton-Perez (2014), Weakened tropical circulation and reduced precipitation in response to geoengineering, *Environ. Res. Lett., 9*(1), 014001, doi:10.1088/1748-9326/9/1/014001.

Fischer, E.M, J. Luterbacher, E. Zorita, S.F.B. Tett, C. Casty, and H. Wanner, (2007), European climate response to tropical volcanic eruptions over the last half millennium, *Geophys. Res. Lett., 34*, L05707, doi:10.1029/2006GL027992.

Flato, G. et al., (2013) Evaluation of Climate Models, in *Climate Change 2013: The Physical Science Basis. Contribution of Working Group I to the Fifth Assessment Report of the Intergovernmental Panel on Climate Change*, edited by T.F. Stocker, D. Qin, G.-K.

Plattner, M. Tignor, S.K. Allen, J. Boschung, A. Nauels, Y. Xia, V. Bex and P.M. Midgley, Cambridge University Press, Cambridge, United Kingdom and New York, NY, USA.

Forster, P. M. D., and M. Collins (2004), Quantifying the water vapour feedback associated with post-Pinatubo global cooling, *Clim. Dyn.*, *23*(2), 207–214, doi:10.1007/s00382-004-0431-z.

Fyfe, J. C., J. N. S. Cole, V. K. Arora, and J. F. Scinocca (2013), Biogeochemical carbon coupling influences global precipitation in geoengineering experiments, *Geophys. Res. Lett.*, *40*(3), 651–655, doi:10.1002/grl.50166.

Gedney, N., P. M. Cox, R. A. Betts, O. Boucher, C. Huntingford, and P. A. Stott (2006), Detection of a direct carbon dioxide effect in continental river runoff records., *Nature*, *439*(7078), 835–8, doi:10.1038/nature04504.

Gent, P. R. et al. (2011), The Community Climate System Model Version 4, *J. Clim.*, *24*(19), 4973–4991, doi:10.1175/2011JCLI4083.1.

Gerten, D., S. Rost, W. von Bloh, and W. Lucht (2008), Causes of change in 20th century global river discharge, *Geophys. Res. Lett.*, *35*(20), L20405, doi:10.1029/2008GL035258.

Gillett, N.P, A.J. Weaver, F.W. Zwiers, and M.F. Wehner (2004), Detection of volcanic influence on global precipitation, *Geophs. Res. Lett.*, *31*, L12217, doi:10.1029/2004GL020044.

Gimeno, L., A. Drumond, R. Nieto, R. M. Trigo, and A. Stohl (2010), On the origin of continental precipitation, *Geophys. Res. Lett.*, *37*(13), L13804, doi:10.1029/2010GL043712.

Giorgetta, M. A. et al. (2013), Climate and carbon cycle changes from 1850 to 2100 in MPI-ESM simulations for the Coupled Model Intercomparison Project phase 5, *J. Adv. Model. Earth Syst.*, *5*(3), 572–597, doi:10.1002/jame.20038.

Gordon, C., C. Cooper, C. A. Senior, H. Banks, J. M. Gregory, T. C. Johns, J. F. B. Mitchell, and R. A. Wood (2000), The simulation of SST, sea ice extents and ocean heat transports in a version of the Hadley Centre coupled model without flux adjustments, *Clim. Dyn.*, *16*(2-3), 147-168, doi: 10.1007/s003820050010.

Gordon, H. B., et al. (2002), The CSIRO Mk3 climate system model, *Tech. Pap. 60*, Atmos. Res., Commonw. Sci. and Ind. Res. Org.,Aspendale, Victoria, Australia.

Gordon, H. B., S. P. O'Farrell, M. A. Collier, M. R. Dix, L. D. Rotstayn, E. A. Kowalczyk, A. C. Hirst, and I. G. Watterson (2010), The CSIRO Mk3.5 Climate Model, technical report no. 21, *Technical Report 021*, CAWCR, Aspendale, Vic., Australia.

Gu, G., and R. F. Adler (2011), Precipitation and Temperature Variations on the Interannual Time Scale: Assessing the Impact of ENSO and Volcanic Eruptions, *J.Clim.*, *24*(9), 2258-2270, doi: 10.1175/2010JCLI3727.1.

Gu, G. J., R. F. Adler, G. J. Huffman, and S. Curtis (2007), Tropical rainfall variability on interannual-to-interdecadal and longer time scales derived from the GPCP monthly product, *J.Clim.*, *20*(15), 4033-4046, doi: 10.1175/JCLI4227.1.

Hansen, J., et al. (2002), Climate forcings in Goddard Institute for Space Studies SI2000 simulations, *J. Geophys. Res*., *107*(D18), 4347 doi:10.1029/2001JD00114.

Haywood, J. M et al., (2010), Observations of the eruption of the Sarychev volcano and simulations using the HadGEM2 climate model, *J. Geophys.Res., 115*, D21212, doi: 10.1029/2010JD014447

Haywood, J. M., A. Jones, N. Bellouin, and D. Stephenson (2013), Asymmetric forcing from stratospheric aerosols impacts Sahelian rainfall, *Nat. Clim. Chang.*, *3*(7), 660–665, doi:10.1038/nclimate1857

Hazeleger, W. et al. (2012) EC-Earth V2.2: description and validation of a new seamless earth system prediction model. *Clim. Dyn. 39*(11), 2611-2629, doi: 10.1007/s00382-011-1228-5

Hegerl, G., and F. Zwiers (2011), Use of models in detection and attribution of climate change, *Wiley Interdiscip. Rev. Clim. Chang.*, *2*(4), 570–591, doi:10.1002/wcc.121.

Hegerl, G. C., T. J. Crowley, S. K. Baum, K. Y. Kim, and W. T. Hyde (2003), Detection of volcanic, solar and greenhouse gas signals in paleo-reconstructions of Northern Hemispheric temperature, *Geophys. Res. Lett.*, *30*(5), 1242, doi:10.1029/2002GL016635.

Hegerl, G., J. Luterbacher, F. Gonzalez-Rouco, S. F. B. Tett, T. Crowley, and E. Xoplaki (2011), Influence of human and natural forcing on European seasonal temperatures, *Nat. Geosci.*, *4*(2), 99-103, doi: 10.1038/NGEO1057.

Hegerl G.C.,et al. (2014) Quantifying changes in the global watercycle. *Bull. Am. Meteorol. Soc.*, resubmitted.

Held, I. M., and B. J. Soden (2006), Robust responses of the hydrological cycle to global warming, *J. Clim.*, *19*(21), 5686-5699, doi: 10.1175/JCLI3990.1.

Hendon, H. H., E.-P. Lim, and H. Nguyen (2014), Seasonal Variations of Subtropical Precipitation Associated with the Southern Annular Mode, *J. Clim.*, *27*(9), 3446–3460, doi:10.1175/JCLI-D-13-00550.1.

Highwood, E. J., and D. S. Stevenson (2003), Atmospheric impact of the 1783–1784 Laki Eruption: Part II Climatic effect of sulphate aerosol, *Atmos. Chem. Phys. Discuss.*, *3*(2), 1177–1189, doi:10.5194/acp-3-1177-2003.

Hurrell, James & National Center for Atmospheric Research Staff (Eds). Last modified 02 Dec 2013. "The Climate Data Guide: Hurrell North Atlantic Oscillation (NAO) Index (station-based)." Retrieved from https://climatedataguide.ucar.edu/climate-data/hurrell-north-atlantic-oscillation-nao-index-station-based.

Iles, C. E., G. C. Hegerl, A. P. Schurer and X. Zhang (2013), The effect of volcanic eruptions on global precipitation, *J. Geophys. Res.,118*(16) , 8770–8786, doi:10.1002/jgrd.50678.

Inness, P., and J. Slingo (2003), Simulation of the Madden-Julian oscillation in a coupled general circulation model. Part I: Comparison with observations and an atmosphere-only GCM, *J. Clim.16*(3), 345–365. doi:10.1175/1520-0442(2003)016<0345:SOTMJO>2.0.CO;2.

IPCC (2013) Summary for Policymakers, in *Climate Change 2013: The Physical Science Basis. Contribution of Working Group I to the Fifth Assessment Report of the Intergovernmental Panel on Climate Change*, edited by T.F. Stocker, D. Qin, G.-K. Plattner, M. Tignor, S.K. Allen, J. Boschung, A. Nauels, Y. Xia, V. Bex and P.M. Midgley, Cambridge University Press, Cambridge, United Kingdom and New York, NY, USA

IPCC (2014) Summary for policymakers, in *Climate Change 2014: Impacts, Adaptation, and Vulnerability. Part A: Global and Sectoral Aspects. Contribution of Working Group II to the Fifth Assessment Report of the Intergovernmental Panel on Climate Change*, edited by C.B. Field et al., Cambridge University Press, Cambridge, United Kingdom and NewYork, NY, USA, pp. 1-32

Iversen, T. et al. (2013), The Norwegian Earth System Model, NorESM1-M – Part 2: Climate response and scenario projections, *Geosci. Model Dev.*, *6*(2), 389–415, doi:10.5194/gmd-6-389-2013.

Jeffrey, S., L. Rotstayn, M. Collier, S. Dravitzki, C. Hamalainen, C. Moeseneder, K. Wong, and J. Syktus (2013), Australia's CMIP5 submission using the CSIRO-Mk3 . 6 model, *Aust. Meteorol. Ocean.*, *63*(1), 1–13.

Jones, G. S., Gregory, J. M., Stott, P. a., Tett, S. F. B., & Thorpe, R. B. (2005). An AOGCM simulation of the climate response to a volcanic super-eruption. *Climate Dynamics*, *25*(7-8), 725–738. doi:10.1007/s00382-005-0066-8

Jones, A., J. Haywood, O. Boucher, B. Kravitz, and A. Robock (2010), Geoengineering by stratospheric SO_2 injection: results from the Met Office HadGEM2 climate model and comparison with the Goddard Institute for Space Studies ModelE, *Atmos. Chem. Phys.*, *10*(13), 5999–6006, doi:10.5194/acp-10-5999-2010.

Jones, C. D. et al. (2011), The HadGEM2-ES implementation of CMIP5 centennial simulations, *Geosci. Model Dev.*, *4*(3), 543–570, doi:10.5194/gmd-4-543-2011.

Joseph, R., and S. Nigam (2006), ENSO evolution and teleconnections in IPCC's twentieth-century climate simulations: Realistic representation?, *J. Clim.*, *19*(17), 4360–4378. doi:10.1175/JCLI3846.1.

Joseph, R., and N. Zeng (2011), Seasonally Modulated Tropical Drought Induced by Volcanic Aerosol, *J. Clim.*, *24*(8), 2045-2060, doi: 10.1175/2009JCLI3170.1.

Joseph, P. V., B. Gokulapalan, A. Nair, and S. S. Wilson (2013), Variability of Summer Monsoon Rainfall in India on Inter-Annual and Decadal Time Scales, *Atmos. Oceanic Sci. Lett.*, *6*(5), 398–403, doi:10.3878/j.issn.1674-2834.13.0044.

Joshi, M. M. and G. S. Jones (2009), The climatic effects of the direct injection of water vapour into the stratosphere by large volcanic eruptions, *Atmos. Chem. Phys.*, *9*(16), 6109–6118. doi: 10.5194/acp-9-6109-2009

Karpechko, A. Y., N. P. Gillett, M. Dall'Amico, and L. J. Gray (2010), Southern Hemisphere atmospheric circulation response to the El Chichón and Pinatubo eruptions in coupled climate models, *Q. J. R. Meteorol. Soc.*, *136*(652), 1813–1822, doi:10.1002/qj.683.

Kenyon, J., and G. C. Hegerl (2008), Influence of modes of climate variability on global temperature extremes, *J. Clim.*, *21*(15), 3872-3889, doi: 10.1175/2008JCLI2125.1.

Kenyon, J., and G. C. Hegerl (2010), Influence of Modes of Climate Variability on Global Precipitation Extremes, *J. Clim.*, *23*(23), 6248-6262, doi: 10.1175/2010JCLI3617.1.

Koenigk, T., L. Brodeau, R. G. Graversen, J. Karlsson, G. Svensson, M. Tjernström, U. Willén, and K. Wyser (2013), Arctic climate change in 21st century CMIP5 simulations with EC-Earth, *Clim. Dyn.*, *40*(11-12), 2719–2743, doi:10.1007/s00382-012-1505-y.

Kravitz, B., A. Robock, P. M. Forster, J. M. Haywood, M. G. Lawrence, and H. Schmidt (2013a), An overview of the Geoengineering Model Intercomparison Project (GeoMIP), *J. Geophys. Res. Atmos.*, *118*(23), 13,103–13,107, doi:10.1002/2013JD020569.

Kravitz, B. et al. (2013b), Climate model response from the Geoengineering Model Intercomparison Project (GeoMIP), *J. Geophys. Res. Atmos.*, *118*(15), 8320–8332, doi:10.1002/jgrd.50646.

Kravitz, B. et al. (2013c), An energetic perspective on hydrological cycle changes in the Geoengineering Model Intercomparison Project, *J. Geophys. Res. Atmos.*, *118*(23), 13,087–13,102, doi:10.1002/2013JD020502.

Labat, D., Y. Goddéris, J. L. Probst, and J. L. Guyot (2004), Evidence for global runoff increase related to climate warming, *Adv. Water Resour.*, *27*(6), 631–642, doi:10.1016/j.advwatres.2004.02.020.

Lambert, F. H., and M. R. Allen (2009), Are Changes in Global Precipitation Constrained by the Tropospheric Energy Budget?, *J. Clim.*, *22*(3), 499–517, doi:10.1175/2008JCLI2135.1.

Lambert, F.H., P.A. Stott, M.R. Allen, and M.A. Palmer (2004), Detection and attribution of changes in 20th century land precipitation. *Geophys. Res. Lett.*, *31*(10), L10203, doi:10.1029/2004GL019545.

Lambert, F.H., N.P. Gillett, D.A. Stone, and C. Huntingford (2005), Attribution studies of observed land precipitation changes with nine coupled models, *Geophys. Res. Lett.*, *32*(18), L18704, doi:10.1029/2005GL023654.

Li, J., and A. Sharma (2013), Evaluation of volcanic aerosol impacts on atmospheric water vapor using CMIP3 and CMIP5 simulations, *J. Geophys. Res. Atmos.*, *118*(10), 4448–4457, doi:10.1002/jgrd.50420.

Liu, C., R. P. Allan, and G. J. Huffman (2012), Co-variation of temperature and precipitation in CMIP5 models and satellite observations, *Geophys. Res. Lett.*, *39*(13), L13803, doi:10.1029/2012GL052093.

Liu, J., B. Wang, M.A.Cane, S.Y. Yim, J.Y. Lee (2013), Divergent global precipitation changes induced by natural versus anthropogenic forcing, *Nature, 493*(7434), 656-659, doi: 10.1038/nature11784.

Marengo, J. A. (2004), Characteristics and spatio-temporal variability of the Amazon River Basin Water Budget, *Clim. Dyn.*, *24*(1), 11–22, doi:10.1007/s00382-004-0461-6.

McHugh, M. J., and J. C Rogers (2001), North Atlantic oscillation influence on precipitation variability around the southeast African convergence zone, *J. Clim.*,*14*(17), 3631–3642, doi: 10.1175/1520-0442(2001)014<3631:NAOIOP>2.0.CO;2

Meehl, G.A., et al., (2007) Global Climate Projections., in *Climate Change 2007: The Physical Science Basis. Contribution of Working Group I to the Fourth Assessment Report of the Intergovernmental Panel on Climate Change*, edited by S.Solomon, D. Qin, M. Manning, Z. Chen, M. Marquis, K.B. Averyt, M. Tignor and H.L. Miller. Cambridge University Press, Cambridge, United Kingdom and New York, NY, USA.

Meehl, G. A. et al. (2012), Climate System Response to External Forcings and Climate Change Projections in CCSM4, *J. Clim.*, *25*(11), 3661–3683, doi:10.1175/JCLI-D-11-00240.1.

Miller, G. H. et al. (2012), Abrupt onset of the Little Ice Age triggered by volcanism and sustained by sea-ice/ocean feedbacks, *Geophys. Res. Lett.*, *39*(2), L02708, doi:10.1029/2011GL050168.

Milliman, J. D., K. L. Farnsworth, P. D. Jones, K. H. Xu, and L. C. Smith (2008), Climatic and anthropogenic factors affecting river discharge to the global ocean, 1951–2000, *Glob. Planet. Change*, *62*(3-4), 187–194, doi:10.1016/j.gloplacha.2008.03.001.

Milly, P. C. D., K. A. Dunne, and A. V. Vecchia (2005), Global pattern of trends in streamflow and water availability in a changing climate., *Nature*, *438*(7066), 347–350, doi:10.1038/nature04312.

Niemeier, U., H. Schmidt, K. Alterskjaer, and J. E. Kristjánsson (2013), Solar irradiance reduction via climate engineering: Impact of different techniques on the energy balance and the hydrological cycle, *J. Geophys. Res. Atmos.*, *118*(21), 11,905–11,917, doi:10.1002/2013JD020445.

Nijjssen, B., G. M. O'Donnell, A. F. Hamlet and D. P. Lettenmaier (2001), Hydrologic sensitivity of global rivers to climate change, *Climatic Change.*, *50*(1-2), 143-175, doi: 10.1023/A:1010616428763

Nilsson, C., C. A. Reidy, M. Dynesius, and C. Revenga (2005), Fragmentation and flow regulation of the world's large river systems., *Science*, *308*(5720), 405–408, doi:10.1126/science.1107887.

Nohara, D., A. Kitoh, M. Hosaka and T. Oki (2006), Impact of climate change on river discharge projected by multimodel ensemble., *J.Hydrometeorol.*,*7*(5), 1076–1089, doi: 10.1175/JHM531.1

O'Gorman, P. a., R. P. Allan, M. P. Byrne, and M. Previdi (2012), Energetic Constraints on Precipitation Under Climate Change, *Surveys in Geophysics*, *33*(3-4), 585–608, doi:10.1007/s10712-011-9159-6.

Oman, L., A. Robock, G. L. Stenchikov, T. Thordarson, D. Koch, D. T. Shindell, and C. Gao (2006a), Modeling the distribution of the volcanic aerosol cloud from the 1783–1784 Laki eruption, *J. Geophys. Res.*, *111*(D12), D12209, doi:10.1029/2005JD006899.

Oman, L., A. Robock, G.L. Stenchikov, and T. Thordarson (2006b), High-latitude eruptions cast shadow over the African monsoon and the flow of the Nile, *Geophys. Res. Lett.*, *33*(18), L18711, doi:10.1029/2006GL027665.

Pardaens, a. K., H. T. Banks, J. M. Gregory, and P. R. Rowntree (2003), Freshwater transports in HadCM3, *Clim. Dyn.*, *21*(2), 177–195, doi:10.1007/s00382-003-0324-6.

Peng, Y, C. Shen, W.C. Wang, and Y. Xu (2010), Response of Summer Precipitation over Eastern China to Large Volcanic Eruptions. *J. Clim.*, *23*(3), 818-824, doi: 10.1175/2009JCLI2950.1.

Piao, S., P. Friedlingstein, P. Ciais, N. de Noblet-Ducoudré, D. Labat, and S. Zaehle (2007), Changes in climate and land use have a larger direct impact than rising CO2 on global river runoff trends., *Proc. Natl. Acad. Sci. U. S. A.*, *104*(39), 15242–7, doi:10.1073/pnas.0707213104.

Polson, D., G. C. Hegerl, X. Zhang, and T. J. Osborn (2013a), Causes of Robust Seasonal Land Precipitation Changes, *J. Clim.*, *26*(17), 6679–6697, doi:10.1175/JCLI-D-12-00474.1.

Polson, D., G. C. Hegerl, R. P. Allan, and B. B. Sarojini (2013b), Have greenhouse gases intensified the contrast between wet and dry regions?, *Geophys. Res. Lett.*, *40*(17), 4783–4787, doi:10.1002/grl.50923.

Pope, V. D., M. L. Gallani, P. R. Rowntree, and R. A. Stratton (2000), The impact of new physical parametrizations in the Hadley Centre climate model: HadAM3, *Clim. Dyn.*, *16*(2-3), 123-146, doi: 10.1007/s003820050009.

Ricke, K. L., M. G. Morgan and M. R. Allen (2010), Regional climate response to solar-radiation management, *Nat. Geosci.*, *3*(8), 537–541, doi:10.1038/ngeo915.

Robock, A. (2000), Volcanic Eruptions and Climate, *Rev. Geophys.*, *38*(2), 191-219, doi: 10.1029/1998RG000054.

Robock, A. and Y. Liu (1994), The volcanic signal in Goddard Institute for Space Studies Three-Dimensional model simulations. *J. Clim.*, *7*(1), 44-55, doi: 10.1175/1520-0442(1994)007<0044:TVSIGI>2.0.CO;2.

Robock, A and J. Mao (1992) Winter warming from large volcanic eruptions. *Geophys. Res. Lett.*, **19**, 2405-2408, doi: 10.1029/92GL02627.

Robock, A., and J. P. Mao (1995), The Volcanic Signal in Surface-Temperature Observations, *J. Clim.*, *8*(5), 1086-1103, doi: 10.1175/1520-0442(1995)008<1086:TVSIST>2.0.CO;2.

Robock, A., L. Oman, and G. L. Stenchikov (2008), Regional climate responses to geoengineering with tropical and Arctic SO 2 injections, *J. Geophys. Res.*, *113*(D16), D16101, doi:10.1029/2008JD010050.

Roscoe, H., and J. Haigh (2007), Influences of ozone depletion, the solar cycle and the QBO on the Southern Annular Mode, *Q. J. R,.133*(628), 1855–1864, doi:10.1002/qj.

Sato, M., J. Hansen, M. McCormick, and J. Pollack (1993), Stratospheric aerosol optical depths, *J. Geophys. Res.*, *98*, 22,987–22,994, doi:10.1029/93JD02553.

Schmidt, G.A et al. (2006) Present-Day Atmospheric Simulations Using GISS ModelE: Comparison to In Situ,Satellite, and Reanalysis Data, *J. Clim.*, *19*(2), 153-192, doi:10.1175/JCLI3612.1

Schmidt, H. et al. (2012), Solar irradiance reduction to counteract radiative forcing from a quadrupling of CO_2: climate responses simulated by four earth system models, *Earth Syst. Dyn.*, *3*(1), 63–78, doi:10.5194/esd-3-63-2012.

Schmidt, H. et al. (2013), Response of the middle atmosphere to anthropogenic and natural forcings in the CMIP5 simulations with the Max Planck Institute Earth system model, *J. Adv. Model. Earth Syst.*, *5*(1), 98–116, doi:10.1002/jame.20014.

Schneider, D. P., C. M. Ammann, B. L. Otto-Bliesner, and D. S. Kaufman (2009), Climate response to large, high-latitude and low-latitude volcanic eruptions in the Community Climate System Model, *J. Geophys. Res.*, *114*, D15101, doi: 10.1029/2008JD011222.

Schurer, A. P., S. F. B. Tett, and G. C. Hegerl (2014), Small influence of solar variability on climate over the past millennium, *Nat. Geosci.*, *7*(2), 104–108, doi:10.1038/ngeo2040.

Scinocca, J. F., N. A. McFarlane, M. Lazare, J. Li, and D. Plummer (2008), Technical Note: The CCCma third generation AGCM and its extension into the middle atmosphere, *Atmos. Chem. Phys.*, *8*(23), 7055–7074, doi:10.5194/acp-8-7055-2008.

Self, S., M. R. Rampino, and M. G. Katz (1997), Volcanic aerosol perturbations and strong El Nino events: No general correlation, *Geophys. Res. Lett.*, *24*(10), 1247–1250, doi:10.1029/97GL01127.

Shindell, D. T. et al. (2013), Interactive ozone and methane chemistry in GISS-E2 historical and future climate simulations, *Atmos. Chem. Phys.*, *13*(5), 2653–2689, doi:10.5194/acp-13-2653-2013.

Soden, B. J., R. T. Wetherald, G. L. Stenchikov, and A. Robock (2002), Global cooling after the eruption of Mount Pinatubo: a test of climate feedback by water vapor., *Science*, *296*(5568), 727–30, doi:10.1126/science.296.5568.727.

Stenchikov, G. L., I. Kirchner, A. Robock, H.-F. Graf, J. C. Antuña, R. G. Grainger, A. Lambert, and L. Thomason (1998), Radiative forcing from the 1991 Mount Pinatubo volcanic eruption, *J. Geophys. Res.*, *103*(D12), 13,837–13,857, doi:10.1029/98JD00693.

Stenchikov, G., K. Hamilton, R. J. Stouffer, A. Robock, V. Ramaswamy, B. Santer, and H. F. Graf (2006), Arctic Oscillation response to volcanic eruptions in the IPCC AR4 climate models, *J. Geophys. Res.*, *111*(D7). D07107, doi:10.1029/2005JD006286.

Stenchikov, G., T. L. Delworth, V. Ramaswamy, R. J. Stouffer, A. Wittenberg, and F. Zeng (2009), Volcanic signals in oceans, *J. Geophys. Res.*, *114*, D16104, doi:10.1029/2008JD011673.

Taylor, K. E., R. J. Stouffer, and G. A. Meehl (2012), An Overview of CMIP5 and the Experiment Design, *Bull. Am. Meteorol. Soc.*, *93*(4), 485–498, doi:10.1175/BAMS-D-11-00094.1.

Tett, S. F. B., R. Betts, T. J. Crowley, J. Gregory, T. C. Johns, A. Jones, T. J. Osborn, E. Ostrom, D. L. Roberts, and M. J. Woodage (2007), The impact of natural and anthropogenic forcings on climate and hydrology since 1550, *Clim. Dyn.*, *28*(1), 3-34, doi: 10.1007/s00382-006-0165-1.

Tilmes, S. et al. (2013), The hydrological impact of geoengineering in the Geoengineering Model Intercomparison Project (GeoMIP), *J. Geophys. Res. Atmos.*, *118*(19), 11,036–11,058, doi:10.1002/jgrd.50868.

Timmreck, C. (2012), Modeling the climatic effects of large explosive volcanic eruptions, *WIREs Clim. Change.*,*3*(6), 545-564, doi: 10.1002/wcc.192.

Timmreck, C., S. J. Lorenz, T. J. Crowley, S. Kinne, T. J. Raddatz, M. A. Thomas, and J. H. Jungclaus (2009), Limited temperature response to the very large AD 1258 volcanic eruption, *Geophys. Res. Lett.*, *36*(21), L21708, doi:10.1029/2009GL040083.

Timmreck, C., H.-F. Graf, D. Zanchettin, S. Hagemann, T. Kleinen, and K. Krüger (2012), Climate response to the Toba super-eruption: Regional changes, *Quat. Int.*, *258*, 30–44, doi:10.1016/j.quaint.2011.10.008.

Toohey, M., K. Krüger, U. Niemeier, and C. Timmreck (2011), The influence of eruption season on the global aerosol evolution and radiative impact of tropical volcanic eruptions, *Atmos. Chem. Phys.*, *11*(23), 12351–12367, doi:10.5194/acp-11-12351-2011.

Trenberth, K.E. (2011) Changes in precipitation with climate change, *Clim. Res.*, *47*(1-2), 123-138, doi: 10.3354/cr00953.

Trenberth, K. E., and A. Dai (2007), Effects of Mount Pinatubo volcanic eruption on the hydrological cycle as an analogue of geoengineering, *Geophys. Res. Lett.*, *34*(15). L15702, doi:10.1029/2007GL030524.

Turner, A. G., P. M. Inness, and J. M. Slingo (2005), The role of the basic state in the ENSO-monsoon relationship and implications for predictability, *Q. J. R. Meteorol. Soc.*, **131**(607), 781–804. doi: 10.1256/qj.04.70.

Voldoire, A. et al. (2012), The CNRM-CM5.1 global climate model: description and basic evaluation, *Clim. Dyn.*, *40*(9-10), 2091–2121, doi:10.1007/s00382-011-1259-y.

Vorosmarty, C. J., B. M. Fekete, and B. A. Tucker. 1998. Global River Discharge, 1807-1991, V[ersion]. 1.1 (RivDIS). Data set. Available on-line [http://www.daac.ornl.gov] from Oak Ridge National Laboratory Distributed Active Archive Center, Oak Ridge, Tennessee, U.S.A. doi:10.3334/ORNLDAAC/199.

Vose, R. S., R. L. Schmoyer, P. M. Steurer, T. C. Peterson, R. Heim, T. R. Karl, and J. Eischeid (1992), The Global Historical Climatology Network: Long-term monthly temperature, precipitation, sea level pressure, and station pressure data, *ORNL/CDIAC*-53, 325 pp., Carbon Dioxide Inf. Anal. Cent., Oak Ridge, Tenn.

Watanabe, M. et al. (2010), Improved Climate Simulation by MIROC5: Mean States, Variability, and Climate Sensitivity, *J. Clim.*, *23*(23), 6312–6335, doi:10.1175/2010JCLI3679.1.

Wegmann, M., S. Brönnimann, J. Bhend, J. Franke, D. Folini, M. Wild, and J. Luterbacher (2014), Volcanic Influence on European Summer Precipitation through Monsoons: Possible Cause for “Years without Summer”, *J. Clim.*, *27*(10), 3683–3691, doi:10.1175/JCLI-D-13-00524.1.

Wielicki, B. a et al. (2002), Evidence for large decadal variability in the tropical mean radiative energy budget, *Science*, *295*(5556), 841–4, doi:10.1126/science.1065837.

Wu, T., R. Yu, and F. Zhang (2008), A Modified Dynamic Framework for the Atmospheric Spectral Model and Its Application, *J. Atmos. Sci.*, *65*(7), 2235–2253, doi:10.1175/2007JAS2514.1.

Wu, T., R. Yu, F. Zhang, Z. Wang, M. Dong, L. Wang, X. Jin, D. Chen, and L. Li (2010), The Beijing Climate Center atmospheric general circulation model: description and its performance for the present-day climate, *Clim. Dyn.*, *34*(1), 123–147, doi:10.1007/s00382-008-0487-2.

Xin, X.G., T.W. Wu, J.L. Li, Z.Z. Wang, W.P. Li and F.H. Wu, (2013), How Well does BCC _ CSM1.1 Reproduce the 20th Century Climate Change over China ?, *Atmos. Oceanic Sci. Lett.*, *6*(1), 21–26.

Yoshimori, M., and A. J. Broccoli (2008), Equilibrium response of an atmosphere-mixed layer ocean model to different radiative forcing agents: Global and zonal mean response, *J. Clim.*, *21*(17), 4399-4423, doi: 10.1175/2008JCLI2172.1.

Yukimoto, S. et al. (2012), A New Global Climate Model of the Meteorological Research Institute: MRI-CGCM3-Model Description and Basic Performance, *J. Meteorol. Soc. Japan*, *90A*(SI), 23–64, doi:10.2151/jmsj.2012-A02.

Zanchettin, D., C. Timmreck, H.-F. Graf, a. Rubino, S. Lorenz, K. Lohmann, K. Krüger, and J. H. Jungclaus (2012), Bi-decadal variability excited in the coupled ocean–atmosphere system by strong tropical volcanic eruptions, *Clim. Dyn.*, *39*(1-2), 419–444, doi:10.1007/s00382-011-1167-1.

Zanchettin, D., C. Timmreck, O. Bothe, S. J. Lorenz, G. Hegerl, H.-F. Graf, J. Luterbacher, and J. H. Jungclaus (2013), Delayed winter warming: A robust decadal response to strong tropical volcanic eruptions?, *Geophys. Res. Lett.*, *40*(1), 204–209, doi:10.1029/2012GL054403.

Zhang, X., F. W. Zwiers, G. C. Hegerl, F. H. Lambert, N. P. Gillett, S. Solomon, P. A. Stott, and T. Nozawa (2007), Detection of human influence on twentieth-century precipitation trends, *Nature.*, *448*(7152), 461-465. doi:10.1038/nature06025.

Zhang, Y., J. M. Wallace, and D. S. Battisti (1997), ENSO-like interdecadal variability: 1900-93, *J. Clim.*, *10*(5), 1004–1020, doi: 10.1175/1520-0442(1997)010<1004:ELIV>2.0.CO;2

Zhong, Y., G. H. Miller, B. L. Otto-Bliesner, M. M. Holland, D. a. Bailey, D. P. Schneider, and a. Geirsdottir (2010), Centennial-scale climate change from decadally-paced explosive volcanism: a coupled sea ice-ocean mechanism, *Clim. Dyn.*, *37*(11-12), 2373–2387, doi:10.1007/s00382-010-0967-z.